KONINKLIJK NEDERLANDS METEOROLOGISCH INSTITUUT

WETENSCHAPPELIJK RAPPORT
SCIENTIFIC REPORT
W.R. 81 - 2

A.G.M. Driedonks

Dynamics of the Well-Mixed
Atmospheric Boundary Layer.

De Bilt 1981

Publikatienummer: K.N.M.I. W.R. 81-2 (FM)

Koninklijk Nederlands Meteorologisch Instituut,
Fysisch Meteorologisch onderzoek,
Postbus 201,
3730 AE De Bilt,
Nederland.

U.D.C.: 551.510.522

VRIJE UNIVERSITEIT TE AMSTERDAM

Dynamics of the Well-Mixed Atmospheric Boundary Layer

ACADEMISCH PROEFSCHRIFT

ter verkrijging van de graad van doctor in
de wiskunde en natuurwetenschappen aan
de Vrije Universiteit te Amsterdam,
op gezag van de rector magnificus
dr. H. Verheul,
hoogleraar in de faculteit der wiskunde en natuurwetenschappen,
in het openbaar te verdedigen
op woensdag 22 april 1981 te 13.30 uur
in het hoofdgebouw der universiteit, De Boelelaan 1105

door

Adrianus Gerhardus Maria Driedonks

geboren te Utrecht

K.N.M.I. - DE BILT, 1981

PROMOTOR : PROF.DR.IR.H.TENNEKES

COREFERENT : PROF.DR.IR.L.WARTENA

CONTENTS

Woord vooraf

Bij het tot stand komen van dit proefschrift hebben een aantal gunstige omstandigheden een rol gespeeld, die ik hier graag wil noemen.
Het KNMI ben ik bijzonder erkentelijk voor de faciliteiten die het mij geboden heeft om dit onderzoek te verrichten en uit te doen groeien tot een dissertatie. Speciaal de infrastructuur, die het mogelijk maakte om de experimenten uit te voeren waarop deze studie gebaseerd is, was van grote betekenis.
De begeleiding door mijn promotor, Henk Tennekes, was voor mij van groot belang. Ik ben je speciaal dankbaar voor je pragmatische adviezen die voortdurend gericht waren op de grote lijn en die mij hebben behoed voor een onvruchtbaar ronddwalen tussen details.
Bert Wartena, de aandacht die je als coreferent aan mijn proefschrift hebt besteed en je kritische opmerkingen heb ik zeer op prijs gesteld.
Veel collega's van de afdeling Fysische Meteorologie hebben via discussies bijgedragen. Met name bedank ik hiervoor Aad van Ulden en Frans Nieuwstadt. In de eerste fase van dit onderzoek was Jaap Wisse hoofd van deze afdeling. Ik ben je zeer erkentelijk voor je steun.
Het experimentele deel van deze studie zou niet mogelijk zijn geweest zonder de inzet van velen, direct of indirect. Mijn dank gaat uit naar iedereen die betrokken is geweest bij de voorbereiding, uitvoering en controle van de metingen bij de 200 m mast in Cabauw en van de radiosonde-opstijgingen. Zonder de steun van de Instrumentele Afdeling, met name de buitendienst, en zonder de assistentie van vele medewerkers van de sectie Fysische Meteorologie, zouden deze experimenten niet mogelijk zijn geweest.
De uiteindelijke vormgeving van dit proefschrift is het resultaat van de vakbekwaamheid van de secretaresses van mijn afdeling, met name Anja van Dolderen en Mej. A.R. Krabman, van de tekenkamer, en van de drukkerij.

Samenvatting

Het onderwerp van deze studie is de ontwikkeling van de atmosferische grenslaag in de loop van een heldere dag. De atmosferische grenslaag is de laag nabij het aardoppervlak waarin de stroming turbulent is. De dikte van deze laag en de eigenschappen ervan kunnen sterk variëren. Oorzaak van de ontwikkeling overdag is de zonnestraling, waardoor het aardoppervlak opgewarmd wordt.

Als begintoestand nemen we de situatie aan het einde van de nacht, rond zonsopkomst. Door de nachtelijke afkoeling is de grenslaag stabiel opgebouwd (de temperatuur neemt toe met de hoogte), waardoor vertikale uitwisseling tegengewerkt wordt. De grenslaag is dan dun (van de orde van 100 m).

Na zonsopkomst verwarmt de zon het aardoppervlak. Doordat dit warmer wordt dan de lucht ontstaan er convectieve, opstijgende bewegingen die de turbulente intensiteit sterk doen toenemen. Door de vergroting van de turbulente energie kan de stabiele opbouw doorbroken worden. Er ontstaat een laag waarin sterke vertikale uitwisseling de temperatuuropbouw adiabatisch (neutraal) maakt en vochtigheid, wind en luchtverontreiniging vertikaal homogeen verdeelt. Deze wordt de menglaag genoemd. Aan de bovenkant van de menglaag is er een scherpe grens tussen de turbulente lucht beneden en de niet-turbulente, nog stabiel gelaagde lucht erboven.

De menglaag verandert voortdurend. Turbulente wervels dringen aan de bovenkant in de niet-turbulente lucht binnen en vangen die in. De voortdurende toevoer van turbulente energie houdt dit proces in stand. De dikte van de menglaag zal dus toenemen in de loop van de dag. Dit proces wordt "entrainment" genoemd. Midden op de dag kan de menglaag gemakkelijk een hoogte van 1000 m bereiken en, afhankelijk van de vochtigheid, kunnen er aan de top cumuluswolken ontstaan.

De bestudering van de groei van de menglaag als functie van de tijd in afhankelijkheid van externe factoren, zoals bijvoorbeeld de warmte-

toevoer vanaf de bodem en de stabiliteit van de lucht erboven, is een belangrijk onderwerp in de grenslaagmeteorologie. Een duidelijke toepassing ligt op het gebied van de luchtverontreiniging. Zolang de pluim van een schoorsteen zich boven de menglaag bevindt zal er geen verontreiniging op grondniveau gevonden worden. Kort nadat de menglaaghoogte de pluim bereikt heeft, zal dit door de vertikale menging wel het geval zijn. De groei van de menglaag zal verder bepalen in hoeverre de luchtverontreiniging verdund kan worden.

Bij de modelvorming voor de groei van de menglaag gaan we uit van een vereenvoudigd beeld van de werkelijkheid. We nemen aan dat de menglaag als volledig vertikaal homogeen beschouwd kan worden. De grens tussen de turbulente menglaag en de stabiele lucht erboven wordt oneindig dun genomen; een discontinuïteit in de waarde van de variabelen markeert deze overgang. Met deze modelveronderstellingen kunnen de voorspelvergelijkingen voor de menglaag in betrekkelijk eenvoudige vorm worden opgeschreven. Zoals altijd het geval is in turbulente stromingen, bevatten deze vergelijkingen een onbekende meer dan het aantal vergelijkingen. Voor een verstandige aanpak van dit probleem moeten we ons realiseren dat turbulente wervels aan de bovenkant van de menglaag relatief warme lucht invangen en naar beneden transporteren. Neerwaarts transport van relatief warme lucht gaat niet vanzelf. Dit kan alleen als er kinetische energie aan de turbulentie wordt onttrokken. De groei van de menglaag hangt dus samen met de hoeveelheid kinetische energie die de turbulentie hiervoor beschikbaar kan stellen. Daarom is het verstandig om als extra vergelijking de vergelijking voor de turbulente kinetische energie te nemen.

De verschillende termen in deze vergelijking moeten geparameteriseerd worden, d.w.z. uitgedrukt in reeds bekende variabelen. Hierbij moeten we ons realiseren dat er, naast convectie, nog andere mechanismen zijn waardoor turbulente kinetische energie geproduceerd kan worden: door wrijving met het aardoppervlak en door een sterke verandering

van de wind aan de top van de menglaag. De parameterisatie van deze processen in de energievergelijking is niet eenvoudig. Fysisch inzicht in de werkzame mechanismen is nodig om tot verstandige schattingen te komen. We hebben een groot aantal mogelijkheden onderzocht. Na analyse bleek dat deze voor een aantal termen niet tot essentieel verschillende formuleringen leidden. Complicaties ontstaan in zeer stabiele situaties. De voorgestelde oplossingen hiervoor zijn niet geheel bevredigend. Omdat de "entrainment" in deze gevallen toch al klein is, is het praktisch belang van dit probleem gering in de atmosferische menglaag. Het effect bleek niet aantoonbaar in onze metingen.

Om de resultaten van de menglaagmodellen te toetsen werd een uitgebreid experimenteel programma uitgevoerd bij de 200 m hoge meteorologische meetmast van het KNMI, te Cabauw. Op tien heldere dagen in 1977 en 1978 werden alle, voor de groei van de menglaag belangrijke, gegevens verzameld. Langs de mast werden de profielen van temperatuur, vochtigheid en wind gemeten. Om deze gegevens ook boven 200 m hoogte te krijgen, werd een groot aantal radiosondes opgelaten. Met behulp van een acoustische radar (Sodar) kon in de ochtend de hoogte van de grenslaag bepaald worden. Ook de fluxen van warmte en vocht vanaf de grond en de wrijving werden gemeten.

Bij het gebruik van atmosferische metingen ter toetsing van modellen moet altijd met een zekere onnauwkeurigheid rekening worden gehouden. Deze is niet zozeer het gevolg van meetfouten maar veel meer van interpretatieproblemen. Een menglaagmodel berust op een geschematiseerd beeld van de werkelijkheid. Metingen wijken hier altijd min of meer af; er is dus een procedure vereist om uit de metingen de modelvariabelen af te leiden. Aan de andere kant moet rekening worden gehouden met de variabiliteit van de atmosfeer zelf. Modellen doen uitspraken over gemiddelde waarde van grootheden. Metingen kunnen deze waarde hoogstens benaderen; ze hebben daardoor statistische fouten. Zo moet bijvoorbeeld een radiosondemeting gezien worden als een momentopname

van de vertikale opbouw. Aan de bovenkant van de menglaag zorgen turbulente wervels voortdurend voor vervormingen van het grensvlak tussen turbulente en niet-turbulente lucht. Bij een schatting van de menghoogte uit een radiosondemeting moet rekening worden gehouden met een toevallige fout ten gevolge van deze vervormingen. Een karakteristieke grootte van deze fout is $\pm$ 100 m midden op de dag.
Bij de beoordeling van modelresultaten moet met deze zaken rekening worden gehouden. Kleine verschillen tussen modellen onderling zijn dus niet van betekenis. Bovendien blijkt bij een analyse van de modelvergelijkingen dat de oplossingen hiervan niet erg gevoelig zijn voor variaties in de waarden van verschillende constanten. Alleen grote verschillen kunnen in de atmosfeer getoetst worden.

Bij de vergelijking tussen modellen hebben we ons geconcentreerd op de voorspelling van de menghoogte h. De resultaten hiervan voor onze tien meetdagen kunnen als volgt worden samengevat:

- In situaties waarin alleen convectieve produktie van turbulentie belangrijk is, verklaart een model dat het neerwaartse transport voor warmte aan de top van de menglaag eenvoudigweg negeert al ongeveer 80% van de waargenomen toename van de menghoogte ("encroachment", vergelijkbaar met de zgn. "Gold-methode"). De resterende 20% wordt goed voorspeld wanneer het neerwaarts warmtetransport ter hoogte h evenredig wordt genomen met het opwaarts warmtetransport vanaf de grond, met een evenredigheidsconstante $c_F = 0.2$. De standaarddeviatie die overblijft is $\pm$ 125 m. Met dit model kan de menghoogte midden op een heldere dag goed berekend worden.
- In de eerste uren na zonsopkomst is de warmtetoevoer vanaf de grond, en daarmee de convectieve productie van turbulentie, nog niet groot. Het is dan noodzakelijk om ook met mechanische productie van turbulentie rekening te houden. Wanneer we de bijdrage hiervan aan het neerwaarts warmtetransport evenredig stellen aan $A(u_*^3/h)(T/g)$, met een evenredigheidsconstante $A = 5$, en deze optellen bij de hierboven genoemde convectieve bijdrage, dan wordt gemiddeld over alle gevallen de opgetreden menghoogte voor 95% goed berekend. De resterende sprei-

ding is ongeveer even groot als de geschatte fouten in de waarnemingen.
- Alle verdere complicaties van het "entrainment"-model leiden tot resultaten die niet significant beter zijn.
- Wanneer we het effect van vocht op de dichtheid in rekening brengen, veranderen de resultaten niet sterk, behalve wanneer de lucht boven de menglaag slechts zwak stabiel is. Dan kan dit effect tot aanzienlijke vergroting van de berekende waarde van h leiden. De overeenstemming met de waarnemingen was dan echter niet goed. De oorzaak hiervan is de onnauwkeurigheid in de meting van vochtigheid met de radiosondes.

We hebben ook de gemiddelde berekende en gemeten waarden van de potentiële temperatuur, vochtigheid en wind in de menglaag vergeleken.
De conclusies zijn:
- De potentiële temperatuur in de menglaag is niet gevoelig voor het gebruikte "entrainment"-model. Hij hangt sterker af van de warmteflux vanaf de grond en van de stabiliteit van de lucht boven de menglaag. De waargenomen temperatuurstijging werd berekend met een resterende standaarddeviatie van $\pm$ 0.5 ^{o}C.
- De vochtigheid werd redelijk goed berekend, op een paar gevallen na. Ook hier geldt dat de externe factoren belangrijker zijn dan het gebruikte model.
- De wind in de menglaag werd slecht voorspeld. Oorzaak hiervan is het feit dat de vergelijkingen oplossingen toelaten in de vorm van inertiaaloscillaties met een amplitude die afhangt van de geostrofische wind, de beginvoorwaarden, de wrijving en de menghoogte zelf. De demping van deze oscillaties is zwak, zodat onnauwkeurigheden in een van deze gegevens een langdurig effect hebben.

Abstract

The evolution of the mixed layer during a clear day can be described with a slab model. The model equations have to be closed by a parameterization of the turbulent kinetic energy budget. Several possibilities for this parameterization are investigated.

For an intermediate range of Richardson numbers (Ri_*) the differences between the parameterizations are minimal. For low values of Ri_* an extra term has to keep the entrainment rate finite. The inclusion of an additional dissipation term is not an adequate remedy for the problems that arise at large values of Ri_*.

In order to assess the practical applicability of these models for the atmosphere, field experiments were carried out on ten clear days in 1977 and 1978. Within the accuracy of the measurements the mixed-layer height in fully convective conditions (at noon) is well predicted by taking a constant heat flux ratio: $-\overline{\theta'w'}_h = +0.2\ \overline{\theta'w'}_o$.

In the early morning hours mechanical entrainment is also important. Good results are obtained by taking: $-\overline{\theta'w'}_h = +0.2\ \overline{\theta'w'}_o + 5\ u_*^3\ T/gh$.

A sensitivity analysis of the model solutions shows that only large differences in the values of the constants lead to significantly different results. Further complications in the entrainment model do not lead to substantial improvement.

The mean potential temperature in the mixed layer is reproduced within $\pm$ 0.5 ^{o}C. The mean humidity is less well predicted. Both are rather insensitive to the choice of a particular entrainment formulation.

The results for the mixed-layer wind are poor. Errors in the initial conditions and forcing functions cause spurious oscillations of the wind vector in the models.

1. INTRODUCTION

1.1. Statement of the problem.

This study deals with the unsteady behavior of the atmospheric boundary layer in the morning hours of a clear day. After sunrise the stably stratified boundary layer which has been formed during the night is being heated from below. Turbulence is produced by convective and mechanical mixing. In a layer near the ground this turbulence is capable of overcoming the stable stratification and to form a mixed layer in which many properties tend to be distributed in a vertically homogeneous way. Due to the sustained production of turbulence and to the continuing heat input this mixed layer grows into the stable layer aloft and entrains air from above which has other properties than the mixed layer itself (other temperature, other humidity, other pollutant concentrations). The depth as well as the properties of the mixed layer will continuously change in time.

It is the purpose of a mixed-layer model to predict this time dependence as a function of initial and boundary conditions. Such a mixed-layer model has to parameterize the amount of turbulent kinetic energy that is available for entrainment. For this parameterization several assumptions have to be made. Depending on the sophistication of these assumptions and on the processes involved, mixed-layer models of varying complexity may be constructed. It is our purpose to establish the applicability of these models to atmospheric conditions and to investigate what sophistication is needed in order to describe realistically the mixed-layer behavior in the atmosphere on a clear day. For this purpose we carried out a large number of field experiments.

1.2. Relevance of the study.

The atmospheric boundary layer is the region where the atmosphere interacts with the earth's surface. Due to the influence of the properties of the free atmospheric flow aloft and to the influence of the surface itself, the state of the boundary layer may change continuously. In this study we are concerned with situations in which the free atmosphere is quasi-steady on the time scale of a day. We are further dealing with situations in which the incoming radiation at the surface is not severely influenced by cloudiness. Then the boundary layer will be mainly governed by the surface characteristics and by the daily cycle in radiation. In this study we are mainly interested in the daytime part of this cycle.

Turbulence and associated vertical mixing is generally confined to the boundary layer. In case of a mixed layer that is sustained by vigorous turbulence production and capped by a stable non-turbulent region aloft, all conservative variables within the mixed layer are to a large extent distributed homogeneously in the vertical direction. Anything that is entrained from above or injected from below will be fully mixed after a short time.

When, for example, a stack releases polluting material in the stable region, no pollution will be found at ground level. However, when after a certain time the mixed-layer height reaches the height of the stack and its plume, then suddenly the pollution is mixed over the whole depth of the mixed layer, and the concentrations at ground level increase.

Also, when considering the dispersion of pollutants that are released within the mixed layer, it can easily be seen that this process will be strongly influenced by the dynamics of the mixed layer itself.

The prediction of meteorological variables will also depend on the mixed-layer behavior. The maximum surface temperature reached on a sunny day is a well-known example. Also, the humidity and the wind at low levels are strongly influenced. When the mixed-layer depth reaches the condensation level, cumulus clouds are formed.

For all these problems it is of great importance to have insight in the dynamic behavior of the mixed layer.

1.3. Outline of the thesis.

We collected a large number of full-scale atmospheric measurements on the dynamics of the mixed layer. It is our purpose to compare the results of various models with this data set.

Therefore, first a critical review of mixed-layer models is required. Since a mixed layer may form not only in the atmospheric boundary layer, but also in the upper layer of the ocean, we will have to review both types of geophysical flow. Besides, several interesting laboratory experiments on this subject have been carried out, which are extensively used in establishing the model parameters.

Further, a description of the observation system and of the data set is required. Since it is by no means trivial to retrieve appropriate data from the actual observations, the procedure is presented in detail.

A comparison of the results of various mixed-layer model calculations with the data set tries to assess their value for atmospheric conditions. A test on the sensitivity of the models to their intrinsic parameters and to the initial and boundary conditions is carried out in order to investigate the variation between the models caused by typical measuring errors or the natural variability of atmospheric forcing.

2. GENERAL ANALYSIS OF THE PROBLEM

One of the most pronounced features of turbulent flow is its diffusive capability. In turbulent flow the diffusion of momentum, heat, and of passive contaminants, for example air pollution, is by several orders of magnitude faster than in laminar flow. Therefore mean gradients of any property will tend to smear out, except in regions where they are maintained by a boundary condition, in particular by the presence of a wall.

Another feature of turbulent flow is its behavior at a free boundary. At the interface of a turbulent flow with a non-turbulent environment, such as the upper edge of a wall-bounded shear flow or the edges of a jet, turbulent eddies will entrain originally non-turbulent fluid into the turbulent region. So turbulent flow at a free surface will tend to expand.

Both features, mixing and entrainment, play an important role in the description of the evolution of a turbulent flow. When turbulence is continuously supplied with kinetic energy, it will occupy the largest available volume and distribute all properties nearly homogeneously, as can be seen by the simple stirring of a cup of milk-powdered coffee.

There is however a property of the fluid which can have considerable effect on the process of mixing. That is the case when the fluid is stably stratified, i.e. when the density distribution is such that vertical accelerations are counteracted by buoyancy forces in the presence of a gravity field.

The effect of a stable density stratification on mixing and entrainment may be quite obvious from observations in nature. In case of a low-level atmospheric temperature inversion the visitor of an industrial area observes that the vertical mixing of pollutants is inhibited, keeping them concentrated near the ground. Another common example may be found at home. It is a well-known phenomenon that the warmest air is found at the top of a room, and the way in which the air is mixed is very important for our

comfort. The oceans are also usually stably stratified with the warmest water at the top. If wind blows over the sea surface and produces turbulence in the water, mixing can take place only over a limited depth.

The dynamical effect of stable stratification manifests itself through the buoyancy force, which acts as a restoring force whenever fluid is displaced vertically from its equilibrium position. In order to move a fluid parcel vertically over a small distance d in an environment with a potential density gradient $d\rho/dz$, the amount of work to be done is $\frac{1}{2} gd^2(-d\rho/dz)$, where g is the gravity acceleration. This amount of work has to be supplied by the agency producing the displacement. So for turbulent eddies acting in a stably stratified fluid, negative buoyancy acts as a sink for turbulent kinetic energy. If this loss exceeds the net production, the character of the flow can change drastically.

This effect of the stratification on the flow character is clearly demonstrated in the daily cycle of the atmospheric boundary layer over land under clear-sky conditions. During the night there is a net outgoing radiation from the surface, cooling the adjacent air. The density stratification becomes stable and turbulence can be maintained only in a shallow layer near the surface, where the wind shear is largest. The resulting nocturnal boundary-layer height is much shallower than it would have been in a neutrally buoyant atmosphere. In daytime the picture reverses. By convection from the heated surface, kinetic energy is continuously supplied to the turbulence. Part of this production of turbulent kinetic energy may be used to overcome the stable stratification, so that the boundary layer is able to intrude into the stable air aloft. In the unstable boundary layer itself turbulence is quite vigorous and is able to mix effectively. Vertical mixing is an adiabatic process and thus all properties that are conserved under this process will tend to be distributed in a vertically

homogeneous way. This concerns potential temperature (not the temperature itself), specific humidity, momentum, and passive contaminants. Large gradients are only found at the top of the mixed layer (and at the bottom). At the top, stable non-turbulent air is entrained at a rate which depends on the net available kinetic energy.

In order to illustrate the effect of mixing on the shape of the vertical density profile, we consider a flow with a constant potential density gradient $d\rho/dz$ and with a constant velocity gradient dU/dz. We mix this fluid over a vertical distance H (see Figure 2.1).

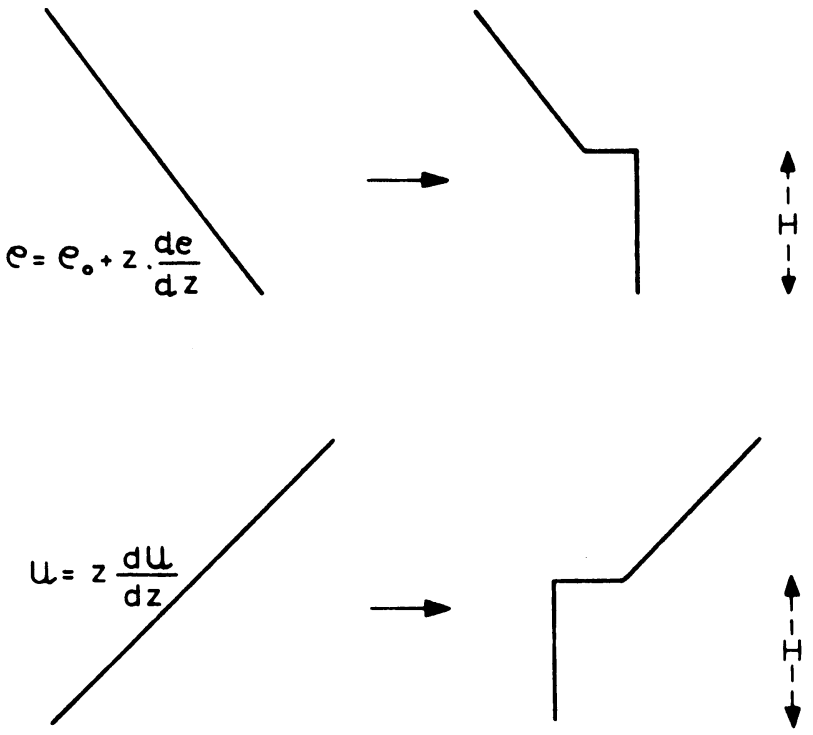

Figure 2.1. Profiles in a stably stratified flow before (left) and after (right) mixing over a distance H.

The potential energy $PE = \int_0^H gz\rho(z)dz$ changes due to the mixing with an amount

$$\Delta PE = -\frac{1}{12} \cdot g.H^3.(d\rho/dz).$$

The difference in the kinetic energy KE is

$$\Delta KE = -\frac{1}{24} \rho_o H^3.(dU/dz)^2,$$

where the Boussinesq approximation has been used ($H.d\rho/dz << \rho_o$). The ratio of the increase in potential energy and the release of kinetic energy is

$$\frac{\Delta PE}{\Delta KE} = 2 \cdot \frac{g}{\rho_o} \cdot \frac{-d\rho/dz}{(dU/dz)^2} = 2\ Ri,$$

where Ri is the Richardson number. If $Ri > \frac{1}{2}$ there is more energy required to mix the fluid than there is available in the velocity shear. Thus a layer for which $Ri > \frac{1}{2}$ can only be mixed and lead to non-uniform profiles as in Fig. 2.1 when there is an external source of turbulent kinetic energy. This is the case in a convective atmospheric boundary layer because of the continuous production of turbulence by convection from the surface.

When this external source of turbulent kinetic energy is strong enough to overcome the stable stratification, a layer with a small density gradient is formed, which is capped by a sharp interface with a much stronger density gradient than in the stable fluid above. There is ample evidence that in that case the vertical density profile has a structure as depicted in Fig. 2.2.

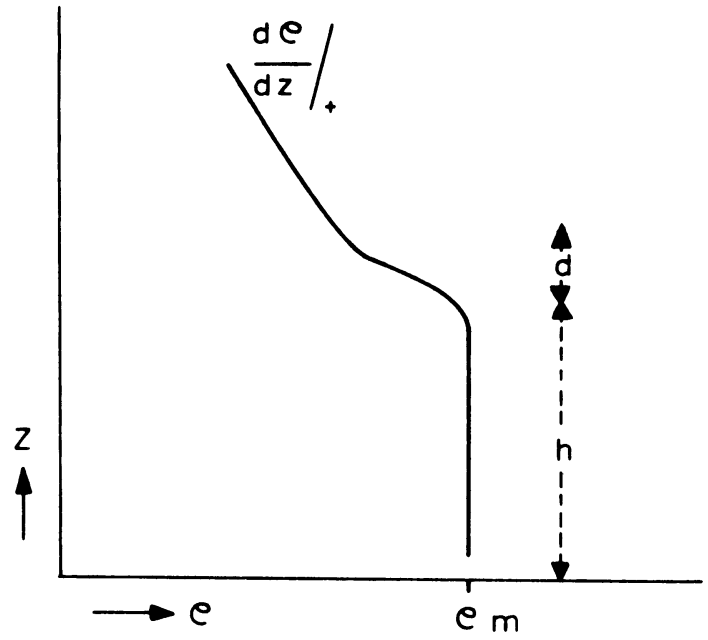

Figure 2.2. Distribution of mean potential density ρ *in a stratified flow with externally generated turbulence.*

A layer of thickness h is well mixed with representative density ρ_m. In a layer of thickness d turbulence is intruding into the stable, quiet layer above with density gradient $(d\rho/dz)_+$. The turbulence in the interfacial layer d is quite intermittent.

The state of affairs pictured in Fig. 2.2 has been confirmed for various types of flow. It was observed in laboratory experiments for mixed layers in a stratified water tank, either driven by convection from below (Willis and Deardorff, 1974; Heidt, 1977) or driven by a stress applied at the top surface (Kato and Phillips, 1969; Kantha, 1975; Kantha et al., 1977),

or driven by an oscillating grid at the surface (Turner, 1968, 1973; Crapper and Linden, 1974; Linden, 1975; Thompson and Turner, 1975; Wolanski and Brush, 1975).

The same profiles have also been observed in the upper layer of the ocean (see e.g. Kraus, 1977) and in the unstable atmospheric boundary layer (Clarke et al., 1971; Coulman, 1978a,b; Klöppel et al., 1978; Stilke et al., 1976; Yamamoto, 1977; Jensen and Lenschow, 1978, and others).

When there is a mechanism that continuously supplies kinetic energy to the turbulence in the mixed layer, its thickness h will tend to increase, and the mean potential density within the layer will change. The increase in h is a consequence of entrainment of originally non-turbulent air from the stable layer above, which is caught up in the mixed layer. This entrainment is caused by turbulent eddies which intrude into the stable layer. In a convective mixed layer these eddies may be identified as the convective plumes or billows with a length scale comparable to the mixed-layer height. Several interesting studies have been made on the details of the entrainment process, theoretically (Phillips, 1972; Manton, 1977, 1978; Mahrt, 1979) as well as experimentally (Rayment and Readings, 1974; Arnold and Rowland, 1976). From these studies the following qualitative conclusions about the entrainment process can be drawn:

a. Entrainment is a one-way process. It occurs only in one direction, into the non-turbulent region.
b. Large turbulent eddies, such as convective plumes or billows, act to distort the local interface between turbulent and non-turbulent air.
c. The actual entrainment of mass is caused by small-scale eddies at the edges of the large ones.
d. The local interface between turbulent and non-turbulent air is always very thin (a few meters), but there may be undulations which have a large amplitude (up to $\sim$ 100 m in the atmosphere).

The modeling of entrainment by considering the dynamics of individual turbulent eddies is quite illuminating when trying to understand the details of the entrainment process. However, we are interested in the entrainment rate on time- and space-scales which are large compared with those of individual penetrating elements. In that case it seems more suitable to consider all the turbulent eddies as deviations from a mean state and to try to model the overall net effect of them on the entrainment.

We will now review this type of entrainment modeling.

3. MIXED-LAYER MODELING

3.1. Turbulence production mechanisms.

In a stratified flow a mixed layer will be formed when enough energy is supplied to the turbulence. In geophysical flows the mechanisms for the generation of turbulent kinetic energy may be classified into the following types:

a. Mechanical production.
Mechanical production of turbulent kinetic energy occurs e.g. by the working of the wind at a water surface, resulting in breaking waves and wind shear in the upper water layer. In the atmosphere, wind shear in the surface layer is a well-known production mechanism. Turbulence may also be produced at the interface between turbulent and non-turbulent flow when there is a difference in mean wind speed between the mixed layer and the stable layer.

b. Convective production.
Convective production of turbulence in the atmosphere originates from a temperature difference between the surface and the air. In the ocean downward convection may be caused by evaporation from the surface and therefore increased salinity at the top, or by radiative cooling of the water surface. An interesting experiment was carried out by Farmer (1975) on downward convection of water below an iced surface. This downward convection is caused there by radiative absorption, which heats the water and therefore increases its density because the initial temperature is below 4 ^{o}C.

In real geophysical flows more than one of these production mechanisms are acting simultaneously. Their interaction is one of the fundamental problems of mixed-layer models (and of turbulence in general).

In laboratory flows it is possible to isolate one of these production mechanisms and to study its influence. The effect of a wind stress at the ocean surface was simulated by Kato and Phillips

(1969) and Kantha et al. (1977) in an annular water tank. The simulation of the effect of breaking waves may be carried out by an oscillating grid at the surface of a stratified fluid (see e.g. Turner, 1973; Linden, 1975). Convective mixed layers are simulated by heating the bottom of a stratified water tank (Deardorff et al., 1969; Willis and Deardorff, 1974; Heidt, 1977). The results of these experiments are extensively used in mixed-layer models. However, their interpretation may be complicated due to the effects of the side-walls of the experimental set-up (Thompson, 1979) or due to the ambiguity in the identification of the relevant production mechanism (Tennekes and Driedonks, 1981).

3.2. The conservation equations in general.

Every mixed-layer model has to originate from the general conservation equations for a turbulent flow. In order to proceed then, closure assumptions have to be made.

We will state here these general conservation equations. The following simplifying assumptions are made about the type of flow to be described:

- We treat the equations in one-dimensional form (vertical). No horizontal advection terms are included. However, since local vertical gradients may be very large, we retain a mean vertical advection velocity $\overline{w}$ (subsidence).
- No effects of condensation and cloud formation are taken into account.
- Molecular transport is neglected.

With these assumptions the set of conservation equations for the mean flow reads in the Boussinesq approximation (see e.g. Monin and Yaglom, 1971, ch.3; Busch, 1973; Kraus, 1977):

a. The equations for the mean horizontal momentum,

$$\frac{\partial \underset{\sim}{\overline{U}}_H}{\partial t} + \overline{w}\,\frac{\partial \underset{\sim}{\overline{U}}_H}{\partial z} = -\frac{1}{\rho_o}\,\underset{\sim}{\nabla}_H \cdot p - f\,\underset{\sim}{\eta} \times \underset{\sim}{\overline{U}}_H + \frac{\partial}{\partial z}\,\frac{\underset{\sim}{\tau}_H}{\rho_o} \,. \qquad (3.1)$$

b. The continuity equation,

$$\underset{\sim}{\nabla}_H \cdot \underset{\sim}{\bar{U}}_H = 0. \tag{3.2}$$

c. The conservation of energy,

$$\rho_o c_p \frac{\partial \bar{\Theta}}{\partial t} + \frac{\partial}{\partial z} (\rho_o c_p \overline{w'\theta'}) + \rho_o c_p \bar{w} \frac{\partial \bar{\Theta}}{\partial z} = \rho_o c_p Q_T . \tag{3.3}$$

d. The species conservation equations (e.g. for salinity S or specific humidity q),

$$\frac{\partial \bar{C}}{\partial t} + \frac{\partial}{\partial z} (\overline{w'c'}) + \bar{w} \frac{\partial \bar{C}}{\partial z} = 0. \tag{3.4}$$

e. An equation of state, relating the state variables.
This equation of state is different for the atmosphere and for the ocean.

In the atmosphere the perfect gas law may be applied, also when moist air is considered. In that case the temperature has to be replaced by the virtual temperature $\tilde{T}_v = \tilde{T}(1 + 0.61\ \tilde{q})$ where the $\sim$ indicates a state variable. In the Boussinesq approximation this perfect gas law reduces to:

$$\frac{\rho}{\rho_o} = - \frac{\theta_v}{T_{vo}} . \tag{3.5}$$

where $\theta_v = \theta(1 + 0.61\ q) + 0.61\ q\ T_o$ and $T_{vo} = T_o$.
Here the index o denotes the reference state.

In the ocean the following expansion for ρ in terms of small deviations in temperature (θ) and salinity (S) from a reference state may be used:

$$\frac{\rho}{\rho_o} = - \alpha \, \theta + \beta \, S. \tag{3.6}$$

(Note the meaning of the variables in (3.1)-(3.6) from the list of symbols).

As will be clear from the general discussion on entrainment in stratified flow, an important role is played by the buoyancy, defined by

$$b = - \frac{g}{\rho_o} \rho. \tag{3.7}$$

From eqs. (3.3)-(3.6) an explicit equation for b can easily be derived. For the atmosphere and for the ocean it reads repectively:

$$\frac{\partial \bar{b}}{\partial t} + \frac{\partial}{\partial z} (\overline{w'b'}) + \bar{w} \frac{\partial \bar{b}}{\partial z} = + \frac{g}{T_o} Q_T \, , \tag{3.8a}$$

and

$$\frac{\partial \bar{b}}{\partial t} + \frac{\partial}{\partial z} (\overline{w'b'}) + \bar{w} \frac{\partial \bar{b}}{\partial z} = g \, \alpha \, Q_T. \tag{3.8b}$$

A central problem in entrainment in stratified flows is the transformation of kinetic energy of the turbulence into potential energy of the density stratification. Therefore we will have to inspect closely the equation for turbulent kinetic energy (TKE), which reads (Tennekes and Lumley, 1972):

$$\frac{\partial e}{\partial t} + \bar{w} \frac{\partial e}{\partial z} = \frac{1}{\rho_o} \underset{\sim}{\tau}_H \cdot \frac{\partial \underset{\sim}{U}_H}{\partial z} - \frac{g}{\rho_o} \overline{\rho' w'} - \frac{\partial}{\partial z} \left(\overline{ew'} + \frac{\overline{p'w'}}{\rho_o} \right) - \varepsilon, \tag{3.9}$$

where e is the turbulent kinetic energy per unit mass ($e = \frac{1}{2} (\overline{u'^2} + \overline{v'^2} + \overline{w'^2})$) and ε is the viscous dissipation. We will return to this TKE equation later.

A solution of the system of equations (3.1)-(3.6) cannot be achieved, because the number of unknowns is larger than the number of equations. Some assumptions have to be made in order to close the system.
These closure assumptions can be made in various ways. We will discuss them shortly.

- Gradient-transfer approach.
  The well-known gradient-transfer assumption amounts to the expression for the vertical turbulent transport of some variable a in the form:

$$\overline{a'w'} = -K_a \frac{\partial \bar{a}}{\partial z} ,$$

  where K_a is the turbulent eddy viscosity, which depends on the flow structure.
  This gradient-transfer approach was applied to the mixed-layer problem by some authors (Munk and Anderson, 1948; Pandolfo and Jacobs, 1972; Kraus, 1972; Mellor and Yamada, 1974; Mellor and Durbin, 1975). However, it was shown by Zeman (1975) that in a convective mixed layer gradient transfer is not applicable and may even lead to the wrong sign of the transport (see Fig. 3.1, page 16).
  It may therefore be argued that a gradient-transfer approach is not suitable to buoyancy-driven mixed-layers. We will not pursue this further.

- Second-order closure.
  A more complex class of closure techniques requires an extra set of equations for the turbulent transports themselves. In these equations new unknowns occur, which have to be modeled (see e.g. Zeman, 1975; Zeman and Lumley, 1976; Mellor and Yamada, 1975; Wyngaard et al., 1974; André et al., 1978; and many others). The results of these second-order closure models are quite impressive and they produce realistic results for the mean quantities and for the turbulent fluxes in the mixed

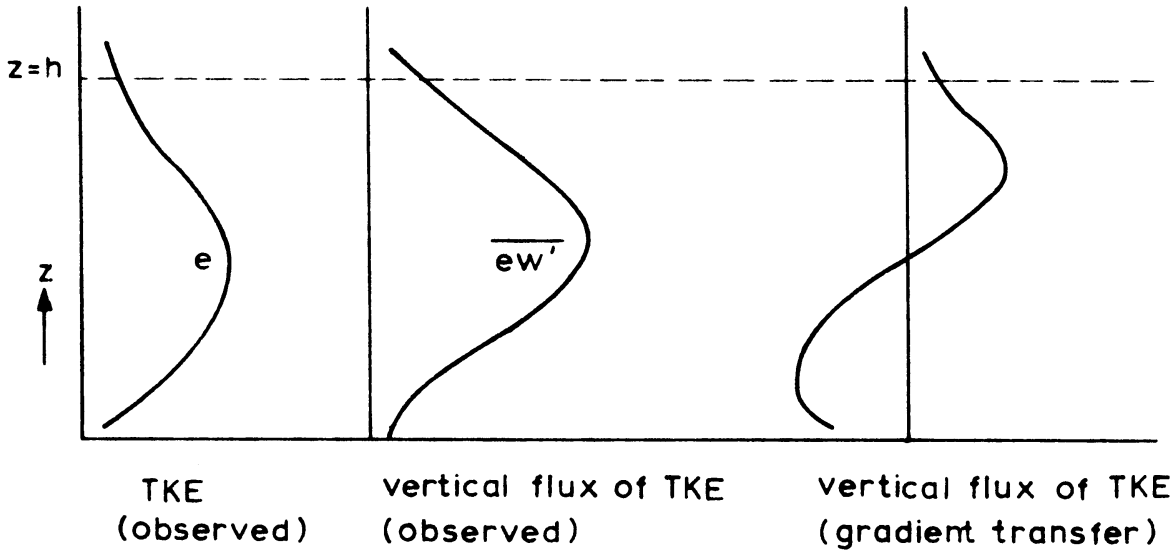

Figure 3.1. Observed profiles of TKE (e) and the flux of TKE $\overline{ew'}$ *and the profile of* $\overline{ew'}$ *according to gradient transfer.*

layer. However, these models require a large computational effort and the theoretical foundations are still subject to discussion. We will not pursue them further here, also because in our opinion full-scale experiments involve too many experimental uncertainties as to be able to test the assumptions of these second-order closure models accurately.

When applying the governing equations (3.1)-(3.6) to the problem of a mixed layer, which has a typical structure as shown in Fig. 2.2, it is possible to make use of observed properties of this mixed layer in order to develop slab models, which we discuss in the next section.

3.3. One-dimensional slab models.

It is well known that in a stratified fluid where turbulent mixing is quite vigorous, a typical structure as depicted in Fig. 2.2 will develop. A mixed layer is formed in which all conservative properties are to a large extent uniformly distributed and which is separated from the non-turbulent fluid by a relatively sharp interface. The mixed layer may be considered as a uniform slab (which means that e.g. the density flux profile is linear). On this basis many models have been developed, so called mixed-layer or bulk-layer models, which make use of the eqs. (3.1)-(3.6) in integrated form and which use several assumptions based on observations.

These mixed layer models use in general the following assumptions:

a. Within the bulk of the mixed layer vertical gradients of any conservative mean variable, such as potential temperature, potential density, salinity, or momentum, are small.
b. Compared to the height of the mixed layer the thickness of the interface between turbulent and non-turbulent fluid is small.
c. The thickness of the surface layer where sharp gradients may occur is small with respect to the thickness of the mixed layer.

On the basis of these assumptions and the situation of Fig. 2.2 an appealing simple model was constructed for which the basic ideas had first been developed by Ball (1960), Turner and Kraus (1967), Kraus and Turner (1967), and Lilly (1968). This model has been productively used and elaborated by Betts (1973), Carson (1973), Tennekes (1973, 1975), Zilitinkevich (1975), Stull (1976a,b), Deardorff (1973, 1974a,b), Mahrt and Lenschow (1976), Zeman (1975), Zeman and Tennekes (1977) for the mixed layer in the atmosphere, and by e.g. Pollard et al. (1973), Niiler (1975), Niiler and Kraus (1977), Garnich and Kitaigorodskii (1977, 1978) for the mixed layer in the ocean. Many other references can be cited, see Zilitinkevich (1979) or Tennekes and Driedonks (1980).

In this simple model the assumption b. listed above is used to replace the interface between turbulent and non-turbulent fluid by a jump discontinuity in the mean profiles. This jump model or zero-order discontinuity model is depicted in Fig. 3.2.

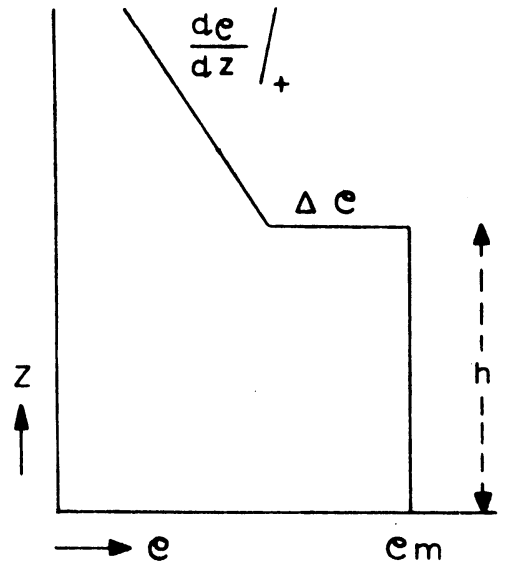

Figure 3.2. Characteristic vertical profile in a jump model for the mixed layer.

What are the consequences of the jump model for the governing equations?

From model assumption a. it follows that within the bulk of the mixed layer all flow variables that are conservative under adiabatic mixing may be characterized by a value independent of z. We will denote these values by the index m. Furthermore the values of the mean variables just above the mixed layer are denoted by an index +. The situation of the mixed layer at any time is then characterized by its height h and by Φ_m and $\Delta\Phi = \Phi_+ - \Phi_m$ for all flow variables Φ.

From eqs. (3.1)-(3.6) and (3.8) a set of equations for Φ_m and $\Delta\Phi$ may be derived. In order to do this, one must recognize the following mathematical identity:

$$\Phi_+ = \lim_{\varepsilon \downarrow 0} \Phi\,(t;\, x(t), y(t),\, h(x(t),y(t),t) + \varepsilon).$$

From this definition we can derive the following expression for the rate of change of Φ_+:

$$\frac{d\Phi_+}{dt} = \left(\frac{\partial\Phi}{\partial t}\right)_+ + \left(\underset{\sim}{U}_H \cdot \underset{\sim}{\nabla}_H \Phi\right)_+ + \left(\frac{\partial\Phi}{\partial z}\right)_+ \cdot \frac{dh}{dt}$$

$$= \left(\frac{d\Phi}{dt}\right)_+ + \left(\frac{\partial\Phi}{\partial z}\right)_+ \left(\frac{dh}{dt} - \overline{w}_h\right) . \qquad (3.10)$$

For Φ_m it is easy to see that:

$$\frac{d\Phi_m}{dt} = \left(\frac{d\Phi}{dt}\right)_m . \qquad (3.11)$$

Using (3.10) and (3.11), we can now easily derive equations for Φ_m and $\Delta\Phi = \Phi_+ - \Phi_m$ from eqs. (3.1)-(3.4) and (3.8), where Φ is $\overline{U}$, $\overline{V}$, $\overline{\Theta}$, $\overline{C}$, $\overline{b}$, respectively.

We then arrive at the following equations for U_m, V_m, Θ_m, C_m, b_m and their jumps at the mixed-layer top ΔU, ΔV, $\Delta\Theta$, ΔC and Δb.

(The pressure gradient is replaced by the in meteorological applications more common geostrophic wind, defined by: $U_g = -\frac{1}{f\rho}\frac{\partial p}{\partial y}$, $V_g = \frac{1}{f\rho}\frac{\partial p}{\partial x}$).

$$\frac{dU_m}{dt} = f(V_m - V_{gm}) + (\overline{u'w'}_o - \overline{u'w'}_h)/h \ , \tag{3.12}$$

$$\frac{dV_m}{dt} = -f(U_m - U_{gm}) + (\overline{v'w'}_o - \overline{v'w'}_h)/h \ , \tag{3.13}$$

$$\frac{d\Theta_m}{dt} = (\overline{\theta'w'}_o - \overline{\theta'w'}_h)/h + Q_T^m \ , \tag{3.14}$$

$$\frac{dC_m}{dt} = (\overline{c'w'}_o - \overline{c'w'}_h)/h \ , \tag{3.15}$$

$$\frac{db_m}{dt} = (\overline{b'w'}_o - \overline{b'w'}_h)/h + Q_b^m \ , \tag{3.16}$$

$$\frac{d\Delta U}{dt} = \left(\frac{\partial \bar{U}}{\partial z}\right)_+ \left(\frac{dh}{dt} - \bar{w}_h\right) - (\overline{u'w'}_o - \overline{u'w'}_h)/h + f\Delta V + fV_g\Delta\rho/\rho_o \ , \tag{3.17}$$

$$\frac{d\Delta V}{dt} = \left(\frac{\partial \bar{V}}{\partial z}\right)_+ \left(\frac{dh}{dt} - \bar{w}_h\right) - (\overline{v'w'}_o - \overline{v'w'}_h)/h - f\Delta U - fU_g\Delta\rho/\rho_o \ , \tag{3.18}$$

$$\frac{d\Delta\Theta}{dt} = \left(\frac{\partial \bar{\Theta}}{\partial z}\right)_+ \left(\frac{dh}{dt} - \bar{w}_h\right) - \frac{d\Theta_m}{dt} + Q_T^+ \ , \tag{3.19}$$

$$\frac{d\Delta C}{dt} = \left(\frac{\partial \bar{C}}{\partial z}\right) \left(\frac{dh}{dt} - \bar{w}_h\right) - \frac{dC_m}{dt} \ , \tag{3.20}$$

$$\frac{d\Delta b}{dt} = \left(\frac{\partial \bar{b}}{\partial z}\right)_+ \left(\frac{dh}{dt} - \bar{w}_h\right) - \frac{db_m}{dt} + Q_b^+ \ . \tag{3.21}$$

The values of U_{gm}, V_{gm} denote the average values of the geostrophic wind components within the mixed layer. The same holds for the source terms Q_T^m and Q_b^m (Q_b is given by the right hand side of (3.8)). In the atmosphere these source terms are small (see page 88). The last terms on the right of (3.17) and (3.18) are derived from terms $f(V_{gm}-V_g^+)$, and $f(U_{gm}-U_g^+)$ by recognition of pressure continuity across the interface. The wind components U_g and V_g in (3.17), (3.18) are average values of U_{gm} and U_g^+, respectively V_{gm} and V_g^+. These last terms are small.

The set of equations (3.12)-(3.21) constitutes 10 equations with 16 unknowns (including h). We assume the conditions at $z = 0$ and at $z > h$ to be known, as well as $\overline{w}_h$.

An important extra set of equations may be derived from the flux boundary conditions at $z = h$. For the fluxes $\overline{u'w'}_h$, $\overline{\theta'w'}_h$, $\overline{v'w'}_h$, $\overline{c'w'}_h$, $\overline{b'w'}_h$, equations can be derived by integrating eqs. (3.1), (3.3), (3.4) and (3.8) from $h-\varepsilon$ to $h+\varepsilon$, applying Leibniz's rule for the integrals and taking the limit for $\varepsilon \downarrow 0$ (Lilly, 1968).
The results are:

$$-\overline{u'w'}_h = \Delta U \left(\frac{dh}{dt} - \overline{w}_h \right), \tag{3.22}$$

$$-\overline{v'w'}_h = \Delta V \left(\frac{dh}{dt} - \overline{w}_h \right), \tag{3.23}$$

$$-\overline{\theta'w'}_h = \Delta\theta \left(\frac{dh}{dt} - \overline{w}_h \right), \tag{3.24}$$

$$-\overline{c'w'}_h = \Delta C \left(\frac{dh}{dt} - \overline{w}_h \right), \tag{3.25}$$

$$-\overline{b'w'}_h = \Delta b \left(\frac{dh}{dt} - \overline{w}_h \right). \tag{3.26}$$

The set of equations (3.12)-(3.26) now still contains one unknown in excess of the number of equations. In order to be able to solve the system we need an additional relation

between the unknowns and the boundary conditions.

As the process of entrainment is closely related to the energy that is made available from the turbulence to overcome the buoyancy forces, it is quite natural that the equation for turbulent kinetic energy is called for. The various terms in this equation have to be parameterized in order to get an extra equation for the energetics of the entrainment and to close the system of equations (3.12)-(3.26).

The parameterization of this budget of turbulent kinetic energy is the fundamental problem in entrainment prediction. We will discuss this in the next sections.

3.4. The turbulent kinetic energy budget.

The budget for turbulent kinetic energy (TKE) reads (Tennekes and Lumley, 1972):

$$\frac{de}{dt} = \frac{1}{\rho_o} \underset{\sim}{\tau}_H \cdot \frac{\partial \underset{\sim}{U}_H}{\partial z} + \overline{b'w'} - \frac{\partial}{\partial z}\left(ew' + \frac{p'w'}{\rho_o}\right) - \varepsilon. \qquad (3.27)$$

(T) (P) (B) (F) (D)

We first give a physical interpretation of the various terms in e.g. (3.27).

The term T = de/dt is the rate of change of TKE. We will consider situations that are horizontally homogeneous. However, we retain a mean vertical velocity, since it may be associated with large vertical gradients at z = h. So $T = \partial e/\partial t + \overline{w}\, \partial e/\partial z$.

The term $P = (\underset{\sim}{\tau}_H/\rho_o).(\partial \underset{\sim}{U}_H/\partial z)$ gives the mechanical production of TKE by the interaction of the stress with the mean vertical shear. In a mixed layer this term is zero

nearly everywhere. Only at the edges, where $\partial \underset{\sim}{U}_H/\partial z \neq 0$, it can contribute appreciably.

The term $B = \overline{b'w'}$ is the buoyant production (or destruction) of TKE. In a mixed layer it varies linearly between the surface and its top.

The term $F = -\frac{\partial}{\partial z}\left(\overline{ew'} + \frac{\overline{p'w'}}{\rho_o}\right)$ represents the divergence (or convergence) of turbulent transport of TKE and pressure fluctuations. This term deals with the redistribution of TKE by turbulent motion. In a convective mixed layer it is a very important term.

The last term $D = -\varepsilon$ is the dissipation rate of TKE into heat. In a fully developed turbulent flow this dissipation usually is very large and about equal to the TKE production.

In order to be able to solve the mixed-layer equations we have to derive from eq. (3.27) a relation between the unknown variables. Therefore all terms in (3.27) have to be parameterized and the constants involved must then follow from experiments.

The parameterization of eq. (3.27) has given rise to a huge amount of literature. Extensive records of references may be found in Tennekes and Driedonks (1981) and Zilitinkevich et al. (1979). The reasons for the difficulties in this parameterization must lie in the nature of a turbulent flow in general. It is well known that for most non-decaying turbulent flows the production rate of turbulent kinetic energy is about equal to the dissipation rate, i.e. kinetic energy is supplied to the large eddies, but about an equal amount is dissipated into heat on the very small scales (Tennekes and Lumley, 1972). For entraining turbulent flows then the complicating fact exists that the net amount of kinetic energy that is available for entrainment is only a very small fraction of the total kinetic energy that is produced within the bulk of the flow. By far the greatest part of this production is removed by dissipation. We thus have to realize that in scaling eq. (3.27) we are trying to estimate

a small term (the entrainment) as a difference between large terms (the bulk production and dissipation).

We illustrate this with a purely convective mixed layer in the atmosphere, without any other buoyancy effects than those caused by temperature, such that $\overline{b'w'} = \frac{g}{T_o} \overline{\theta'w'}$. In this layer the heat flux profile is linear, as given in Fig. 3.3.

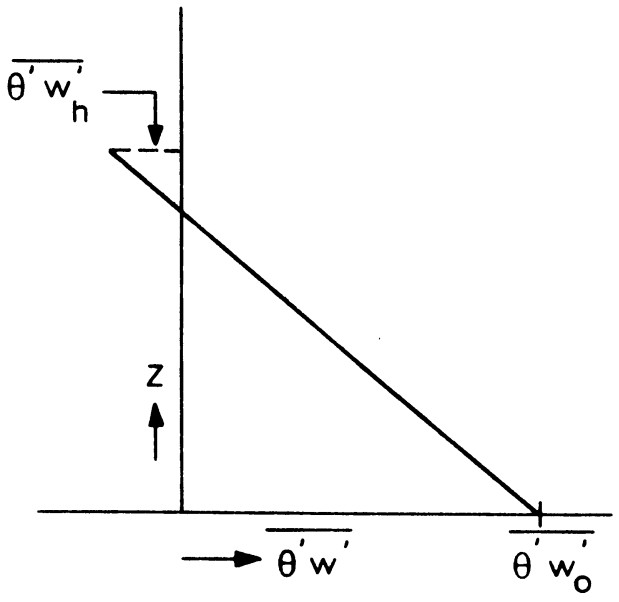

Figure 3.3. Heat flux profile in a convective mixed layer.

The ratio of the negative heat flux at the inversion base to the positive heat flux at the surface is $a_F = -\overline{\theta w}_h / \overline{\theta w}_o$. Now the ratio of the destruction of kinetic energy by buoyancy (the negative area in Fig. 3.3) to the production of kinetic energy by buoyancy (the positive area in Fig. 3.3) is equal to a_F^2.

A usual value is $c_F = 0.2$, so that only 4% of the total TKE-production is used to overcome the negative buoyancy at $z = h$. The rest is lost to dissipation.

In the parameterization of eq. (3.27) two main approaches can be taken. We may first integrate eq. (3.27) from $z = 0$ to $z = h$ and then try to assess the entrainment as the difference between bulk production and dissipation, or we may apply eq. (3.27) locally at the entrainment interface and estimate all the terms right there. The former approach is usually taken in oceanic models, the latter is often used in atmospheric models. These different ways to look at eq. (3.27) do not solve the problem in any substantial way; in integrated models the dissipation plays a central role, in local models the flux convergence is the most important term. We will now try to review both methods and to achieve conclusions on the usefulness of different entrainment models.

3.5. Parametric models based on the integrated kinetic energy budget.

From the model assumption that in the mixed layer all mean flow variables, that are conserved under vertical adiabatic mixing, are independent of z, it follows immediately that the profiles of the vertical fluxes of those quantities are linear. In particular this holds for the buoyancy flux $\overline{b'w'}$, which thus can be integrated over the mixed layer to give the rate of change of potential energy:

$$\int_0^h \overline{b'w'}\, dz = \tfrac{1}{2}\, h\, (\overline{b'w'}_o + \overline{b'w'}_h) \,. \qquad (3.28)$$

Upon integrating eq. (3.27) over the mixed layer from $z = 0$ to $z = h$, arranging the interfacial buoyancy flux to the left, we get:

$$- \tfrac{1}{2} h \overline{b'w'}_h = \int_0^h \frac{\tau_H}{\rho_o} \cdot \frac{\partial U_H}{\partial z} dz + \tfrac{1}{2} h \overline{b'w'}_o$$

I II III

$$- \left(\overline{ew'} + \frac{\overline{p'w'}}{\rho_o} \right)_h + \left(\overline{ew'} + \frac{\overline{p'w'}}{\rho_o} \right)_o$$

IV V

$$- \int_0^h \varepsilon \, dz - \int_0^h \frac{de}{dt} dz. \qquad (3.29)$$

VI VII

The right hand side of eq. (3.29) thus gives the net amount of vertically integrated TKE that is available per unit time to overcome the negative buoyancy at the inversion base.

A sequence of papers in which the various terms on the right hand side of (3.29) are parameterized started with Turner and Kraus (1967) and Kraus and Turner (1967). They applied (3.29) to the upper layer in the ocean, forced by a wind stress. In that case there is no buoyancy flux from the surface, so term III is zero. They furthermore neglected dissipation (term VI) and storage of TKE (term VII), as well as the energy flux at the entrainment interface (term IV). There results a balance between the entrainment flux (term I) and the mechanical production (term II) plus the flux of energy at the surface

(term V). They estimated II+V to be proportional to u_*^3 where u_* is the friction velocity near the surface.
Using these parameterizations there results from (3.29) and (3.26):

$$h\,\Delta b\left(\frac{dh}{dt} - \overline{w}_h\right) = A\,u_*^3 .$$

With $\overline{w}_h = 0$ there results:

$$\frac{1}{u_*}\,\frac{dh}{dt} = A\,\frac{u_*^2}{h\Delta b} = A\,.\,Ri_*^{-1}. \qquad (3.30)$$

This result was also found in the laboratory experiments of Kato and Phillips (1969). They concluded that the constant of proportionality in (3.30) was about 2.5. In analogous experiments, however, Kantha et al. (1977) later found a proportionality factor of 5, and at the same time showed that a simple relation like (3.30) is only approximately valid for a limited range of Ri_* ($90 < Ri_* < 400$).

In the case of a convectively-driven mixed layer, term II (mechanical production) is zero, and with the same assumptions on the other terms as those of Kraus and Turner (1967), we are left with a balance between the entrainment flux (I) and the buoyancy flux at the surface (term III) plus the kinetic energy flux from the surface (V):

$$-\tfrac{1}{2}\,h\,\overline{b'w'}_h = \tfrac{1}{2}\,h\,\overline{b'w'}_o + \left(\overline{ew'} + \frac{\overline{p'w'}}{\rho_o}\right)_o . \qquad (3.31)$$

When we define a convective velocity scale w_* as

$$w_*^3 = h\,.\,\overline{b'w'}_o , \qquad (3.32)$$

and furthermore parameterize the last term on the right-hand side of (3.31) to be proportional to w_*^3 (which is a reasonable assumption in convective conditions as shown by Mahrt and Lenschow (1976)), then (3.31) amounts to:

$$- \overline{b'w'}_h = c. \overline{b'w'}_o \ , \tag{3.33}$$

which is the same entrainment relation as proposed by Tennekes (1973) from a simplified local energy budget (to which we return later). With (3.26) (and $\overline{w}_h = 0$), (3.33) is equivalent to the convective counterpart of (3.30):

$$\frac{1}{w_*} \frac{dh}{dt} = c. \frac{w_*^2}{h.\Delta b} = c.Ri_*^{-1} \ . \tag{3.34}$$

In order to get from (3.29) entrainment relations of type (3.30) or (3.34), i.e. a Ri_*^{-1} dependence, it is in fact not necessary to neglect dissipation altogether. If we scale the total production of TKE on the cube of some turbulence velocity scale σ_w, i.e. on σ_w^3 (where $\sigma_w \equiv u_*$ in mechanically-driven mixed layers and $\sigma_w \equiv w_*$ in convectively-driven mixed layers), and if we scale the flux of TKE at the surface (term V) also on σ_w^3 and neglect for a moment terms IV and VII, then we are left with the balance:

$$- \tfrac{1}{2} h \overline{b'w'}_h = A \ . \ \sigma_w^3 - \int_0^h \varepsilon \, dz. \tag{3.35}$$

A Ri_*^{-1} relation for the non-dimensional entrainment rate may now be derived from (3.35) by taking the integral dissipation proportional to σ_w^3; this is related to an energy cascade (Tennekes and Lumley, 1972), in which the dissipation is proportional to the production.

This argument was generalized by Turner (1968), who stated that the rate of change of potential energy of the mixed layer (i.e.

terms I + III) is proportional to the surface input rate of TKE, i.e. $\sim u_*^3$. There is however no a priori justification for this assumption and further analysis of laboratory experiments (Kantha et al., 1977; Kato and Phillips, 1969) showed that it does not hold for very low and for very large Richardson numbers.
Also, in experiments in which mixing was not generated by applying a stress at the surface (as in the aforementioned experiments) but by the stirring of the fluid by means of an oscillating grid (Thompson and Turner, 1975), it was shown by Linden (1975) that this assumption is not correct. He demonstrated that the potential energy change of the mixed layer is proportional to the kinetic energy that is available at the entrainment interface, which is not simply proportional to the energy input by the oscillating grid at the surface.
In fact, in these experiments deviations of the Ri_*^{-1} dependence as given by (3.30) or (3.34) occurred, which are attributed to the fact that the parameterization of (3.29) as given above is not valid under all circumstances.

In order to get more general results, several attempts were made to model the various terms of the TKE-equation (3.29) in more detail.
Significant contributions to this parameterization were given by Niiler (1975), Resnyanski (1975), Kim (1976), de Szoeke and Rhines (1976), Niiler (1977), Niiler and Kraus (1977), Garwood (1977), Garnich and Kitaygorodskiy (1977 and 1978). These papers deal with the deepening of the upper mixed layer of the ocean. Slightly different but essentially the same type of modeling was applied to the convective atmospheric boundary layer by Stull (1976 a,b), Mahrt and Lenschow (1976), and by Kitaygorodskiy and Kozhelupava (1978).

First we consider term II, the integral mechanical production in the mixed layer. Since the velocity will be well mixed within the bulk of the layer (one of the model assumptions), contributions to this term can come only from the region near the surface and

from the region near the interface where a velocity jump $\Delta\underset{\sim}{U}$ is allowed.
If we consider these separate contributions we obtain:

$$II = II_{\delta} + II_{h} \,,$$

where

$$II_{\delta} = \int_{o}^{\delta} \underset{\sim}{\tau}_{H} \cdot \frac{\partial \underset{\sim}{U}_{H}}{\partial z} \, dz \approx u_{*}^{2} \, (u_{\delta} - u_{o}) \sim u_{*}^{3} \,,$$

$$II_{h} = \int_{h}^{h+\varepsilon} \underset{\sim}{\tau}_{H} \cdot \frac{\partial \underset{\sim}{U}_{H}}{\partial z} \, dz \approx \underset{\sim}{\tau}_{h} \cdot \Delta\underset{\sim}{U} \sim |\Delta\underset{\sim}{U}|^{2} \left(\frac{dh}{dt} - \overline{w}_{h} \right) . \qquad (3.36)$$

(Niiler, 1975; Niiler and Kraus, 1977; Garnich and Kitaygorodskiy, 1977 and 1978).
The scaling of this mechanical production term is unlikely to depend explicitly on a convective velocity scale w_{*}, but scales only on u_{*} and $|\Delta\underset{\sim}{U}|$.

The role of the wind shear at the interface (i.e. the term $II_{h} \sim |\Delta U|^{2} \, (dh/dt - \overline{w}_{h})$ was explicitly investigated by Pollard et al. (1973), for a situation in which the acceleration of the mixed layer in the ocean by the wind is important. They considered situations in which there is no buoyancy flux at the surface ($\overline{b'w'}_{o} = 0$) and furthermore stated that the work of the wind stress at the surface mainly generates inertial motions within the mixed layer and that the stirring of the surface by the wind and transport of turbulent kinetic energy from the surface to the entrainment interface is less important. They thus neglected all terms in the energy equation (3.29) that are associated with the generation of turbulence at the surface (term II_{δ}) or with turbulent transports (terms IV and V) or with dissipation or instationarity

(terms VI and VII). What is left is a balance between the interfacial buoyancy flux and the energy generated by the difference in momentum (terms I and II_h), i.e.

$$-\tfrac{1}{2}\, h\, \overline{b'w'}_h \sim |\Delta \underset{\sim}{U}|^2 \left(\frac{dh}{dt} - w_h\right).$$

Realizing that $-\overline{b'w'}_h = \Delta b\ (dh/dt - \bar{w}_h)$ their result is that entrainment is governed by:

$$Ri_b = \frac{\Delta b.h}{|\Delta \underset{\sim}{U}|^2} = \text{constant}. \qquad (3.37)$$

This simple result states that for wind-driven flows the mixed-layer depth h and the mean momentum difference adjust always in such a way that the bulk Richardson number remains constant. Later it was shown by Price (1979) and Thompson (1979) that a reinterpretation of the laboratory experiments of Kato and Phillips (1969) and Kantha et al. (1977) confirms that in accelerating flows entrainment is governed by a relation of type (3.37). Thus it is quite clear now that the entrainment mechanism as proposed by Pollard et al. (1973) is important when sudden wind changes over the ocean occur and that a term of type $II_h = |\Delta \underset{\sim}{U}|^2\ dh/dt$ must be taken into account in a parameterization of the turbulent kinetic energy budget.

From other studies (Denman, 1973; Denman and Miyake, 1973; de Szoeke and Rhines, 1976) it is also clear that this mechanism is only part of the story in oceanic mixing. In reality sudden accelerations do not occur very frequently and in most cases the turbulent kinetic energy fluxes do make an important contribution to the supply of kinetic energy for mixing. Therefore, general entrainment models should also include terms like $II_\delta \sim u_*^3$. We also

have to look at the other terms of (3.29). These include the energy flux at the interface ($[\overline{ew'} + \overline{p'w'}/\rho_o]_h$, term IV), the energy flux at the surface ($[\overline{ew'} + \overline{p'w'}/\rho_o]_o$, term V), the dissipation (term VI) and the instationarity (term VII).

The energy flux at the surface ($[\overline{ew'} + \overline{p'w'}/\rho_o]_o$, term V) is a production term, associated with the rate of work done by pressure perturbations over the waves at the ocean surface and with the direct input of turbulent kinetic energy by breaking waves. This production is in general scaled as u_*^3 (Niiler and Kraus, 1977). In convective conditions this energy input is negligibly small (Mahrt and Lenschow, 1976).

The energy flux at the interface ($[\overline{ew'} + \overline{p'w'}/\rho_o]_h$, term V) and the instationarity ($\int_o^h de/dt\, dz$, term VII) represent relatively small losses (Zilitinkevich, 1979), associated with the energy that is needed to spin up the initially quiet entrained fluid to the turbulence level of the mixed layer. This energy is of the order of $\sigma_w^2\, dh/dt$ (Niiler and Kraus, 1977; Zilitinkevich, 1979). Also, in term V the energy losses are represented which are due to the generation of internal waves that propagate away from the interface into the quiet, stably stratified fluid. This expenditure of kinetic energy is neglected by most authors.

The parameterization of the terms discussed so far amounts to:

$$\int_o^h \underset{\sim}{\tau}_H \cdot \frac{\partial \underset{\sim}{U}_H}{\partial z}\, dz - [\overline{ew'} + \overline{p'w'}/\rho_o]_h + [\overline{ew'} + \overline{p'w'}/\rho_o]_o$$

$$- \int_o^h \frac{de}{dt}\, dz = A_1 u_*^3 + A_2 |\Delta \underset{\sim}{U}|^2 \left(\frac{dh}{dt} - \bar{w}_h\right) + A_3 \sigma_w^2 \left(\frac{dh}{dt} - \bar{w}_h\right), \quad (3.38)$$

(Niiler and Kraus, 1977; de Szoeke and Rhines, 1976; Garnich and Kitaygorodskiy, 1977 and 1978; Zilitinkevich, 1979). Here A_1-A_3 are adjustable constants.

The most controversial term in the parameterization of the turbulent kinetic energy budget in integrated form is the integral dissipation rate, $\int_o^h \varepsilon \, dz$, term VI in eq. (3.29). Since it is well known that in turbulent flows by far the largest part of the energy that is produced is also dissipated into heat, this integral dissipation will surely be a very large term. In fully developed turbulent flow there is an energy cascade transferring energy from large eddies with length-scale h down to the viscous scale where the dissipation takes place. In that case the integral dissipation may be estimated as σ_w^3 (Tennekes and Lumley, 1972), where σ_w is a turbulent velocity scale. It is not obvious however that this parameterization is correct here, since the mean shear in the mixed layer is small, and the stirring is effectively done only in small regions near the surface and near the interface. Besides, there is also energy produced by the buoyancy flux. It is assumed by most authors that the integral dissipation is composed of terms which are individually proportional to the various turbulence generating processes, i.e.

$$\int_o^h \varepsilon \, dz = \alpha_1 u_*^3 + \alpha_2 |\Delta \underset{\sim}{U}|^2 \left(\frac{dh}{dt} - \overline{w}_h \right) + \alpha_3 . (h . \overline{b'w'}_o) \, , \qquad (3.39)$$

where α_1-α_3 are adjustable constants and $h.\overline{b'w'}_o = w_*^3$ (Niiler and Kraus, 1977).

Garnich and Kitaygorodskiy (1977, 1978) argue that α_1-α_3 are not constants but that they depend on the Richardson number Ri_*. The functional form of this dependence and the values of some new constants are derived by using the results of the laboratory experiments of Turner (1973), Kato and Phillips (1969) and Kantha et al (1977). The results of the latter two experiments, however, are still subject of discussion (Price, 1979; Thompson, 1979). Especially, concerns have been voiced whether the limited size of the experimental apparatus influences the measurements. Therefore it seems a bit premature to

elaborate eq. (3.39) further at the moment. It is clear that more laboratory experiments are needed to settle these questions.

From the foregoing survey of the modeling of the integral form of the TKE budget (3.29) it will be clear that it is very difficult to give parameterizations which are generally valid when several turbulent production mechanisms are acting simultaneously. There is a range of proposed parameterizations and it is sure that during the development of an entraining flow different regimes exist in which one term is more important than the others (de Szoeke and Rhines, 1976). As a summary of the parameterizations of the various terms in (3.29) we now write it in the total form:

$$- h \overline{b'w'}_h = B_1 u_*^3 + B_2 |\Delta U|^2 \left(\frac{dh}{dt} - \overline{w}_h \right) + B_3 w_*^3 + B_4 \sigma_w^2 \left(\frac{dh}{dt} - \overline{w}_h \right), \tag{3.40}$$

where B_1-B_4 are experimental factors (which may turn out to be functions of non-dimensional flow variables), and σ_w is a characteristic turbulent velocity scale which is a combination of w_* and u_* (we return to this later).

The values of B_1-B_4 are as yet not well determined from experiments. For our purpose of using (3.40) for the atmosphere in convective situations, it seems best to start from the following values:

$$\begin{aligned} B_1 &= 2.5 \quad \text{(Kato and Phillips, 1969) or} \\ &\quad\ 5 \quad \text{(Kantha et al., 1977)} \\ B_2 &= 0.7 \quad \text{(Price et al., 1978)} \\ B_3 &= 0.2 \quad \text{(Tennekes, 1973)} \\ B_4 &= 1.5 \quad \text{(see later in this study).} \end{aligned} \tag{3.41}$$

In this section we have been concerned with the parameterization of the turbulent kinetic energy budget in integrated form (from z = 0 to z = h). Now we will look closer at the local form of the energy budget at the inversion base.

3.6. Parametric models based on the kinetic energy budget at the entrainment interface.

As we have seen in the foregoing section, the parameterization of the integrated turbulent kinetic energy equation is very difficult because of the important role of the integral dissipation. It is not easy to parameterize a small difference between large terms (production and dissipation).

At the edges of an entraining turbulent flow, however, it is known that the local dissipation is a relatively small term (Tennekes and Lumley, 1972). That means that in the local energy budget, applied at the mixed layer height h, dissipation is not very important. Therefore an investigation of the local form of the TKE budget was started by Tennekes (1973).

We once again give this TKE budget, now applied at z = h:

$$\left(\frac{de}{dt}\right)_h = \frac{1}{\rho_o}\left(\underset{\sim}{\tau}_H \cdot \frac{\partial \underset{\sim}{U}_H}{\partial z}\right)_h + \overline{b'w'}_h - \frac{\partial}{\partial z}\left(\overline{ew'} + \overline{p'w'}/\rho_o\right)\Big|_h - \epsilon_h \qquad (3.42)$$

$$T_h \qquad P_h \qquad B_h \qquad F_h \qquad D_h$$

The physical interpretation of the various terms in (3.42) is already given in section 3.4 in a general way. In applying (3.42) at z = h we are able to extract some more information about these terms.

The term T_h always represents a loss, since at level z = h turbulent kinetic energy has to be spent on the spinning up of entrained non-turbulent fluid to the level of turbulence in the mixed layer.

The term P_h is positive (or zero) and gives the mechanically produced TKE at the interface.

The term B_h is always negative, since at height h fluid is transported against the buoyancy force.

The term F_h is generally positive. Turbulent kinetic energy is transported from the bulk of the mixed layer towards the interface. The flux convergence is an important term in the local energy budget (in the integrated form it is only present as a boundary condition). When we consider cases with $P_h = 0$, i.e. only convective mixing, then it is the only term in (3.42) which is positive!

The term D_h is the dissipation rate and therefore always negative. It is in most cases not a very large term.

The elaboration of the parameterization of the various terms in (3.42) started with Tennekes (1973) and grew more complex with the work of Zilitinkevich (1975), Tennekes (1975), Zeman (1975), and Zeman and Tennekes (1977). These authors are mainly concerned with a convective atmospheric boundary layer. Most of the arguments, however, have been extended to cases where mechanical mixing is also important.

Tennekes (1973) proposed a drastically simplified form of (3.42). He considered situations in which T_h is small (as is usually the case). Furthermore he considered situations without wind shear at the interface, i.e. $P_h = 0$, and he argued the dissipation rate D_h to be small at the outer edge of an entraining turbulent flow. (More generally, he assumed that mechanical energy produced at the interface is locally dissipated, i.e. $P_h = D_h$).
These assumptions reduce (3.42) to:

$$B_h + F_h = 0. \tag{3.43}$$

He furthermore stated F_h to be proportional to σ_w^3/h,

$$F_h = c_F \sigma_w^3/h, \tag{3.44}$$

where σ_w is the relevant turbulent velocity scale in the mixed layer. Then, with (3.26), (3.43) can be written as:

$$\frac{1}{\sigma_w}\left(\frac{dh}{dt} - \overline{w}_h\right) = c_F \frac{\sigma_w^2}{h\Delta b} = c_F \, Ri_*^{-1}. \tag{3.45}$$

In a mixed layer, which is dominated by convection from the surface, σ_w is proportional to w_* (defined by (3.32)). In that case, (3.43) and (3.44) amount to:

$$\overline{b'w'}_h = - c_F \, \overline{b'w'}_o \; (= - c_F \, w_*^3/h), \tag{3.46}$$

which in a dry convective atmospheric boundary layer reduces to:

$$- \overline{\theta'w'}_h = c_F \, \overline{\theta'w'}_o \quad \left(= c_F \frac{w_*^3 T_o}{gh}\right), \tag{3.47}$$

i.e. the downward heat flux at the inversion base is proportional to the upward heat flux at the surface. This proportionality is postulated or derived by a considerable list of authors (Ball, 1960; Lilly, 1968; Carson, 1973; Betts, 1973; Tennekes, 1973; Stull, 1976a,b). The value of the coefficient c_F varies between 0 and 1. Stull (1976b) summarizes all available experimental results and gives $c_F = 0.2$ as an optimum value. The wide range of reported values of c_F indicates that the assumptions leading to (3.46) are not always correct and that good experimental results are difficult to obtain.

When turbulence is maintained primarily by shear production in the surface layer, then the relevant velocity scale for σ_w is u_*. In that case, (3.43) and (3.44) lead for a dry atmospheric boundary layer to

$$- \overline{\theta'w'}_h = A \frac{u_*^3 T_o}{g\, h} . \tag{3.48}$$

If $\overline{w}_h = 0$, this can be written as:

$$\frac{1}{u_*} \frac{dh}{dt} = A\, Ri_*^{-1} . \tag{3.49}$$

This is the same relation as (3.30), which was derived from a simplified integrated TKE budget. As we have seen, Kato and Phillips (1969) and Kantha et al. (1977) gave experimental values of $A = 2.5$ and $A \approx 5$ respectively for a range of intermediate Richardson numbers.

In cases where both convective and mechanical production of turbulence is important, σ_w has to be an appropriate combination of w_* and u_*, incorporating the correct limits (3.47) and (3.48). This means that σ_w should reduce to w_* in convective conditions and that σ_w must be proportional to u_* in mechanically driven mixed layers. Tennekes (1973) suggested that the fluxes of convective and mechanical energy should be additive:

$$\sigma_w^3 = w_*^3 + (A/c_F)\, u_*^3 . \tag{3.50}$$

This results in a parameterization of the energy budget in the form

$$- \overline{\theta'w'}_h = c_F \overline{\theta'w'}_o + A \frac{u_*^3 T_o}{g\, h} , \tag{3.51}$$

for a dry atmospheric boundary layer. This form is equivalent to

the parameteriztion of the integrated energy budget (3.40), when we omit there the second and fourth term on the right hand side.

Although the simplified energy budget (3.43) is attractive and often works quite well, it is not generally valid since it cannot deal with some limiting cases. When we consider $\gamma_b = \left(\frac{db}{dz}\right)_+ = 0$ and $\Delta b \to 0$ (the latter surely occurs when the boundary layer is heated), then the buoyancy flux at the inversion base must reduce to zero, while dh/dt must remain finite, since a turbulent boundary layer can grow into a neutral environment obviously only at a finite speed. However, due to (3.43) and (3.44), B_h is independent of either Δb or γ_b and so $dh/dt \to \infty$ as $\Delta b \to 0$, $\gamma_b = 0$, which is unrealistic. This inconsistency was pointed out by Zilitinkevich (1975), who attributed it to the removal of term T_h. He argued that in cases where Δb and γ_b are small, the amount of TKE which is needed to spin up the entrained, non-turbulent, fluid to the level of turbulence in the mixed layer, cannot be neglected with respect to the energy spent on buoyancy destruction ($\overline{b'w'}_h$), as was done in (3.43). He proposed a more general form of the energy budget:

$$T_h = B_h + F_h. \tag{3.52}$$

The term F_h may still be parameterized according to (3.44), but an estimate for T_h has to be obtained in a different way. We assume that in a coordinate system that rises with the mixed layer h, the energy does not change with time, i.e. $\frac{d}{dt} e(h(t)) = 0$. Since

$$\frac{d}{dt} e(h(t)) = \frac{de}{dt}\Big/_{z=h} + \frac{\partial e}{\partial z}\Big/_{z=h} \cdot \left(\frac{dh}{dt} - \overline{w}_h\right), \text{ this gives:}$$

$$T_h = \frac{de}{dt}\Big/_{z=h} = -\frac{\partial e}{\partial z}\Big/_{z=h} \cdot \left(\frac{dh}{dt} - \bar{w}_h\right). \tag{3.53}$$

The profile of TKE in a convective mixed layer has a shape as given in Fig. 3.1. We parameterize $(\partial e/\partial z)_h$ as being proportional to $-\sigma_w^2/h$, where σ_w is a characteristic turbulent velocity scale in the bulk of the mixed layer. The term T_h thus is parameterized as:

$$T_h = c_T \frac{\sigma_w^2}{h} \left(\frac{dh}{dt} - \bar{w}_h\right), \tag{3.54}$$

where c_T is a proportionality factor.
With (3.44) and (3.54) we can write (3.52) as

$$-\overline{b'w'}_h = c_F \sigma_w^3/h - c_T(\sigma_w^2/h)\ (dh/dt - \bar{w}_h). \tag{3.55}$$

Rearranging terms in (3.55) and using (3.26), we get the Tennekes/Zilitinkevich entrainment relation:

$$\frac{dh}{dt} - \bar{w}_h = \frac{c_F \sigma_w}{Ri_* + c_T}. \tag{3.56}$$

Comparing this with (3.45), we see that both entrainment relations are the same for $Ri_* >> c_T$. The reason for including the term T_h becomes clear for $Ri_* << c_T$. In contrast to (3.45), the entrainment rate remains finite for $Ri_* \to 0$, and is bounded by

$$\lim_{Ri_* \to 0} \left(\frac{dh}{dt} - \bar{w}_h\right) = \frac{c_F}{c_T} \sigma_w. \tag{3.57}$$

The values of c_F and c_T must follow from experiments. The value of c_F has already been fixed at 0.2 as a best value from experiments in which c_T presumably does not play an important role (Stull, 1976b; Willis and Deardorff, 1974). The value of c_T

must then follow from experiments with $\gamma_b = 0$ and small Ri_*. For convective situations such experiments are not available, but Deardorff (1974a) found from computer simulations that

$$\lim_{\substack{Ri_* \to 0 \\ u_* = 0}} \left(\frac{dh}{dt} - \overline{w}_h \right) \approx 0.2\, w_* \,. \tag{3.58}$$

For the growth of a mechanically driven boundary layer which entrains into a neutral environment (and with $Ri_* = 0$), experimental results indicate (Tennekes and Lumley, 1972) that

$$\frac{dh}{dt} - \overline{w}_h \approx 0.3\, u_* \,. \tag{3.59}$$

In order to determine c_T from (3.57)-(3.59) we now have to establish a relation between σ_w and w_* and u_*.

We want to emphasize here that σ_w is not so much the really measured vertical variance but must be regarded as the scaling velocity for turbulent fluctuations in the bulk of the mixed layer. Proportionality factors may always be absorbed by c_F or c_T. This point was not always clearly realized by Zilitinkevich (1975), Tennekes (1975), André et al. (1978), for which reason they mixed up a number of experimental data on σ_w from different experiments. This led to a variety of proposed values for c_F and c_T, which in our opinion should not be used in the context of this parameterization. We prefer to define the scaling velocity σ_w by the interpolation formula (3.50): $\sigma_w^3 = w_*^3 + (A/c_F)u_*^3$. For convective situations $\sigma_w = w_*$, for mechanically forced situations $\sigma_w = (A/c_F)^{1/3}\, u_*$. We are now ready to combine these data to get an estimate for c_T.

Unfortunately, in the determination of c_T from (3.50) and (3.57)-(3.59) an inconsistency shows up. From the result for a convective boundary layer that grows into a neutral environment, eq. (3.58),

it follows that $c_F/c_T = 0.2$, since then $\sigma_w = w_*$. With $c_F = 0.2$ this leads to a value $c_T = 1$.
From the result for a mechanically driven boundary layer that grows into a neutral environment, eq. (3.59), it follows that $(c_F/c_T).(A/c_F)^{1/3} = 0.3$, since in this case $\sigma_w^3 = (A/c_F)u_*^3$. With $c_F = 0.2$, the value of c_T depends on A: if A = 2.5 then $c_T = 1.5$, and if A = 5 then $c_T = 1.9$.
Obviously the experiments do not give a definitive answer on the value of c_T. As an average we take $c_T = 1.5$.

So far, the Tennekes/Zilitinkevich parameterization of the TKE budget, (3.52)-(3.56), is capable of dealing with situations with moderate Ri_* as well as with the limit for $Ri_* \to 0$. For most practical applications in the atmosphere this seems sufficient. However, in the ocean very large Ri_* occur frequently, and we have to check if (3.56) describes mixed-layer growth properly in these circumstances. From (3.56) it follows that the non-dimensional entrainment rate $(1/\sigma_w)dh/dt$ goes to zero according to Ri_*^{-1} for large Ri_* (we assume that $\overline{w}_h = 0$). In (3.55) this means that $\overline{b'w'}_h$ remains non-zero for all Ri_*. There is ample experimental evidence, however, that for large Ri_*, $(1/\sigma_w)dh/dt$ goes to zero faster than Ri_*^{-1} (Linden, 1975; Kato and Phillips, 1969; Kantha et al., 1977). This means that $\overline{b'w'}_h$ should go to zero too, in contrast to (3.55). In order to allow for this behavior, an extra loss term in case of large Ri_* and large γ_b must be included in the energy budget. For this purpose, Zeman (1975) and Zeman and Tennekes (1977) included the dissipation term D_h in the energy budget. They call it the anomalous dissipation. Only that part of it is interesting which is not proportional to σ_w^3/h (which could simply have been absorbed in c_F). This anomalous dissipation is considered to be determined by an energy cascade in the vicinity of the inversion base:

$$D_h = - c_D \sigma_w^3/d, \qquad (3.60)$$

where d is a relevant length scale for the turbulence near the

interface. Zeman (1975) argues that d is proportional to the penetration depth of turbulent eddies arriving at the inversion base. This penetration depth has a maximum value determined by a simple energy consideration:

$$\tfrac{1}{2}\,\sigma_w^{\,2} = \Delta b.d + \tfrac{1}{2}\,\omega_B^{\,2}.d^2, \qquad (3.61)$$

where $\omega_B = \gamma_b^{\frac{1}{2}}$ is the Brunt-Vaisala frequency. Eq. (3.61) is applied by Zeman and Tennekes (1977) to situations with small Δb and large γ_b. Then the first term on the right hand side of (3.61) is not important and there results:

$$d = \sigma_w/\omega_B \qquad (3.62)$$

which makes the parameterized dissipation (3.60) equal to

$$d_h = - c_D\,\sigma_w^{\,2}\,\omega_B\,. \qquad (3.63)$$

The inversion-base dissipation through an energy cascade is not the only possible extra loss of energy. In the case of $\gamma_b \neq 0$ energy may also be radiated away from the interface into the stable layer by internal waves generated by disturbances at the inversion base. An estimate of the divergence of the energy flux, associated with these internal waves, was given by Linden (1975):

$$\text{Internal wave energy loss} \sim d^2\omega_B^{\,3}. \qquad (3.64)$$

With d given by (3.62) this energy loss is proportional to (3.63) and can be incorporated in the constant c_D. This encourages the assumption that (3.63) represents all energy losses that do not scale on h.

The Zeman/Tennekes parameterization of the TKE budget, including the Zilitinkevich term T_h and the inversion base dissipation D_h, thus amounts to:

$$c_T \frac{\sigma_w^2}{h} \left(\frac{dh}{dt} - \bar{w}_h \right) = \overline{b'w'}_h + c_F \frac{\sigma_w^3}{h} - c_D \sigma_w^2 \omega_B \,. \qquad (3.65)$$

Since an equation of type (3.65) can not handle situations where there is no entrainment at all, we must constrain its applicability to cases in which $|F_h| > |D_h|$, i.e. $\omega_B h/\sigma_w > c_F/c_D$. In practice this condition will hardly be violated.

The use of (3.62) as an expression for the length scale d results from (3.61) under the assumption that Δb does not play an important role compared to $\gamma_b.d$, i.e. d is mainly determined by the stable gradient aloft. In early morning situations in the atmosphere and in the many situations in the ocean, however, the buoyancy jump may be large and its effect on the length scale d through (3.61) can not be neglected. When Δb is large, d will be given by $d \sim \sigma_w^2/\Delta b$ (see 3.61), and the parameterization of D_h, (3.60), leads to $D_h = -c_D \sigma_w \Delta b = -c_D(\sigma_w^3/h)Ri_* = -(c_D/c_F)F_h Ri_*$. This means that in that case D_h exceeds F_h when $Ri_* > c_F/c_D$. The value of c_F/c_D is ≈ 20 (Zeman, 1975) and so in situations with large Ri_* it will very often occur that $D_h > -F_h$, which gives unrealistic results. Thus, for large Δb but small γ_b, we do not think that (3.60) and (3.61) give a proper parameterization of the extra energy losses.

As an alternative to the introduction of D_h in the TKE budget for the purpose of dealing with large Ri_*, Garnich and Kitaygorodskiy (1977, 1978) made the coefficients c_F, c_T dependent on the Richardson number. The functional form of this dependence and the new constants involved are to be determined from experiments. An additional term of type (3.63) may also be introduced then, to account for internal waves.

Although this approach is quite general and leads to results which have the correct behavior in various limiting cases

(which is mainly caused by the functional form of c_F, c_T etc.), we think that this approach is based on too few experiments to justify such a new complication.

It is evident that the issue of the dissipation term is far from being settled at the moment. Results obtained by new, carefully designed, laboratory experiments have be awaited, since full-scale measurements in the atmosphere and ocean are not capable of resolving this matter. For the moment we adhere to the Zeman/Tennekes formulation (3.63).

The evaluation of constants in eq. (3.65) was done by Zeman (1975) on the basis of the experiments of Willis and Deardorff (1974) and Kato and Phillips (1969). This evaluation was carried out with a relation for σ_w, w_* and u_* that is based on the assumption that kinetic energy is a linear combination of convective and mechanical contributions, i.e.

$$\sigma_w^2 = w_*^2 + \eta^2 u_*^2. \tag{3.66}$$

This interpolation formula is different from (3.50), in which the energy <u>fluxes</u> were added. Both forms have correct behavior in the limits for $w_* = 0$ and $u_* = 0$, and neither of these interpolation formulae can be derived from a local energy budget only. However, (3.50) is supported by the integrated energy budget parameterization (3.40). When we omit there the second and fourth term on the right hand side, the buoyancy flux at the interface is related to the sum of the cube of w_* and u_*. Therefore we prefer to use (3.50) rather than (3.66) as an interpolation formula for σ_w. Since in the experiments that were used for the determination of the constants either w_* or u_* was zero, the values of c_F, c_D, c_T and η do not depend on the interpolation formula (the value of η^3 is equivalent to A/c_F in (3.50)). We therefore use, instead of (3.66):

$$\sigma_w^3 = w_*^3 + \eta^3 u_*^3 . \tag{3.67}$$

Zeman used the experiments of Willis and Deardorff (1974) to determine c_F, c_D and c_T. These experiments deal with convective entrainment in a stratified water tank in which the lower surface is heated. Two cases are reported with different values for ω_B. The measured heat flux ratios $-\overline{\theta'w'}_h/\overline{\theta'w'}_o$ are different in these two cases which allows for the determination of c_F, c_D and c_T. The value of η was estimated by fitting to the results of Kato and Phillips (1969). The resulting values of the constants determined by Zeman were: $c_F = 0.5$, $c_D = 0.024$, $c_T = 3.55$ and $\eta = 2$.
As was shown by André et al. (1978), the experimental data of Willis and Deardorff used by Zeman contain a wrong calibration factor. A reanalysis of this data leads to the following values of the constants:

$$c_F = 0.6 \quad c_D = 0.03 \quad c_T = 4.3 \quad \eta = 2 \ . \tag{3.68}$$

The much larger values given by Artaz and André (1980) are based on a miscalculation.
We want to point out here that because of the inclusion of all the parameterized terms in (3.65) the values of <u>all</u> the constants have changed considerably compared to the earlier versions, (3.46) and (3.55).

In situations with appreciable wind shear at the interface between turbulent and non-turbulent fluid the term $P_h = (1/\rho_o)(\underset{\sim}{\tau}_H \cdot \partial \underset{\sim}{U}_H/\partial z)\Big|_{z=h}$ may generate significant turbulence. It is likely that a large part of this locally generated turbulence is also dissipated locally, making the parameterization of the net effect rather difficult. The approach taken by Zeman and Tennekes (1977) is essentially based on the use of the length scale d for dissipation (3.62) to estimate the wind shear. The use of expression (3.62) is however of doubtful value in this case, since it is derived as the maximum overshooting distance of convective billows. Besides, they have to make several other assumptions and statements on this term P_h, which makes their

approach in our opinion a bit too speculative. For the parameterization of this term, we prefer to use an expression based on the length scale h, and in agreement with the results of the parameterization of the integrated TKE budget (section 3.5). We therefore postulate that

$$P_h = c_M \frac{|\Delta \underset{\sim}{U}|^2}{h} \left(\frac{dh}{dt} - \overline{w}_h \right), \tag{3.69}$$

where $\Delta \underset{\sim}{U}$ is the difference in wind speed (vectorial) over the entrainment interface. The factor c_M accounts for the assumption that we regard P_h as the difference between local mechanical production and dissipation (see also (3.38), (3.39) and (3.40)). The value of c_M is about 0.7 (see (3.41), where $c_M = B_2$). Incorporating (3.69) in (3.42) and parameterizing the other terms according to (3.65), we obtain

$$\overline{-b'w'}_h = c_M \cdot \frac{|\Delta \underset{\sim}{U}|^2}{h} \left(\frac{dh}{dt} - \overline{w}_h \right) + c_F \frac{\sigma_w^3}{h} - c_T \frac{\sigma_w^2}{h} \cdot \left(\frac{dh}{dt} - \overline{w}_h \right) - c_D \sigma_w^2 \omega_B, \tag{3.70}$$

where σ_w is defined by $\sigma_w^3 = w_*^3 + \eta^3 u_*^3$, with the constants given by (3.68).

3.7. Recapitulation.

In the foregoing sections we have derived a set of equations (3.12)-(3.26) that govern the dynamics of a slab model or jump model for the mixed layer. This system of equations is not closed. The turbulent kinetic energy budget (3.27) is used as an additional equation. The various terms in this equation have to be parameterized in terms of the variables of eqs. (3.12)-(3.26) and the boundary conditions and forcing functions. For this parameterization two main lines can be chosen: the turbulent kinetic energy budget can be parameterized after integration over the mixed layer or it can be parameterized in local form at the interface between turbulent and non-turbulent fluid. Although there are differences between these two methods, the results are not substantially different and neither method resolves the problems in a conclusive way.

From the parameterization of the TKE budget in integrated form we conclude from section 3.5 that the following relation results:

$$-h.\overline{b'w'}_h = B_1 u_*^3 + B_2 |\Delta \underset{\sim}{U}|^2 \left(\frac{dh}{dt} - \overline{w}_h \right) + B_3 w_*^3 + B_4 \sigma_w^2 \left(\frac{dh}{dt} - \overline{w}_h \right). \quad (3.71)$$

The factors B_1-B_4 may be dependent on the Richardson number $Ri_* = h.\Delta b/\sigma_w^2$. We will however not pursue this further. Instead, we use for practical applications: $B_1 \approx 2.5$-5, $B_2 \approx 0.7$, $B_3 \approx 0.2$, $B_4 \approx 1.5$. For σ_w we use the interpolation formula $\sigma_w^3 = w_*^3 + (A/B_3)u_*^3$, with $A = 2.5$-5.

From the parameterization of the local energy budget (section 3.6) two models arise.

The Tennekes/Zilitinkevich model deals with situations with small and intermediate values of Ri_* and of the stable buoyancy gradient γ_b, for situations without wind shear at the interface:

$$-\overline{b'w'}_h = c_F\,\sigma_w^3/h - c_T(\sigma_w^2/h)\left(\frac{dh}{dt} - \bar{w}_h\right), \qquad (3.72)$$

where $\sigma_w^3 = w_*^3 + \left(A/c_F\right)u_*^3$.
The coefficients c_F, c_T and A were estimated as: $c_F \approx 0.2$, $c_T \approx 1.5$, $A \approx 2.5\text{-}5$.

The Zeman/Tennekes model may also be capable to deal with situations with large γ_b. When we also account for the generation of turbulence at the inversion base (minus its dissipation) there results:

$$-\overline{b'w'}_h = c_F\sigma_w^3/h - c_T(\sigma_w^2/h)\left(\frac{dh}{dt} - \bar{w}_h\right) - c_D\sigma_w^2\omega_B + c_M\frac{|\Delta U|^2}{h}\left(\frac{dh}{dt} - \bar{w}_h\right). \qquad (3.73)$$

where now σ_w is defined by $\sigma_w^3 = w_*^3 + \eta^3 u_*^3$.
The set of constants differ from the values in (3.72) and are given by:
$c_F \approx 0.6$, $c_T \approx 4.3$, $c_D \approx 0.03$, $\eta = 2$ (see 3.68).
The value of c_M is about 0.7 as in (3.69).

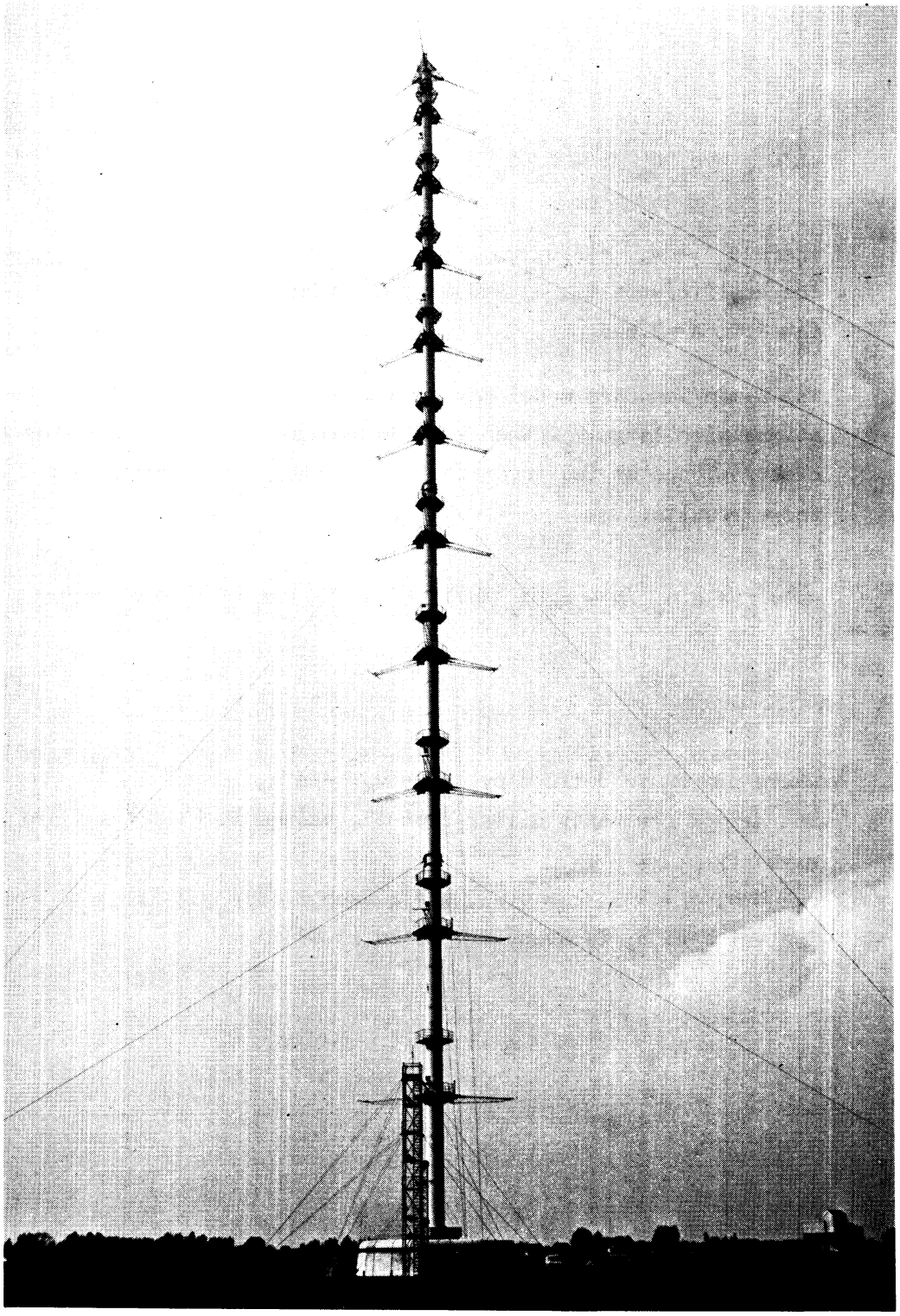

Figure 4.1. The 200 m mast at Cabauw (courtesy J.G. van der Vliet).

4. THE OBSERVATIONAL SYSTEM

Since it is our purpose to compare the mixed-layer models discussed in the foregoing section with a data set obtained in the atmosphere, we carried out an extensive observation programme on the behavior of the mixed-layer variables, the initial and boundary conditions and the forcing functions, and the vertical fluxes of momentum, heat and moisture.

The observations of the vertical profiles of mean and turbulent quantities were done at the 200 m mast at Cabauw, in the center of the Netherlands (Van Ulden et al., 1976; Driedonks et al., 1978). This mast was designed specially for meteorological purposes and is therefore well suited for boundary-layer observations.

At this mast a continuous measuring programme is carried out, which gives data on the vertical profiles of mean wind speed and direction, temperature and visibility. These data are supported by measurements of global and net radiation, mixing height, precipitation and humidity. Besides, the various components of the surface energy balance are monitored.

Under selected atmospheric conditions these measurements may be supplemented by turbulence measurements at several heights and by frequently released radiosondes, which measure temperature, humidity and pressure.

4.1. General description of the 200 m mast.

The 200 m mast (Fig. 4.1) is located at $51^{\circ}58'$N and $4^{\circ}56'$ E, near the village of Cabauw, in the center of the Netherlands (Fig. 4.2). In the NW direction the North Sea is about 50 km away. The surroundings of the mast are topographically flat within a radius of at least 20 km. Typical features are meadows, with occasionally lines of trees, river dikes, and small villages. In Fig. 4.3 a map of the 3.5 x 2.5 km^2 area around the mast is given showing in detail the topographical situation.

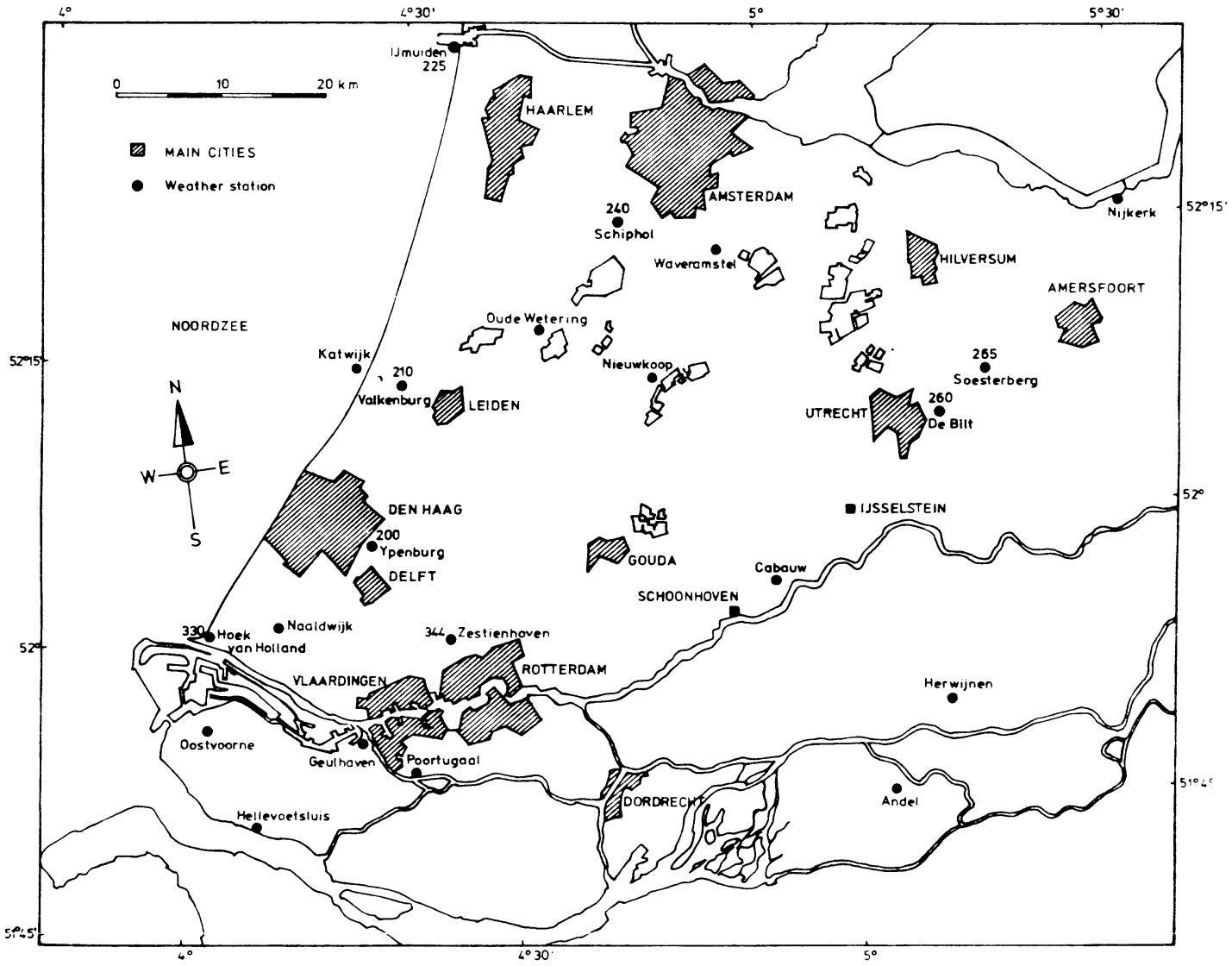

Figure 4.2. Location of Cabauw (center) in the Netherlands.

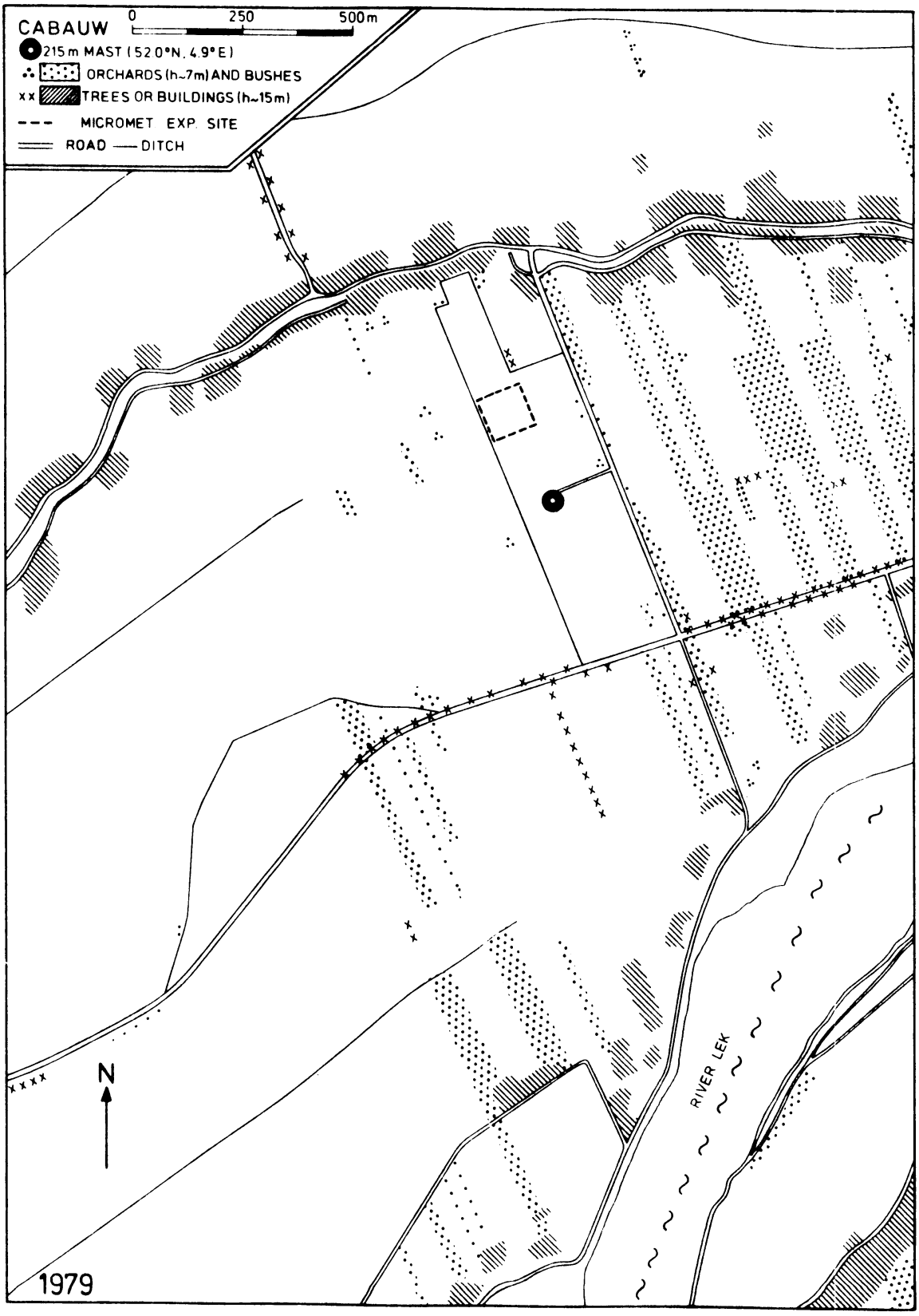

Figure 4.3. Close surroundings of the 200 m mast.

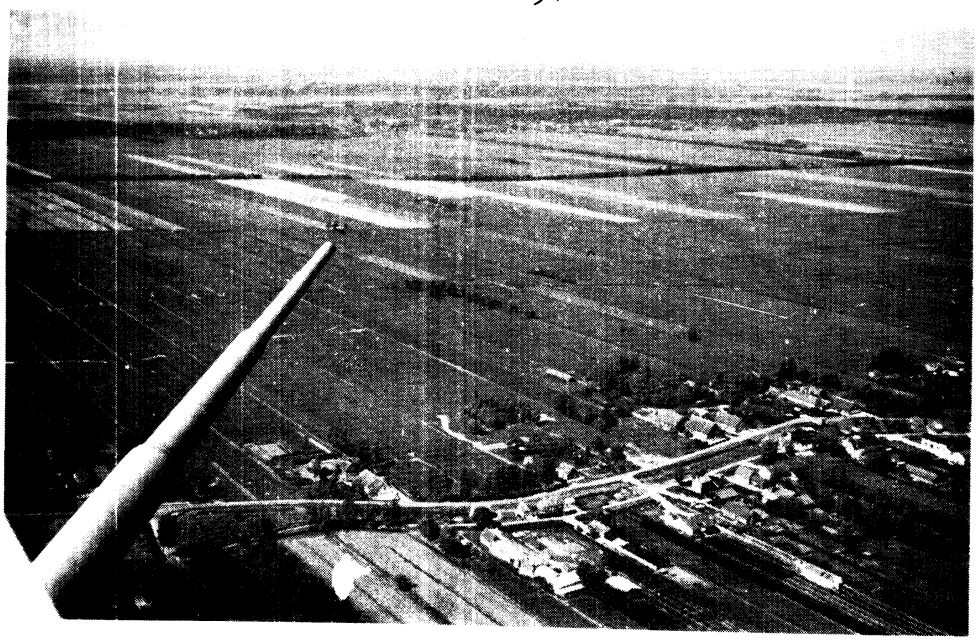

(a)

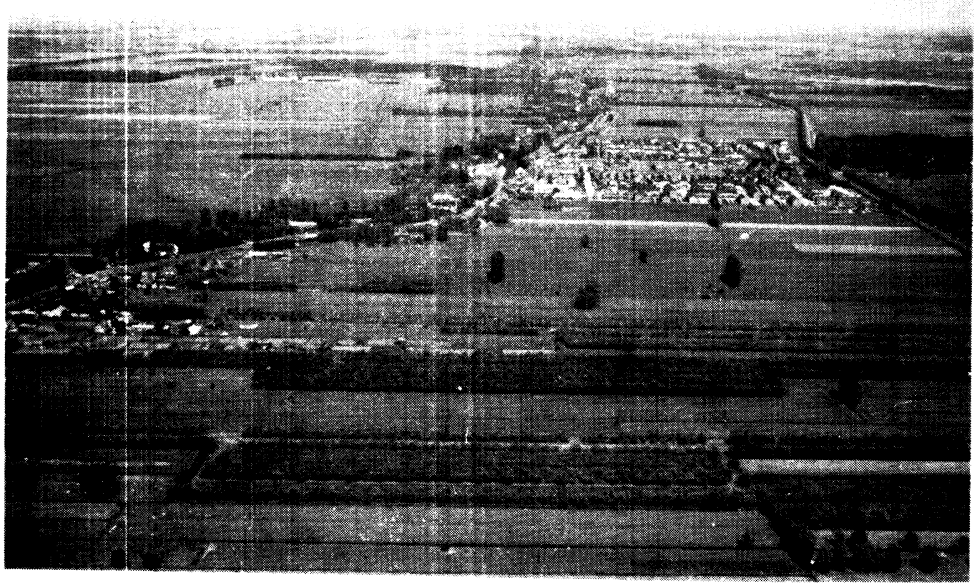

(b)

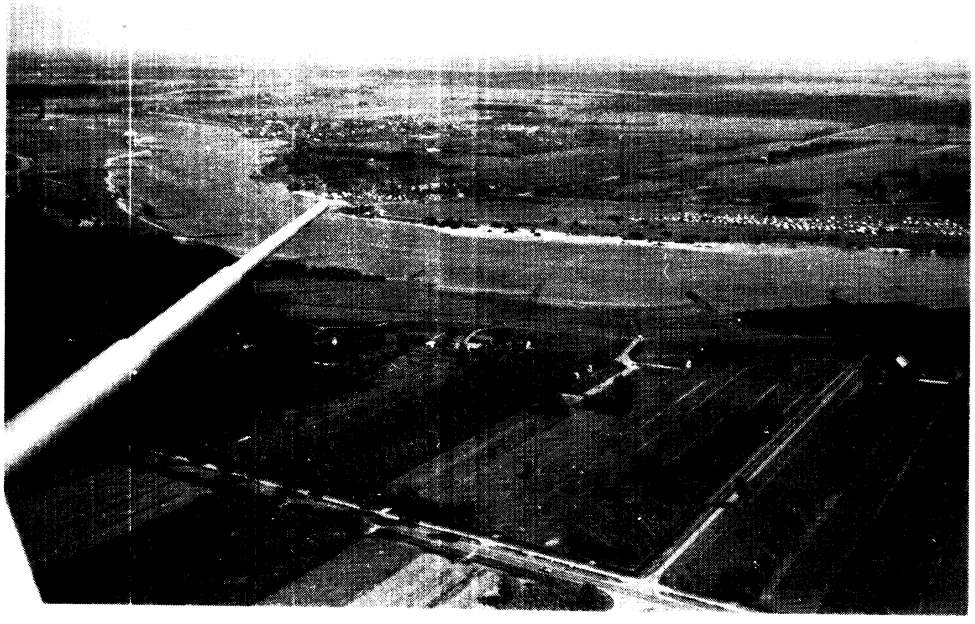

(c)

Figure 4.4. Eastwards views from 215 m height at Cabauw (a) 350°-035° (b) 050°-095° (c) 110°-155° (courtesy Dr. J. Wieringa)

(a)

(b)

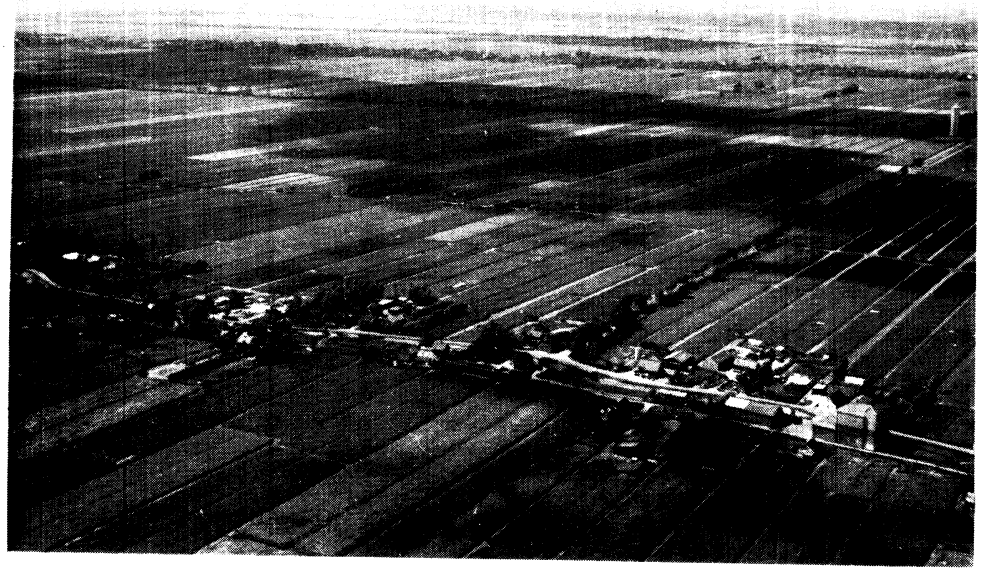

(c)

Figure 4.5. Westwards views from 215 m height at Cabauw (a) 175°-220° (b) 215°-260° (c) 285°-330° (courtesy Dr. J. Wieringa)

The photographs in Fig. 4.4 and 4.5 overlook about the same area. The surface roughness length z_o has been determined from gustiness measurements of the wind speed at a height of 10 m (Wieringa, 1973). Its value varies with direction and season according to table 4.1 (page 58).

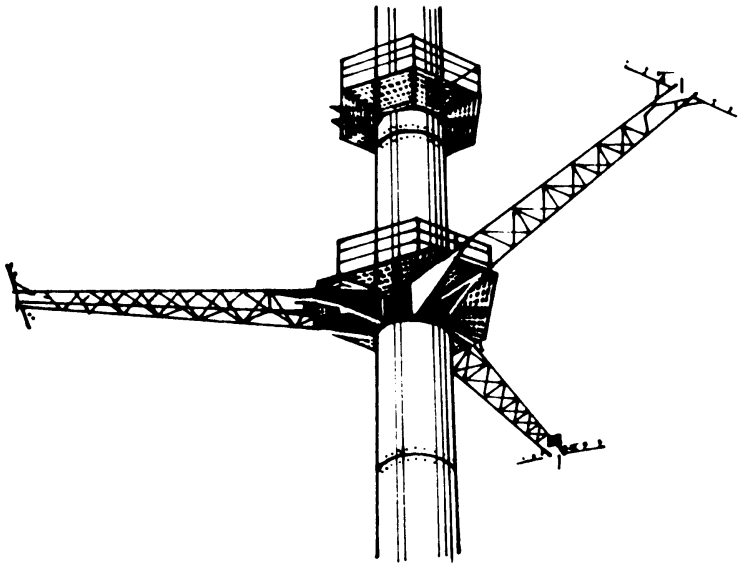

Figure 4.6. Construction of a section of the 200 m mast. At height intervals of 20 m measuring equipment can be installed at the end of three booms.

In Fig. 4.6 the general features of the mast construction are shown. The mast proper is a closed cylinder of 2 m diameter with an elevator inside. At height intervals of 20 m, booms are installed in three directions. Each boom extends ca. 10 m beyond the cylinder surface. In this way, the influence of the

mast itself on the measurements is restricted to less thans 1% (Gill et al., 1967). The booms can be swiveled upward hydraulically for instrument servicing. At the end of each boom two lateral extensions (ca. 1 m long) carry the instruments. To minimize the influence of the boom itself on the measurements, the instrument plugs are extended 0.5 m above the cross booms.

Around the foot of the mast a 3 m high, 9 m wide building contains the registration facilities. In order to get data from levels below 20 m, two auxiliary 20-m masts are installed, one about 40 m SE and one about 60 m NW of the main mast.

The surface energy balance (net radiation, soil heat flux, sensible and laten heat flux in the air) is monitored on a plot of 100 x 100 m^2, about 200 m N of the main mast (see Fig. 4.3). There the soil has been carefully equalized, without disturbance of the original soil profile, which consists of a 60 cm thick layer of heavy river clay covering a thick layer of peat. The plot is drained at a depth of 65 cm. Vegetation is grass with a height of about 10 cm.

Table 4.1. Roughness length z_o at Cabauw as a function of wind direction, derived from gustiness measurements at 10 m.

	May-October	November-April
350 ≤ dd < 20	.21	.20
20 ≤ dd < 50	.18	.14
50 ≤ dd < 80	.23	.17
80 ≤ dd < 110	.25	.12
110 ≤ dd < 140	.19	.12
140 ≤ dd < 170	.19	.10
170 ≤ dd < 200	.19	.10
200 ≤ dd < 230	.17	.10
230 ≤ dd < 260	.07	.06
260 ≤ dd < 290	.08	.10
290 ≤ dd < 320	.12	.11
320 ≤ dd < 350	.11	.09

4.2. Mean profiles and supplementary data.

Data are obtained continuously on the vertical profiles of wind speed and direction, temperature and visibility. These vertical profiles are supplemented by measurements of humidity, global and net radiation, and precipitation.

In table 4.2 (page 60) these measurements are summarized. The surface energy balance measurements, to be discussed later, are also included.

This measuring programme was in operation without substantial changes during 1977 and 1978. In 1981 a new programme will be started with other specifications on heights and instruments.

We will now discuss in detail the instrumentation as it was used in 1977/1978.

Temperature is measured differentially with ventilated, shielded thermocouples (Slob, 1978). In order to keep the circulation in the shield independent of the wind speed in the air, a rather high (9 m/s) ventilation speed is applied. At the lowest and highest measuring level the chain of thermocouples is connected with a zero reference to get absolute temperature values. The overall accuracy of the measured temperature differences is about 0.03 ^{o}C in dry weather conditions. Moisture on the thermocouples at high relative humidity, during and after precipitation or fog, is a still unsolved instrumental problem.

Wind speed and wind direction are measured by means of cup anemometers and wind vanes (Monna and Driedonks, 1979). The cup anemometers have a low starting speed (0.6 m/s) and a response length of 2.9 m. The wind vanes have a damping ratio of 0.36 and a damped wave-length of 3.8 m. The wind speed as measured will still suffer from errors due to overspeeding and obstacle interference. The relative accuracy in the wind speed is about 0.1 m/s. The accuracy of the wind direction is about 2^{o}.

Table 4.2. Continuously measured parameters at the 200 m mast (1977/1978).

element	instrument or method	height	sampling time (s)	recording device
wind speed	cup anemometers	1.5,5,10,20,40, 80, 120,160,200	120	paper tape
wind direction	wind vane	20,40,80,120, 160,200	120	paper tape
temperature	ventilated thermo-couples	0.5,1.5,5,10,20, 40,80,120,160,200	120	paper tape
visibility	transmissometer	1,5,10,20,40,60, 100,140,180	84	Honeywell multipoint
radiation				
global	Kipp(Moll-Gorczynski)	2,213	600	printing
net	Suomi net radiometer	2	600	counters
humidity	wet bulb	2,213	84	multipoint recorder
precipitation	rain gauge	ground level	84	multipoint recorder
O_3,NO,NO_2,SO_2	Philips monitor	3,108,208	300	remote
mixing height	acoustic sounder (monostatic,AeroVironment)	0-1000	15	facsimile recorder
surface energy balance components	Bowen ratio	ground level	600	minicomputer

For fog research, horizontal visibility is measured by transmissometers. The projector is attached to the end of a boom and the detector to a balcony near the mast at the same level, providing a base length of about 11 m.

Global radiation is measured with Kipp-type instruments (Moll-Gorczynski). Net radiation is measured with Suomi net radiometers and Funk radiometers. The latter were used in connection with the surface energy balance measurements and turned out to be of better quality than the Suomi's. Therefore we used the Funk radiometer data when net radiation was required.

Humidity is determined with the aid of ventilated wet bulb thermocouples (Slob, 1978). Rainfall is continuously monitored with a rain gauge, as it may cause considerable errors in the measurements of temperature.

A monostatic acoustic sounder (AeroVironment Inc.) was installed for general and continuous monitoring of the lowest kilometer of the atmosphere (Van Dop et al., 1977). This acoustic sounder was particularly useful during our mixed-layer experiments since from its registration the height of the turbulent boundary layer may be determined with good accuracy if it is within the instrument's range.

4.3. Surface energy balance measurements.

The various components of the surface energy balance are measured on a plot of 100 x 100 m^2, about 200 m North of the main mast (see fig. 4.3). These measurements are based on the equation of conservation of energy at the soil surface, which reads:

$$Q^* + H + LE + G = 0. \qquad (4.1)$$

Here Q^* is the net radiation; H is the flux of sensible heat into the air and thus equal to $\rho_o c_p \overline{w'\theta'}_o$; LE is the flux of latent heat into the air and thus equal to $\rho_o L\overline{w'q'}_o$ where L is the latent heat of evaporation; G is the soil heat flux into the

ground (usually only a small fraction of Q^* in daytime). All fluxes are positive when directed from the soil surface.

The net radiation Q^* is measured by means of a Funk radiometer, the soil heat flux by means of soil heat flux plates (diameter 10 cm, thickness 0.5 cm) at a depth of 5 and 20 cm at three different locations on the field. At one place the temperature profile within the soil is measured by means of electrical resistance elements. From these, the soil heat flux may also be estimated.

The two other unknowns in (4.1), H and LE, are indirectly determined by measuring the Bowen ratio B = H/LE. With the assumption that heat and moisture transports may be represented by gradient-transfer relations with the same eddy diffusivities,

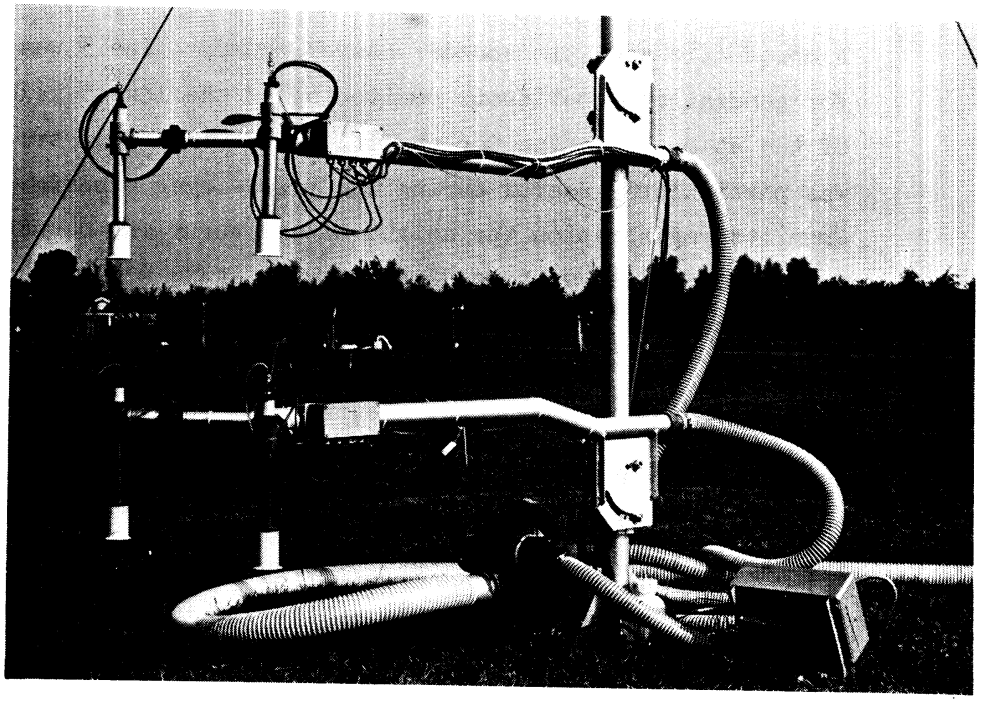

Figure 4.7. The Bowen ratio is determined by measuring the vertical differences in dry and wet bulb temperature.

i.e. $\overline{w'\theta'} = -K\,\partial\bar{\theta}/\partial z$ and $\overline{w'q'} = -K\,\partial\bar{q}/\partial z$, the Bowen ratio is proportional to the ratio of the gradients of temperature and specific humidity close to the ground. The gradients are approximated by measuring the differences in temperature and humidity at two heights close to the ground. Actually, the Bowen ratio was determined from the differences in dry and wet bulb temperature at two heights (usually 1.1 and 0.45 m) along a small mast (see Fig. 4.7). When B = H/LE is given, eq. (4.1) can be solved for H and LE.

4.4. Turbulence measurements.

Under selected atmospheric conditions the turbulent fluxes of momentum, heat and moisture can be measured at several levels up to 200 m. Due to the considerable effort required to carry out these experiments and to process the data, it is not possible to

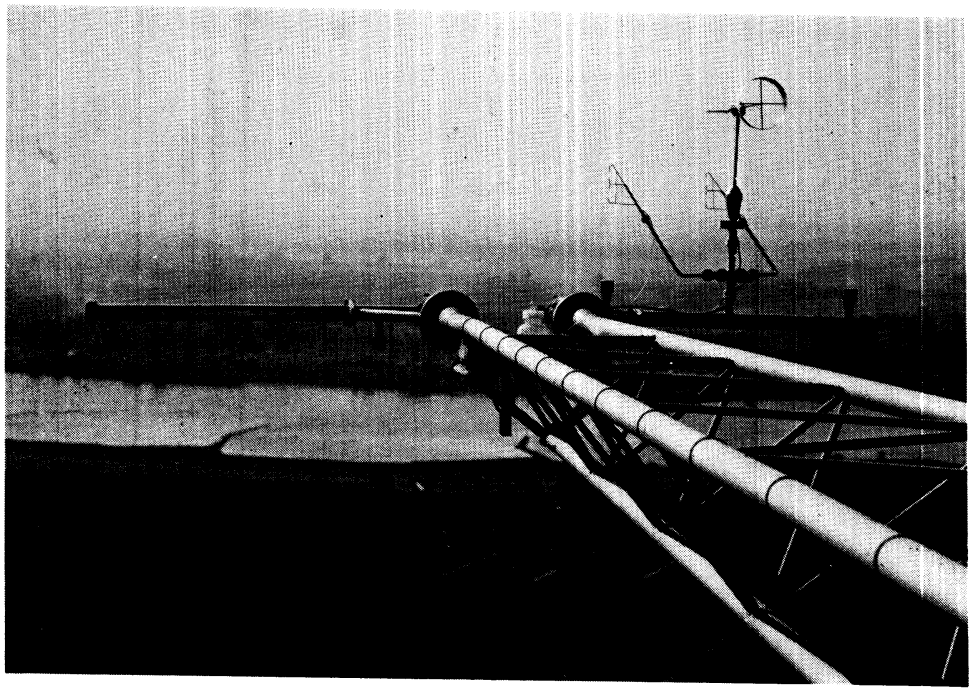

Figure 4.8. Turbulence measuring array installed on a mast boom. The temperature sensors are placed on both sides of the trivane and turned to face the mean wind.

Table 4.3. Turbulence measurements as carried out on most of the days described.

element	instrument	height	sampling frequency (Hz)	recording device
3-dimensional wind vector	trivane	20,40,80,120 160,200	5	Hewlett & Packard 21MX minicomputer on magnetic tape
temperature fluctuations (dry bulb)	unventilated thermocouples	20,40,80,120 160,200	5	idem
temperature fluctuations (wet bulb)	unventilated thermocouples	20,120	5	idem

run them continuously.

The instrumentation used for these turbulence measurements is subject to many changes and improvements. Also, the facilities for these measurements, such as height resolution and registration devices, are continuously evolving. We will describe here the basic characteristics of the instruments as they were used throughout most of the measuring periods.

Turbulence measurements give data on the following variables: the three components of the wind vector u, v, w measured with a mechanical wind sensor delivering the speed and two angles of the wind vector, the dry bulb temperature T measured with a fast response thermocouple, and the wet bulb temperature T_w (the latter was only occasionally included). The total array of turbulence measuring equipment is shown in Fig. 4.8. In table 4.3 a summary is given of the turbulence measurements that were performed on most of the measuring days.

Turbulent wind components are measured with a trivane (Fig. 4.9). This sensor has been developed at the Royal Netherlands Meteorological Institute (Wieringa, 1967, 1972; Monna and Driedonks, 1979). A propeller at one end of a freely rotating rod is kept in the wind direction by an annular fin at the opposite end. The propeller rotation speed is measured with a photo-chopper system, the azimuth and elevation angle of the rod are measured with two potentiometers. The position of the vertical axis of the instrument with respect to the true vertical is measured by two electrolytic water levels with an accuracy of 0.2°. The measured elevation angles are corrected for this deviation by a coordinate transformation afterwards. From wind tunnel experiments the response characteristics were deduced (Monna and Driedonks, 1979). The propeller has a first-order response length of 0.5 m, the vane part has an undamped wave length of 3.3 m and a damping ratio of 0.56.

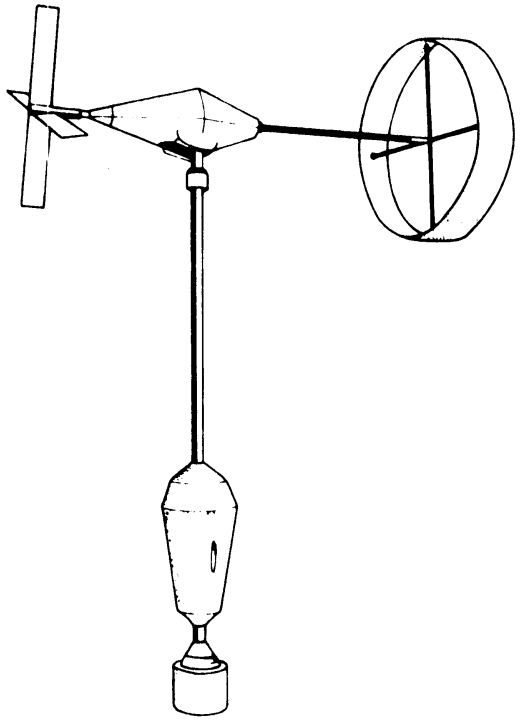

Figure 4.9. Trivane.

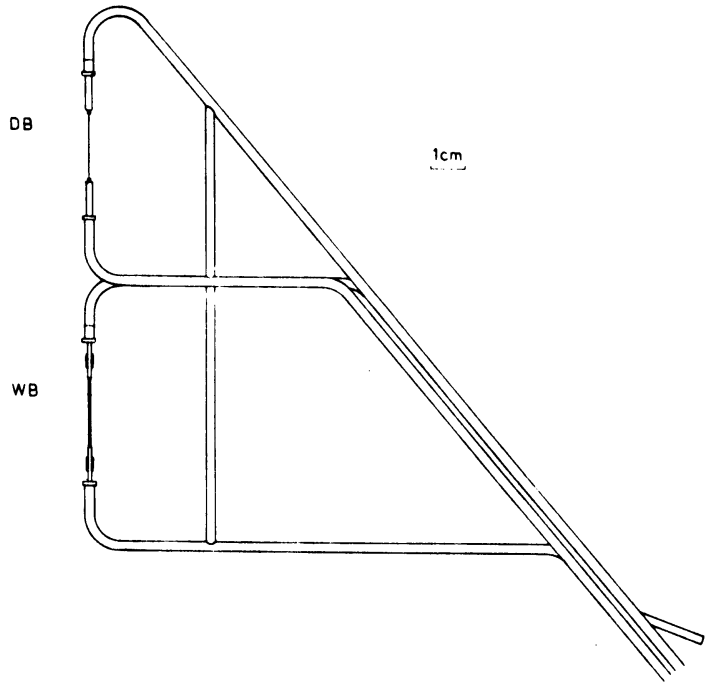

Figure 4.10. Temperature sensor for fluctuations in dry bulb (DB) and wet bulb (WB) temperature.

Temperature fluctuations are measured with a pair of unventilated thermocouples (chromel-alumel), placed on both sides of the trivane, about 1 m apart. The thermocouple-frame can be turned, so as to face the mean wind (see Fig. 4.8). Each thermocouple is accompanied by a wet bulb sensor to measure humidity fluctuations (Fig. 4.10). The response of such an array of thermocouples is primarily determined by the distance between the sensors and it may be considered equivalent to a first-order sensor with a response length of $\sim$ 0.5 m (Wieringa and Van Lindert, 1971).

In appendix A the implications of the sensor's characteristics for their response on periodic forcings are given (attenuation and phase shift). It can be seen that the trivane and thermocouples form a matched array which can reliably measure turbulent fluctuations down to $\sim$ 5 m wave length (with less than 15% attenuation).

This response length has a consequence for the minimum height at which the instruments can be used, since the spectra of turbulence depend on height. As we aim to measure turbulent fluxes with these instruments, it is necessary that the spectral bandwidth of the instruments should contain most of the spectral flux distribution as well (on the high-frequency side). That means that the instrumental high-frequency cut-off has to lie well within the inertial subrange of the spectra, so that only a small fraction of the flux is not resolved. From the spectra of Kaimal (1972) it was concluded that a non-dimensional frequency $f = nz/\bar{U}$ of at least 5 has to be resolved, in order to proceed at least one half of a decade into the inertial subrange (n is the frequency). So the minimum height for the instruments has to be $z_{min} = 5\ L$, where L is the smallest wave length reliably measured. For our measurements we are therefore confined to a minimum height of about 20 m.

4.5. Radiosondes.

In order to calculate the deepening of the mixed layer in daytime, data on the structure of the stable air aloft are required. That is one reason for the use of radio soundings on the measuring days. The other reason is of course that from radiosonde data the height of the mixed layer may be inferred when it is above 200 m.

The radiosondes used on the measuring days were of type VIZ 1207. During an ascent, the sondes give sequentially data on temperature, humidity, and pressure. Since the humidity data are less accurate than the temperature data, the sondes were modified in such a way that the time spent on temperature measurements was favoured at the expense of the humidity signal. Moreover, the signal transmitter of the sonde was cut off at a height of about 3000 m so as to be able to launch the next one.

The time lag of the temperature sensor (resistance element) was measured in the wind tunnel to be 5 s when ventilation is forced by an updraft speed of $\sim$ 3 m/s. In some cases with sharp temperature gradients it was necessary to take this time lag into account (appendix B).

The position of the radiosonde was measured with a theodolite every 30 s. Together with the height from the pressure data transmitted by the sonde, it is possible to construct the wind profile.

4.6. Data processing.

All the signals from instruments installed at the mast are converted and amplified at the observation height to a DC value between -10 and +10 V. To protect the signals from interference currents they are split up into two balanced signals of different polarity and transmitted to ground level. In the registration building these two signals are subtracted again and ready for registration.

The signals from the continuous measuring programme are digitized and stored on paper tape every 120 s. Further data processing is done with a Burroughs B6700 computer at the KNMI. There the data are reduced to 30 min. averages.

The data from turbulence measurements and the surface energy balance field are handled by a Hewlett and Packard 21 MX minicomputer. The turbulence data are sampled with a frequency of 5 Hz and stored on magnetic tape. Further processing of these data again is done with the large computer at the KNMI. An extensive description of this computer processing, including data checks etc., is given in Driedonks et al. (1980).

5. DATA SET

5.1. Measuring campaigns.

Data were obtained on the dynamic behavior of the boundary layer during daytime on 10 days in 1977 and 1978. The measuring campaigns were started at about sunrise and continued till late in the afternoon. On each day the following subsets of data were obtained:

a. Measurements of the mean profiles of temperature, wind speed and wind direction along the 200 m mast. Averaging time 30 min. See table 4.2 (page 60).

b. Measurements of turbulence along the 200 m mast. These include turbulent fluctuations of the wind vector (u', v',w'), of temperature (T') and of humidity (q'). Usually the measuring heights were 20, 40, 80, 120, 160, 200 m for wind and temperature fluctuations, and 20, 120 m for humidity fluctuations.

c. Measurements of the various components of the surface energy balance. Important data from these measurements are the net radiation and the surface fluxes of sensible and latent heat. Averaging time 30 min.

d. Measurements with a monostatic acoustic echo sounder (sodar). From these, the height of the turbulent boundary layer in the early morning hours can be determined directly.

e. Measurements with radiosondes of the vertical profiles of temperature, humidity, wind speed and wind direction, up to a height of about 3000 m in Cabauw. The radiosonde ascent of 1200 gmt in De Bilt ($\pm$ 25 km in distance) was also used.

In table 5.1 a summary is given of the data sets that are available on each of these 10 measuring days. We do not list the measurements done before sunrise. The end of a run depends on the type of measurement. We do not list the measurements after the change in sign of the surface heat flux in the afternoon.

Table 5.1 Data sets available for the 10 measuring days in 1977 and 1978 (all times are in GMT)

date	day number *	mean profiles	turbulence data	surface energy balance	acoustic sounder	radiosondes (launching times)
5/8/77	77217	4.00-14.30	4.00-12.00	4.00-14.30	yes	6.04 7.02 7.49 8.49 9.22 10.05 12.00
5/9/77	77248	4.30-14.00	4.30-10.30	4.30-14.00	yes	5.38 6.33 8.29 12.00
14/9/77	77257	5.00-12.00 15.00-16.00	5.00-11.30	6.30-16.00	yes	12.00
19/9/77	77262	5.00-16.30	5.00-11.00	6.00-16.30	yes	5.19 6.52 9.12 10.20 12.00
30/5/78	78150	3.30-16.00	3.30-16.00	3.30-16.00	yes	6.09 7.50 12.00
31/5/78	78151	3.30-16.00	3.30-16.00	3.30-16.00	yes	4.01 5.56 7.48 8.50 12.00
1/6/78	78152	3.30-15.30	3.30-15.30	3.30-15.30	yes	5.03 6.30 7.56 9.46 12.00
26/9/78	78269	5.30-14.00	6.30-15.30	6.30-14.00	no	5.31 6.55 8.21 9.16 12.00
12/10/78	78285	6.00-15.00	6.00-15.00	6.00-15.00	no	6.01 6.47 7.24 8.13 9.41 10.19 10.57 12.00 12.57 13.53
13/10/78	78286	6.00-15.00	6.00-15.00	6.00-15.00	no	6.34 7.15 8.01 8.42 9.27 10.04 10.36 12.00

* the first two digits in the day number represent the year (-1900), the last three digits represent the number of the day in that year (001 = jan. 1 etc.).

5.2. Problems in relating the measurements to model variables.

The mixed-layer models discussed in chapter 3 are based on a simplified, schematic picture of the mixed layers observed in nature. Therefore the extraction of the relevant model variables from measurements is by no means a trivial task and has to be described in detail. The problem in this extraction arises mainly from the use of ensemble-averaged values of the variables in the mixed-layer models and the difficulty in the estimation of these from one-dimensional measurements under instationary conditions.

We may illustrate this on the definition of the mixed-layer height h. In mixed-layer models h(t) is considered to be an ensemble average. In measurements over horizontally homogeneous terrain one could estimate h(t) as a horizontal average of the local values h'(x,t). This local, instantaneous interface height h'(x,t) may fluctuate considerably from one place to another (see Fig. 5.1).

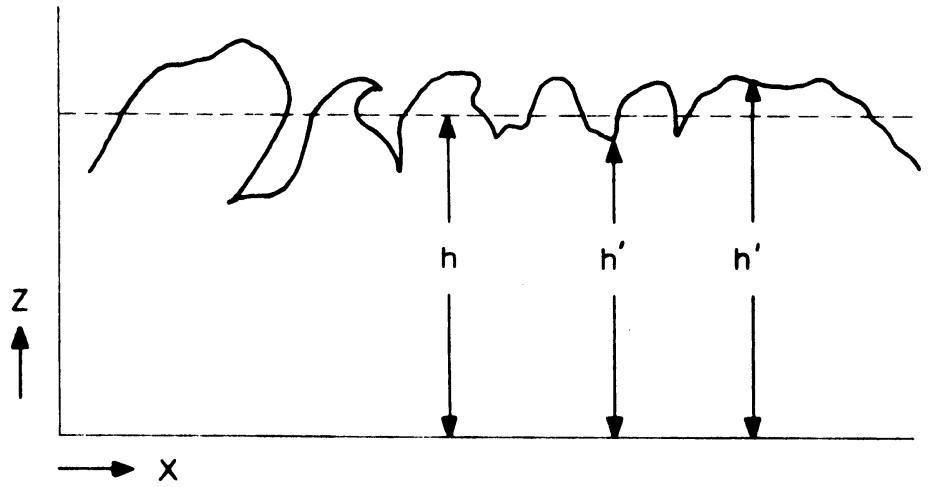

Figure 5.1. The horizontally averaged value of the mixed-layer height h and its local value h', at a certain time t.

In our situation we were not able to average over a horizontal plane, but took measurements along a one-dimensional mast, with one fixed monostatic sodar and with "one-dimensional" radiosondes.

With a radiosonde we infer the mixed-layer height from the "instantaneous" temperature profile. This value is related to h' and so an error has to be taken into account according to the estimated variation of h' around h. An estimate for this variation, var (h'), may be taken as the maximum penetration depth of large eddies into the stable layer, given by (3.61). When Δb is small compared to $\gamma_b.d$, which is usually the case at noon on convective days, we estimate $\text{var}(h') \approx \sigma_w/\omega_B$, where ω_B is the Brunt-Vaisala frequency ($\omega_B = \gamma_b^{\frac{1}{2}}$). For typical values σ_w = 1 m/s, γ_θ = 0.003 K/m, g/T_o = 1/30, the inaccuracy in h determined from a radiosonde ascent is 100 m.

With a sodar one gets a direct estimate of h', more or less continuously (every 15 sec.). To estimate h, we must average h' over a time T which is large with respect to the time scale of the variations in h'. This time scale is associated with the Eulerian time scale of the mixed-layer turbulence. This Eulerian time scale is of the order of h/U_m, where U_m is the mean wind speed in the mixed layer. So we must choose $T >> h/U_m$. This removes the fluctuating component from the mixed layer height. However, we must also take care of the instationarity in h itself, i.e. h = h(t). If we write $\overline{h}^T$ for the mixed layer height from the sodar, averaged over time T, and further take h''(t) as the difference between h'(t) and h(t), i.e. h'(t) = h(t) + h''(t), we get

$$\overline{h}^T_{sodar} = \frac{1}{T}\int_{t-T/2}^{t+T/2} h(t')dt' + \frac{1}{T}\int_{t-T/2}^{t+T/2} h''(t')dt'. \qquad (5.1)$$

The last term in (5.1) is zero, since we take $T >> h/U_m$.

If furthermore dh/dt is constant during the averaging time T, then $\overline{h}^{T}_{sodar}$ is an unbiased estimate of h(t), i.e.

$$\overline{h}^{T}_{sodar} = h(t). \qquad (5.2)$$

Since the sodar gives data only in the early morning hours, when the inversion does not rise very fast, the second criterion (dh/dt = constant) is met for a time T of about 30 min. The Eulerian turbulent time scale h/U_m is typically of the order of a few minutes. Therefore the first criterion ($T >> h/U_m$) is also met for T = 30 min. We thus may assume that (5.2) holds for the mixed layer height from the sodar averaged over T = 30 min.

The determination of h (and the corresponding mixed-layer variables Θ_m etc.) from a measured temperature profile poses some particular problems. Along our mast we have measurements of temperature at fixed heights. To get stable averages we have to choose an averaging time, much larger than the Eulerian turbulent time scale. During this averaging time, however, the mixed-layer height may vary and thus the temperature in the vicinity of h varies considerably. Even when the jump model would be perfect instantaneously, upon averaging this jump will be smoothed out. Furthermore, it is known that even instantaneous ensemble-averaging would not give the schematic jump in the profiles, which can be seen when averaging a mixed-layer variable horizontally in Fig. 5.1.
In any case we will end up with a measured profile in which the "jump" is smoothed out over a certain region and we will have to define a procedure in order to transform the measured profiles into the model profiles (Fig. 5.2).

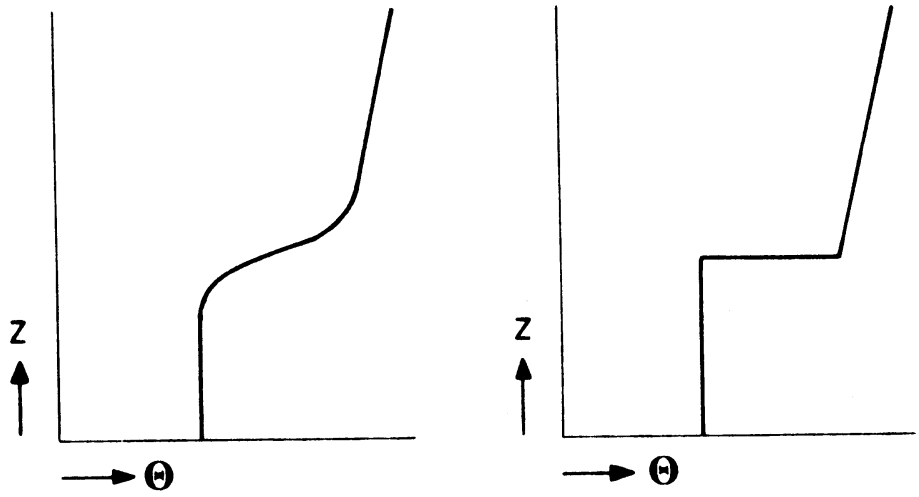

Figure 5.2. Measured profile of Θ (left) has to be transformed into model profile (right).

5.3. The extraction of the model variables.

We will now discuss in detail the various procedures that were followed in order to extract the model variables from the measurements. We will deal only with the variables that are needed for the comparison of integral results from the models, i.e. we compare the models with respect to their solutions for $h(t)$ and $\Phi_m(t)$, where Φ_m may be potential temperature, specific humidity, momentum. Thus the differential equations of section 3.3 are combined with an additional model equation as discussed in sections 3.5 and 3.6, and then integrated. Another, more direct, method to compare various models is to measure all the terms in the turbulent kinetic energy budget individually and compare them with their parameterizations. This, however, is hardly possible from

atmospheric measurements; we abandoned that approach, which will be discussed further in ch. 6.

From ch. 3 it follows that for the integration of the mixed-layer model equations we need the following initial and boundary conditions:

- initial mixed-layer height, h_o
- initial values of all mean variables in the mixed layer, and their jumps at h_o, U_{mo}, ΔU_o; V_{mo}, ΔV_o; θ_{mo}, $\Delta\theta_o$; q_{mo}, Δq_o
- vertical component of gradients of all variables in the stable air aloft. These gradients may be a function of height (and time), $\gamma_u = (\partial\overline{U}/\partial z)_+$; $\gamma_v = (\partial\overline{V}/\partial z)_+$; $\gamma_\theta = (\partial\theta/\partial z)_+$; $\gamma_q = (\partial q/\partial z)_+$
- forcing functions at all times t. (surface sensible heat flux, surface latent heat flux, surface friction, geostrophic wind, mean vertical wind component, radiative fluxes) $\overline{\theta'w'}_o$ (t); $\overline{q'w'}_o$ (t); u_* (t); $\underline{U}_g$, V_g (t); $\overline{w}_h$ (t); Q_T (t)

In order to test the models, we have of course to extract data on $h(t)$, $\theta_m(t)$, $q_m(t)$, $U_m(t)$ and $V_m(t)$ from the measurements.

a. Determination of γ_θ, the gradient of potential temperature in the stable air aloft.

For the determination of γ_θ we used the radio soundings. On most of the measuring days a set of radio soundings was obtained (table 5.1). From the sequence of these soundings the value of θ was taken at a number of heights, to get time

series of $\Theta(z,t)$. In order to take into account possible temperature advection, it was investigated whether a significant trend in $\Theta(z,t)$ with time was present. Only in one case there was a significant trend.

The mean value of all the individual measurements at a height z was then taken to construct a temperature profile in the stable layer aloft. Taking into account the accuracy of this averaged profile ($\pm$ 0.5 ^{o}C) we then determined characteristic points where the temperature gradient changed significantly. This resulted in a number of values of γ_θ for different height intervals.

b. Determination of the mixed-layer height h and the mixed-layer potential temperature Θ_m.

As we have seen in the foregoing section there are some basic problems in the determination of h from measurements. Since our procedure to determine h is closely related to that for Θ_m, we discuss them together.
For the definition of h several approaches can be used. Some definitions, generally used in combination with numerical model calculations, use the height where the turbulent fluxes have decreased to a certain small percentage of their surface value. Deardorff (1974a) used for h the height where the heat flux has a minimum value, i.e. $-\partial\overline{\theta'w'}/\partial z = \partial\bar{\Theta}/\partial t = 0$. This definition of h is not very appropriate in our case, since measured fluxes are not available above a height of 200 m, and anyway they show too much scatter for using them in such a definition.

Since we are mainly dealing with situations in which the heating of the mixed layer plays an important role, we followed another procedure, which conserves the total heat deficit of the mixed layer with respect to the air aloft (Fig. 5.3).

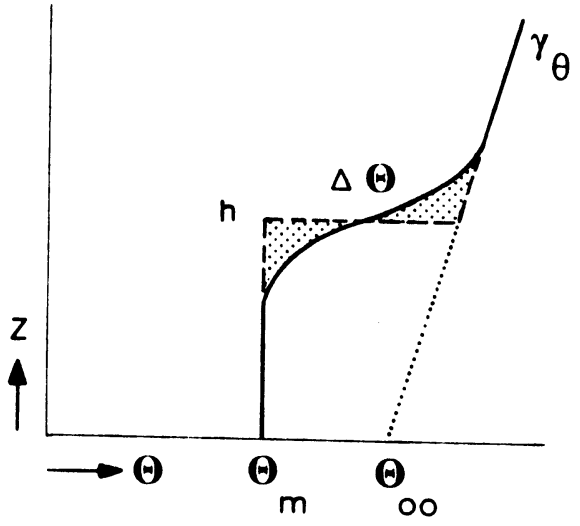

Figure 5.3 Measured profile of Θ (——) and model adaption (- -). The total heat deficit with respect to the reference profile (....) is conserved (shaded areas are equal).

If we define a reference profile $\Theta = \Theta_{oo} + \gamma_\theta z$, then the heat deficit with respect to this profile has to be conserved, i.e.

$$\int_o^\infty \left(\Theta_{oo} + \gamma_\theta z - \Theta_{obs}(z)\right) dz = \int_o^\infty \left(\Theta_{oo} + \gamma_\theta z - \Theta_{model}(z)\right) dz$$

$$= h.\Delta\Theta - \tfrac{1}{2}\,\gamma_\theta h^2. \qquad (5.3)$$

This heat deficit is an important parameter, since its rate of change is directly related to the total sensible heat input:

$$(h.\Delta\Theta - \tfrac{1}{2}\gamma_\theta h^2) - (h_o\Delta\Theta_o - \tfrac{1}{2}\gamma_\theta h_o^2) = \int_{t_o}^{t} \overline{\theta'w'}_o(t')dt' \qquad (5.4)$$

Thus a profile transformation that does not conserve the heat deficit will not be in agreement with the measured heat flux integral.

The condition (5.3) in itself is not enough to determine both h and Θ_m from an observed profile. One of these parameters has to be known from other measurements. We consider two cases.

b.1. Early morning situation: mixed-layer height h determined with the acoustic echo sounder.

Shortly after sunrise the boundary layer is not yet in a state of fully developed convection, and the profile of potential temperature is not nearly as well adapted to a mixed layer model as the example shown in Fig. 5.3. Since mixing is not very vigorous yet, the profile resembles the nocturnal temperature profile, and has the typical structure given in Fig. 5.4.

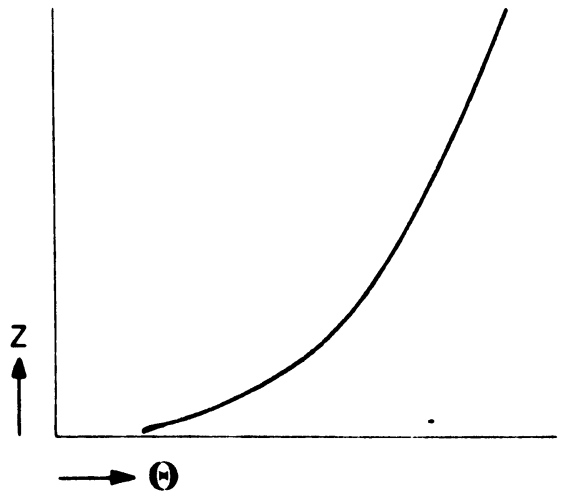

Figure 5.4

Typical vertical profile of potential temperature around sunrise.

Melgarejo and Deardorff (1974) estimated the height of the boundary layer from such a temperature profile as the height where the temperature gradient is within a certain percentage of its value in the air aloft. However, the height of the turbulent layer, which should be taken to be representative for the boundary-layer height, is usually smaller than the height of the ground-based inversion primarily due to the influence of radiational cooling on the temperature profile (Nieuwstadt and Driedonks, 1979; Mahrt et al., 1979; Nieuwstadt, 1980a,b).

We decided to determine the height h in early morning hours from the registration of the acoustic echo sounder. The top of the layer from which this instrument receives backscattered sound corresponds with the height of the turbulent boundary layer. A correction for the length of the acoustic pulse was applied. The total inaccuracy in this procedure gives an estimated error in the boundary-layer height of about 20 m.

When h is determined in this way, we used eq. (5.3) to determine Θ_m and $\Delta\Theta$, using for γ_θ the value of the stable gradient well above z = h (see Fig. 5.5).

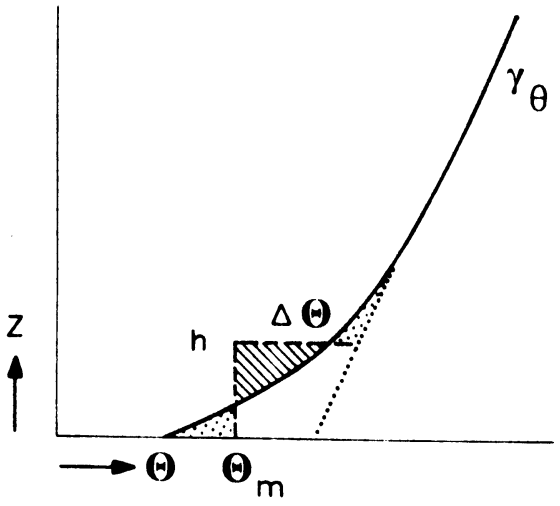

Figure 5.5

Determination of h, Θ_m, $\Delta\Theta$ from a temperature profile around sunrise; h is known from sodar observations; eq. (5.3) is used to determine Θ_m and $\Delta\Theta$ from h, $\Theta_{obs}(z)$ and γ_θ.

This method gives the initial conditions h_o, Θ_{mo}, $\Delta\Theta_o$ at time t_o. For this time we took the time when the surface heat flux gets positive (or is about zero).

This method also gives data on h, Θ_m, $\Delta\Theta$ at later times as long as h could be observed with the sodar and h and Θ_m could not be determined simultaneously from the temperature profile alone.

b.2. Fully developed convection: mixed-layer temperature determined from temperature profile.

When convection is well developed and mixing in the turbulent layer is vigorous, the temperature profile is shaped as in Fig. 5.3: there is a region below h where the temperature is well mixed. The mixed-layer temperature Θ_m can then clearly be defined. This Θ_m and the stable gradient γ_θ well above the inversion, are used in eq. (5.3) to determine both h and $\Delta\Theta$. Thus in case of a well-defined Θ_m the mixed layer variables h, Θ_m, $\Delta\Theta$ can be extracted from the temperature profile alone. This situation usually occurs later on the day and this procedure is applied in particular to the radio soundings.

c. Data on humidity.

Data on the specific humidity q are sparser than on temperature. Measurements along the 200 m mast were available in most cases, but only at a maximum of two heights (20 and 120 m), in some cases only at 20 m. The radiosondes also give rather sparse data on humidity, with vertical spacing of about 60 m. For this reason we did not attempt to determine h independently from the humidity data, but used the mixed-layer height determined from the sodar or from the temperature profile to interpret the humidity profile.
We then have to estimate q_m, Δq, and $\gamma_q = (\partial q/\partial z)_+$.

The gradient in the stable air aloft, $\gamma_q = (\partial q/\partial z)_+$, was determined along the same lines as γ_θ. Thus $q(z,t)$ was averaged in time over all the available radiosondes, and from the resulting averaged profile $q(z)$ in the undisturbed air, values of γ_q for various height intervals were determined. Then also q_+, i.e. the value of q just above z = h, is given by extrapolation.

The value of q_m was determined as the average of the values of q at 20 and 120 m (if h > 120 m); otherwise the value at 20 m was taken. If mast measurements of q were not available, q_m was determined from the radiosondes. The value of the jump Δq is then given by $\Delta q = q_+ - q_m$.

In this way the initial conditions q_{mo}, Δq_o and γ_q are fixed as well as q_m at later times.

d. Data on wind speed and direction.

Mixed-layer models can also predict the time evolution of $U_m(t)$ and $\Delta U(t)$. We thus need the initial values U_{mo}, V_{mo}, ΔU_o, ΔV_o, the stable gradients γ_u, γ_v, and, for verification, data on $U_m(t)$ and $V_m(t)$. Furthermore the geostrophic wind $U_g(t)$, $V_g(t)$ and the surface friction $u_*(t)$ are to be given (see ch. 3). The determination of u_* will be discussed later.

In practice these data are very difficult to obtain from measured profiles. This is mainly caused by the fact that the mixing of momentum in convective conditions is less effective than the mixing of temperature. In cases where temperature is already well-mixed, momentum still may show a considerable gradient within the mixed layer. This occurs especially when h is still rather low (then the surface layer is still a large fraction of the mixed layer).
Fig. 5.6 gives an example.

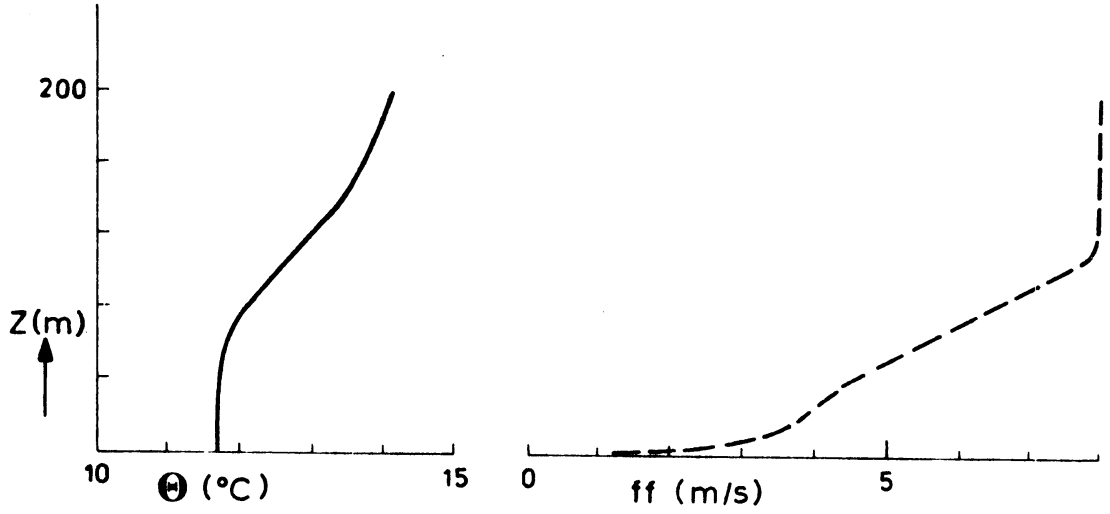

Figure 5.6 Sample profile of Θ and ff up to 200 m. Day 77257, two hours after sunrise, h = 100 (sodar). Θ is already wel mixed below 60 m, but the wind speed still shows a large gradient.

The gradients in the stable air, γ_u and γ_v, were determined along the same lines as γ_θ. The wind data from the individual radiosondes (obtained with theodolite observations) were averaged; from this averaged profile γ_u, γ_v were obtained for several height intervals.

For the determination of U_m, ΔU, V_m, ΔV we used the mixed-layer height h derived earlier. The observed values of U and V below h were vertically averaged to give U_m, V_m. With these values and U_+, V_+ just above z = h as determined from γ_u, γ_v, we estimated ΔU, ΔV.

The geostrophic wind components $U_g(t)$, $V_g(t)$ were calculated from the pressure data of 19 meteorological stations in the Netherlands by a method based on the principal component analysis of a time series of pressure data measured at these stations (Cats, 1977). The geostrophic wind was taken to be independent of height.

e. Data on the surface fluxes.

Turbulent fluxes of momentum, temperature and humidity were measured along the mast (the latter only at two heights). Usually the measuring heights were 20, 40, 80, 120, 160, 200 m. From these measurements the fluxes were calculated with an averaging time of 30 min.

At ground level the turbulent fluxes of sensible and latent heat were measured according to the surface energy balance method, based on the determination of the Bowen ratio (see section 4.3). Averaging time was also 30 min.

The heat flux profile measured along the mast has its lowest point at 20 m. When we assume a linear profile of $\overline{\theta'w'}(z)$ between the surface value $\overline{\theta'w'}_o$ and the value at the top of the mixed layer $\overline{\theta'w'}_h$, then the flux at 20 m, $\overline{\theta'w'}_{20}$, is related to the surface flux by:

$$\overline{\theta'w'}_{20} = \overline{\theta'w'}_o - \frac{20}{h}\left(\overline{\theta'w'}_o - \overline{\theta'w'}_h\right) \qquad (5.5)$$

The correction to be applied to $\overline{\theta'w'}_{20}$ in order to get $\overline{\theta'w'}_o$ thus depends on h and $\overline{\theta'w'}_h$. The latter is not known a priori but may -certainly in early morning hours when h is low and $\overline{\theta'w'}_h$ is mainly determined by mechanical entrainment- be a large fraction of the surface flux (and even exceed it). Thus $\overline{\theta'w'}_{20}$ may differ considerably from $\overline{\theta'w'}_o$ in early morning hours. Later on the day, when h grows large, the second term on the right hand side of (5.5) gets small and the measured flux at 20 m should approach the

surface heat flux. This behavior of the measured flux at 20 m compared to the surface heat flux (as given from the surface energy balance measurements) can be seen in Fig. 5.7 (page 86). Shortly after sunrise the difference may be considerable, in contrast to later times. On days 78151 and 78152 the eddy-correlation fluxes at 20 m are not given because they are suspicious to measuring errors. On these days the heat flux at 20 m obtained from a downward extrapolation of the fluxes at elevated heights exceeded the measured one greatly, even at mid-day.

Thus the difference between the measured flux at 20 m and the surface flux may be explained, at least qualitatively, by (5.5). We conclude that the measured flux at 20 m is not always a good estimate of the surface flux. Therefore at all times we used the data from the surface energy balance measurements as model input.

With respect to the friction velocity u_* (= $(-\overline{u'w'})^{\frac{1}{2}}$) measured at 20 m, no such reference to other, independent, measurements was possible. Therefore we used the available eddy-correlation values of u_* at 20 m whenever the surface friction velocity was required. The value of u_* can also be calculated from the vertical profiles of mean wind and temperature at the lowest levels, using a roughness length of table 4.1 (Nieuwstadt, 1978). These values of u_* agree well with the measured ones. They were used in periods when there were no turbulence measurements.

f. The mean vertical velocity $\overline{w}_h$.

In the formulation of the equations for mixed-layer models in chapter 3, we retained the mean vertical velocity $\overline{w}_h$ at the entrainment interface. From eq. (3.10) we see that $\overline{w}_h$ may be considered as a correction on dh/dt. Therefore we have to compare the relative magnitude of $\overline{w}_h$ and dh/dt in order to assess its importance. We assume that $\overline{w}$ is proportional to the vertical coordinate z, i.e. $\overline{w}_h = \beta h$ with $\beta < 0$ in high pressure areas.

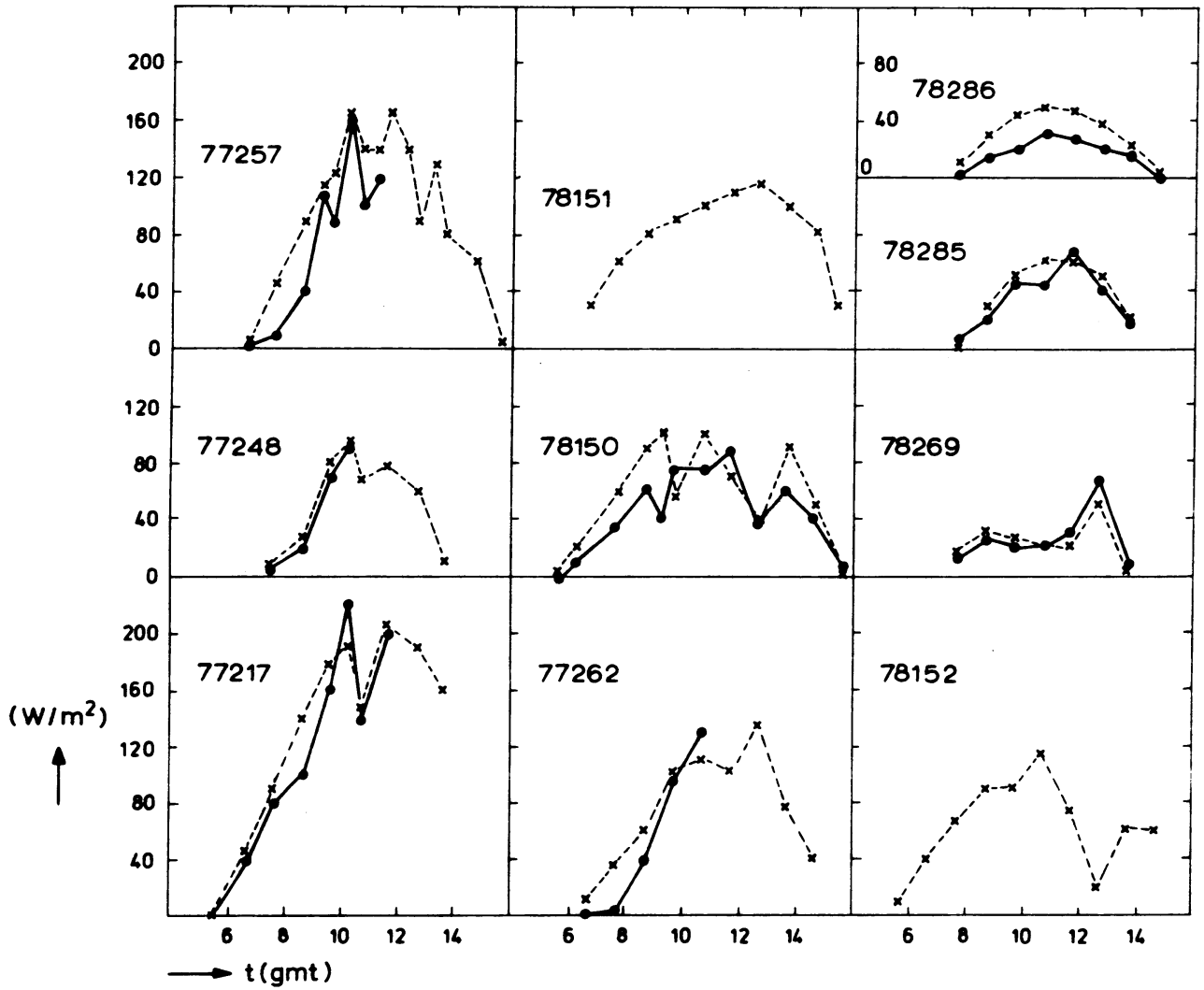

Figure 5.7. Heat flux from eddy-correlation measurement at 20 m (•—•) and from surface energy balance measurements (x--x).

The determination of $\overline{w}_h$ (actually of β) from observations of the horizontal wind is very difficult, since it is associated with the horizontal divergence of the wind field, $\beta = - \nabla_H \cdot \underset{\sim}{U}_H$. This divergence is very sensitive to small errors in the observations (Holton, 1973), and therefore the resulting $\overline{w}_h$ may be contaminated with a large error. In large scale models usually the omega equation (Holton, 1973) is used for the calculation of the vertical wind. This estimate does not depend on the divergence of the measured horizontal wind and gives more accurate results than the continuity equation. However, also from this method the calculated β may be easily in error by 50%.

In order to get more insight in the importance of $\overline{w}_h$ for the mixed-layer dynamics we take a typical value $\overline{w}$ = -2 cm/s at 850 mbar ($\approx$ 1500 m height) and consider various stages in the mixed-layer growth. In the first few hours after sunrise the mixed layer grows quite slowly because the nocturnal inversion has to be eroded and the heat input is still not very large. A typical rise rate is then dh/dt = 50 m/hr. In this stage the mixed-layer height itself is low, typically of the order 150-200 m. Thus $\overline{w}_h$ is then only 10-20% of dh/dt. Later, when the nocturnal inversion has been eroded, the mixed layer grows fast with a typical value of 200 m/hr. Then also, $\overline{w}_h$ is small compared to dh/dt. Eventually, when the mixed layer reaches the height of a strong subsidence inversion, dh/dt will be small again, and in that stage $\overline{w}_h$ may be of the same order of magnitude as dh/dt.

Since our observations of mixed-layer growth did not include this last stage, the effect of $\overline{w}_h$ will be small. Its value at 850 mbar, determined from a large scale model was at most of the order of 1 cm/s. Because of the inaccuracy in the calculation of $\overline{w}_h$ and its small effect in the model, we neglected it altogether and put $\overline{w}_h$ = 0.

g. Radiative fluxes.

In the equations for mixed-layer potential temperature, (3.14), (3.19), the term Q_T allows for diabatic heating associated with long-wave radiative flux divergence. This radiative warming rate has to be compared with the heating by the divergence of the turbulent heat flux in order to assess its importance. The total increase in temperature of the atmospheric mixed layer between sunrise and noon on sunny days is typically 10°C, or 1.5 K/hr. It was shown by Stull (1975), that the effect of radiative flux divergence leads to changes in temperature of at most 1-2 K/day, an order of magnitude smaller than the turbulent effect. We therefore neglected the diabatic heating terms in the model equations. This is of course restricted to the atmosphere. In the ocean radiative absorption is important.

According to the foregoing procedures we extracted the model variables from our observations.
For the ten measuring days they are listed in appendix C.

6. SEVERAL ASPECTS OF COMPARING MIXED-LAYER MODELS WITH OBSERVATIONS

6.1. What model results do we use?

How can we compare mixed-layer models with observations? There are two possibilities.

One is that we could try to evaluate all the terms in the differential equations to see if they indeed describe our observations. A serious disadvantage of this procedure is that the accuracy of differential terms, estimated from measurements, is usually rather poor.

Another method of comparison is to start with the set of differential equations for a mixed-layer model and to integrate numerically in time. We then compare the solutions for the mixed-layer height h(t) and for the mean mixed-layer variables with our observations. A disadvantage of this procedure is that the solutions depend on the initial conditions and on the history of the forcing functions. We now discuss these two methods in more detail.

When we evaluate all the terms in the differential equations, we have to estimate the time derivatives of the mixed-layer variables, and the fluxes of heat etc. at the inversion base. As an illustration we use a dry mixed-layer model. The condition for the heat flux at the inversion base is expressed by eq. (3.24): $-\overline{\theta'w'}_h = \Delta\theta \; dh/dt$. A simple parameterization of the turbulent kinetic energy budget is given in eq. (3.47): $-\overline{\theta'w'}_h = c_F \overline{\theta'w'}_o$. In order to determine the value of such a model we have to estimate dh/dt, $\Delta\theta$, and $\overline{\theta'w'}_h$ from our observations (the surface flux $\overline{\theta'w'}_o$ is measured directly). As we have seen in chapter 5, actually observed profiles deviate from the idealized model situation and we have to apply some transformations to extract the model variables, such as h and $\Delta\theta$. This results in the determination of h itself with reasonable accuracy, but the values of dh/dt can only be estimated with great uncertainty. The determi-

nation of $\overline{\theta'w'}_h$ is even more difficult, because we do not have any direct flux measurements at z = h when h is above mast top (h > 200 m). Then the only possibility for estimating $\overline{\theta'w'}_h$ is to extrapolate a linear profile along the mast up to z = h. It is quite obvious that this will lead only to very crude estimates of $\overline{\theta'w'}_h$. Also when h is below mast top (h < 200 m), $\overline{\theta'w'}_h$ can not be determined accurately from our flux measurements at fixed heights, because of the instationarity in the mixed layer height. Due to this instationarity the averaging time for $\overline{\theta'w'}_h$ must be short (< 30 min.). However, if we average over a short time, the fluxes have a large scatter around their ensemble-averaged value (Wyngaard, 1973). Thus, in investigating the consistency of our observations with the differential equations for a mixed layer, we face large errors in the quantities involved. This makes such an approach quite unattractive, because it is not possible to discriminate between measuring errors and model errors. Therefore we abandoned further attempts in this direction.

The other way to test mixed-layer models is to integrate the governing equations, supplemented by a certain parameterized form of the turbulent kinetic energy budget, and to compare the solutions with the observations. A definitive advantage is that most of these variables are determined with much better accuracy than their derivatives. A disadvantage is that the solutions of a system of differential equations depend on the time history, i.e. on the initial conditions and on the time-dependent forcing functions. Furthermore, it is not a priori clear how sensitive the solutions of a system of coupled differential equations are to a variation of constants in one of them. In particular, it could turn out that relatively large variations in the parameterization of the turbulent kinetic energy budget have only minor effects on the solutions. We will investigate this in the next section, and we will have to be aware of this in the interpretation of our results.

6.2. Sensitivity analysis of the solutions of a convective mixed-layer model.

Since in entrainment models many uncertain coefficients are involved, it is worthwhile to get beforehand some insight in the sensitivity of the model solutions to the various parameters. We will investigate this here on a relatively simple model for convective conditions, for which the equations allow an analytic solution. We take the parameterized turbulent kinetic energy budget in the form of eq. (3.47), i.e. we take the heat flux at the inversion base proportional to the heat flux at the surface:

$$-\overline{\theta'w'}_h = c\,\overline{\theta'w'}_o, \tag{6.1}$$

where we have written c instead of c_F. Furthermore we use the equations for the temperature and the temperature jump:

$$\frac{d\Theta_m}{dt} = (\overline{\theta'w'}_o - \overline{\theta'w'}_h)/h, \tag{6.2}$$

$$\frac{d\,\Delta\Theta}{dt} = \gamma_\theta \frac{dh}{dt} - \frac{d\Theta_m}{dt}, \tag{6.3}$$

and the condition at the interface

$$-\overline{\theta'w'}_h = \Delta\Theta \frac{dh}{dt}. \tag{6.4}$$

After proper substitution, the set of eqs. (6.1)-(6.4) reduces to:

$$c\,\overline{\theta'w'}_o = \Delta\Theta \frac{dh}{dt}, \tag{6.5}$$

$$\frac{d\,\Delta\Theta}{dt} = \gamma_\theta \frac{dh}{dt} - \frac{\overline{\theta'w'}_o}{h}\,(1+c). \tag{6.6}$$

With the initial conditions: $h(t=0)=h_o$, $\Delta\theta(t=0) = \Delta\theta_o$, these equations have an analytic solution in the form:

$$\Delta\theta = \gamma_\theta \frac{c}{1+2c} h + \left(\frac{h_o}{h}\right)^{\frac{1+c}{c}} (\Delta\theta_o - \gamma_\theta \frac{c}{1+2c} h_o). \qquad (6.7)$$

Substitution of (6.7) in (6.5) and integration gives the following implicit solution for h ($\equiv h(t)$):

$$\tfrac{1}{2} \gamma_\theta \frac{c}{1+2c} h^2 - c\left(\frac{h_o}{h}\right)^{\frac{1}{c}} (h_o\Delta\theta_o - \gamma_\theta \frac{c}{1+2c} h_o^2) =$$

$$c \{I(t) + \tfrac{1}{2} \gamma_\theta h_o^2 - h_o\Delta\theta_o\}, \qquad (6.8)$$

where I(t) is the integral of the heat input:

$$I(t) = \int_o^t \overline{\theta'w'}_o(t')\, dt'. \qquad (6.9)$$

Eq. (6.8) gives h(t) as a function of the initial and boundary conditions (through h_o, $\Delta\theta_o$, γ_θ, and I(t)), and of the entrainment coefficient c.

The solution for the temperature θ_m is related to (6.7) and (6.8) by

$$\theta_m(t) - \theta_{mo} = \gamma_\theta (h-h_o) + \Delta\theta_o - \Delta\theta$$

$$= \gamma_\theta \frac{1+c}{1+2c} h - \left(\frac{h_o}{h}\right)^{\frac{1+c}{c}} (\Delta\theta_o - \gamma_\theta \frac{c}{1+2c} h_o) + \Delta\theta_o - \gamma_\theta h_o. \qquad (6.10)$$

A typical value for the entrainment coefficient c is 0.2 (see chapter 3). As a consequence the terms in (6.7), (6.8), and (6.10) in which $(h_o/h)^{1/c}$ is involved, decay very quickly when h starts growing. For example, when c = 0.2 and h = 3 h_o, these terms are only of the order of 0.1% of their initial values. Thus, for $h >> h_o$, we may neglect these terms and approximate (6.7)-(6.10) by

$$\Delta\Theta = \gamma_\theta \frac{c}{1+2c} h \ , \tag{6.11}$$

$$\tfrac{1}{2} \gamma_\theta h^2 = (1+2c)\,(I(t) - \delta_o) \tag{6.12}$$

$$\Theta_m(t) = \Theta_{oo} + \gamma_\theta \frac{1+c}{1+2c} h, \tag{6.13}$$

where $\delta_o = h_o \Delta\Theta_o - \tfrac{1}{2} \gamma_\theta h_o^2$ and $\Theta_{oo} = \Theta_m + \Delta\Theta_o - \gamma_\theta h_o$, see Fig. 6.1.

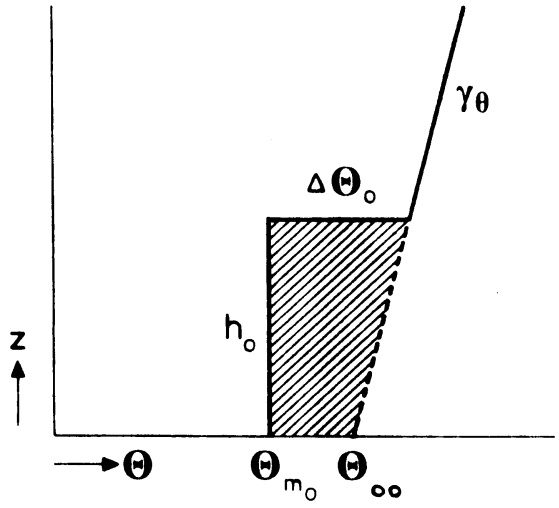

Figure 6.1. Initial temperature profile. The shaded area represents the initial temperature deficit δ_o.

For $t >> o$ (and $h >> h_o$) the effect of the initial conditions on the solutions as given in (6.11)-(6.13) manifests itself only in (6.12) through the initial temperature deficit $\delta_o = h_o \Delta\theta_o - \frac{1}{2} \gamma_\theta h_o^2$. The initial conditions thus play a role only in this combination; the individual values of θ_{mo} and h_o are not important. This justifies our procedure for the selection of proper initial conditions from measured profiles as described in chapter 5. On our measuring days the value of δ_o was on the average 30% of the value of I at noon. Therefore δ_o cannot be neglected in (6.12).

With eqs. (6.11)-(6.13) we now can estimate by partial differentiation the effect of the entrainment coefficient c and of the forcing terms I(t) and γ_θ on the resulting values of h and θ_m.

We first consider the influence of c on h through (6.12). Partial differentiation of this equation with respect to c leads to the result

$$\frac{\Delta h}{h} = \frac{\Delta c}{1+2c} , \qquad (6.14)$$

where Δh is the variation of h when we vary c by an amount Δc. From this relation we see that a change in c from c = 0 to c = 0.2 will cause a change in h of about 20% at noon. The same change in h occurs when c is changed from 0.2 to 0.5.

The variation of h due to a change in the integral heat input I is given by

$$\frac{\Delta h}{h} = 0.5 \frac{\Delta I}{I-\delta_o} . \qquad (6.15)$$

When we use $\delta_o \approx 0.3$ I as the average value from our observations, we see that a change of 30% in the integral heat input causes a change of 20% in h.

A change in the stable lapse rate γ_θ will lead to a change in h according to

$$\frac{\Delta h}{h} = -0.5 \frac{\Delta \gamma_\theta}{\gamma_\theta} . \qquad (6.16)$$

In our measurements the stable lapse rates were of the order of 0.005 K/m. An inaccuracy of 0.001 K/m will then lead to a change in h of about 10%.

From these considerations we see that inaccuracies in I(t) and γ_θ may lead to errors in h which are of the same order of magnitude as those caused by a large variation in the entrainment coefficient c. Therefore it will be difficult to get accurate estimates of c from atmospheric observations.

The influence of a variation in c on the mixed-layer temperature $\theta_m(t)$ is small. It may be estimated by partial differentiation of (6.13):

$$\Delta \theta_m = 2 \frac{(I-\delta_o)c}{h(1+2c)} \Delta c \quad (^\circ C) . \qquad (6.17)$$

Typical values at noon are: $I-\delta_o \approx 1000$ Km, $h \approx 1000$ m. We then see that the change in θ_m caused by a change in c from 0.2 to 0.5 is only very small, less than 0.1 $^\circ$C. This difference can usually be neglected.

The influence of a change in I on θ_m is somewhat larger. From (6.13) and (6.15) we estimate

$$\Delta \theta_m = 0.5 \frac{1+c}{1+2c} \gamma_\theta h \frac{\Delta I}{I-\delta_o} \quad (^\circ C). \qquad (6.18)$$

At noon, $\gamma_\theta h$ is typically 5 $^\circ$C. A change of 20% in I will then change the temperature of the mixed layer at noon with ≈ 0.5 $^\circ$C. This is much larger than could be caused by a change in c. The

mixed-layer temperature is thus more sensitive to a change in the integral heat input than to a change in the entrainment coefficient.

A change in γ_θ will lead to a change in θ_m which may be estimated from (6.13) and (6.16) as

$$\Delta \theta_m = \frac{1+c}{1+2c} \cdot \tfrac{1}{2} h \left(\Delta\gamma_\theta\right) \quad (^oC). \tag{6.19}$$

For typical values c = 0.2, h ≈ 1000 m, we see that a change of $\Delta \gamma_\theta$ = 0.001 K/m causes a change of $\Delta \theta_m$ of about 0.5 ^oC.

What are the conclusions of this sensitivity analysis?
On convective days the initial conditions for h_o and θ_{mo} quickly lose there influence on the solutions for h(t) and $\theta_m(t)$. Only the initial temperature deficit $\delta_o = h_o \Delta\theta_o - \tfrac{1}{2} \gamma_\theta h_o^2$ is important.
The mixed-layer temperature θ_m at noon on convective days can be calculated without paying much attention to the value of the entrainment coefficient c. It is mainly influenced by the integral heat input I and by the stable lapse rate γ_θ.
Although the mixed-layer height h is somewhat more sensitive to variations in the entrainment coefficient than θ_m, it will be difficult to estimate c accurately from atmospheric observations. We saw that a change in c from 0.2 to 0.5 leads to a variation of 20% in h. This is still not very much and the inaccuracy in the determination of h from actual observations (section 5.1) will tend to obscure partly the effect of c.

7. OBSERVATIONS AND CALCULATIONS OF THE MIXED-LAYER HEIGHT

We now want to compare the results of the mixed-layer models with the data of chapter 5, tabulated in appendix C. We have seen that the mixed-layer height is more sensitive to the applied entrainment formulation than the mixed-layer temperature. Therefore we will deal in this chapter with the mixed-layer height prediction. We will use the models of chapter 3, summarized in section 3.7.

Several production mechanisms can contribute to entrainment: convection from the surface, mechanical turbulence caused by friction, and turbulence produced by wind shear at the inversion base. We will mainly deal with the first two mechanisms. Wind shear at the inversion base is discussed in a separate section.

We will start with an investigation of encroachment, i.e. what happens when we completely neglect the negative heat flux at the top of the convectively mixed layer. Then we complicate the entrainment model step by step in order to see what terms do improve the results substantially, and what models only change the results within the scatter of the data.

7.1. Encroachment.

A very simple model for the growth of the mixed layer can be applied to situations which are dominated by convective heating from the surface. The mixed-layer temperature θ_m then will change mainly due to the surface heat input (see section 6.2). The mixed-layer height is growing due to encroachment when we neglect the negative heat flux at the top altogether and instead assume that the temperature just above the mixed layer is always equal to the mixed-layer temperature itself. This is illustrated in Fig. 7.1: the heat supplied from the surface is simply used to fill the original temperature profile.

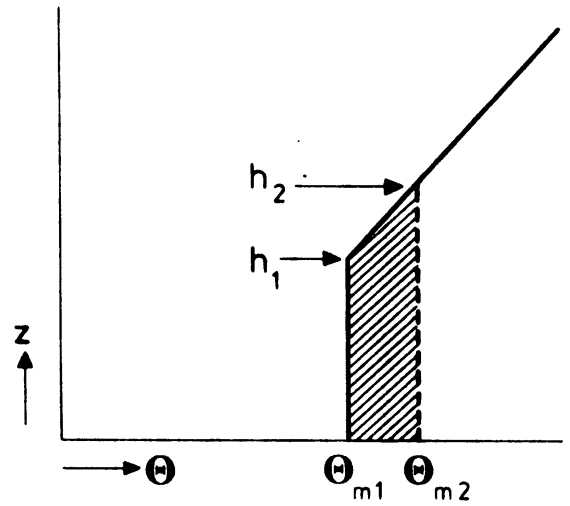

Figure 7.1. Mixed-layer growth due to encroachment. The shaded area represents the heat supplied to the mixed layer between times t_1 and t_2.

The equations for encroachment can be derived from the equations for mixed-layer temperature (3.14), (3.19), (3.23) which we repeat here:

$$\frac{d\Theta_m}{dt} = (\overline{\theta'w'}_o - \overline{\theta'w'}_h)/h \,, \tag{7.1a}$$

$$\frac{d\Delta\Theta}{dt} = \gamma_\theta \frac{dh}{dt} - \frac{d\Theta_m}{dt} \,, \tag{7.1b}$$

$$-\overline{\theta'w'}_h = \Delta\Theta \frac{dh}{dt} \,. \tag{7.1c}$$

The assumption of encroachment supplements these equations by

$$-\overline{\theta'w'}_h = 0. \tag{7.1d}$$

Using (7.1d) we derive from (7.1c) that $dh/dt = 0$ as long as $\Delta\theta > 0$. Only when $\Delta\theta = 0$, dh/dt may be non-zero. Encroachment further assumes

$$\frac{d\Delta\theta}{dt} = 0 \quad \text{if} \quad \Delta\theta = 0. \tag{7.1e}$$

The set of equations (7.1a)-(7.1e) now reduces to the encroachment equations:

$$\text{for} \quad \Delta\theta > 0 \quad \begin{cases} dh/dt = 0 \\ d\theta_m/dt = \overline{\theta'w'}_o/h \\ d\,\Delta\theta/dt = -\overline{\theta'w'}_o/h \end{cases}$$

$$\text{for} \quad \Delta\theta = 0 \quad \begin{cases} dh/dt = \overline{\theta'w'}_o/\gamma_\theta\, h \\ d\theta_m/dt = \overline{\theta'w'}_o/h \\ \Delta\theta = 0 \end{cases} \tag{7.2}$$

In Fig. 7.2 (page 101) the results of the calculations of h(t) with (7.2) are compared with the observations. Here we consider all cases of appendix C without any classification. The scatter is very large and it is also clear that the calculated mixed-layer heights are in general too low. Obviously entrainment has to be taken into account in some way in order to improve the results for all cases. However, encroachment is meant to be used only for fully convective conditions. Therefore we selected those cases from the observations which are only little influenced by mechanical turbulence (the way in which they were selected is

described in the next section). These cases are shown in Fig. 7.3 (page 102). It is clear that in these convective cases encroachment alone can already take care of a large part of the increase in mixed-layer height. Although the calculated values are still too low, the differences are not very large (of the order of 20-30%). These differences will have to be explained by entrainment models.

For the same cases as given in Fig. 7.3, we compared in Fig. 7.4 (page 103) the observed increase in potential temperature $\theta_{m,obs}-\theta_{mo}$ with the values calculated with encroachment. A large part of the observed increase is explained by encroachment. This is not very surprising since we have already seen in section 6.2 that for convective conditions the temperature is quite insensitive to the entrainment.

We will now investigate if we can model the entrainment in such a way that:

- the deviations in Fig. 7.3 become smaller,
- the results in Fig. 7.2 are improved and the scatter is reduced to a value that is comparable with the measuring errors.

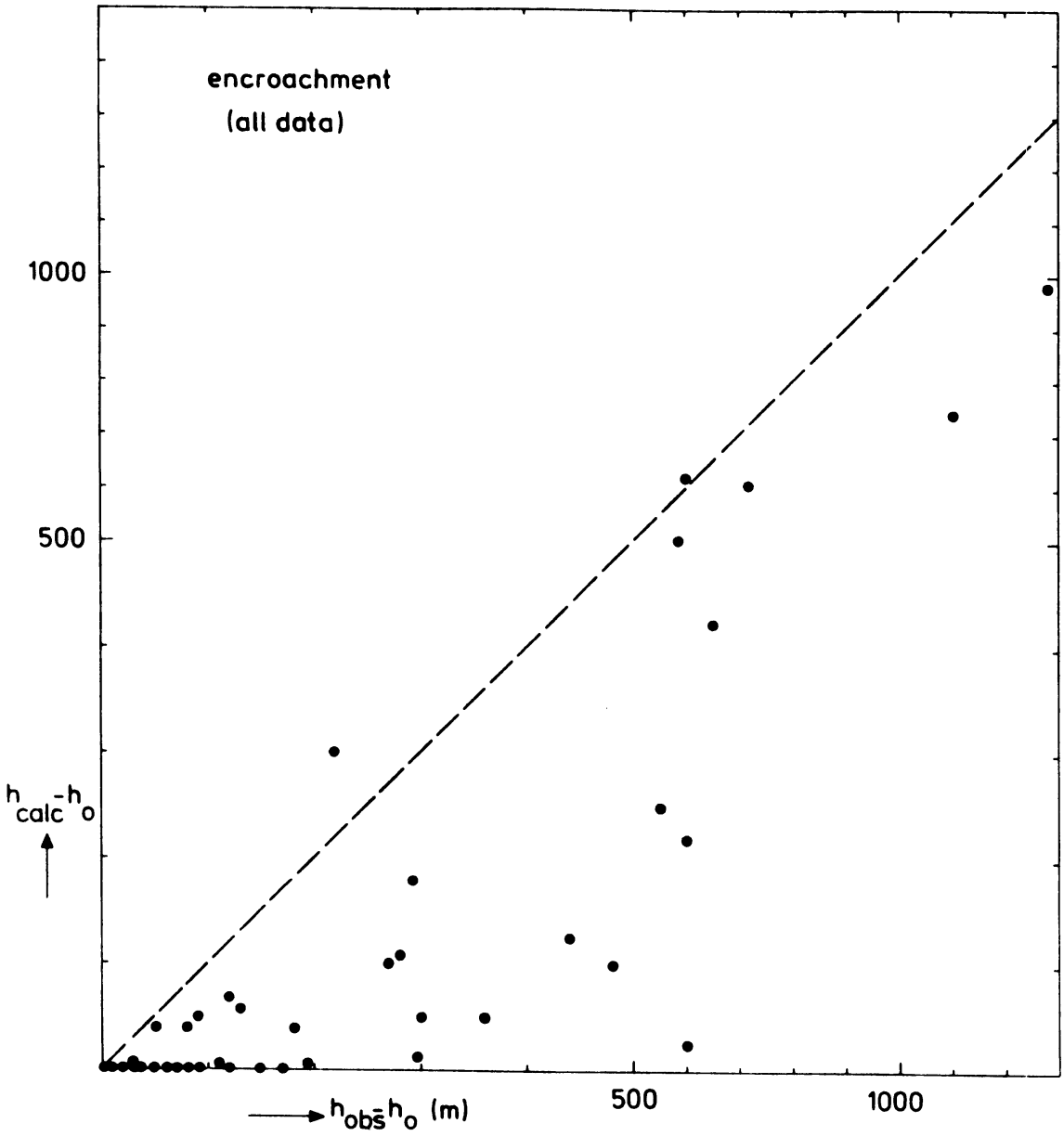

Figure 7.2. Observed mixed-layer height (●) compared with encroachment calculations for all cases.

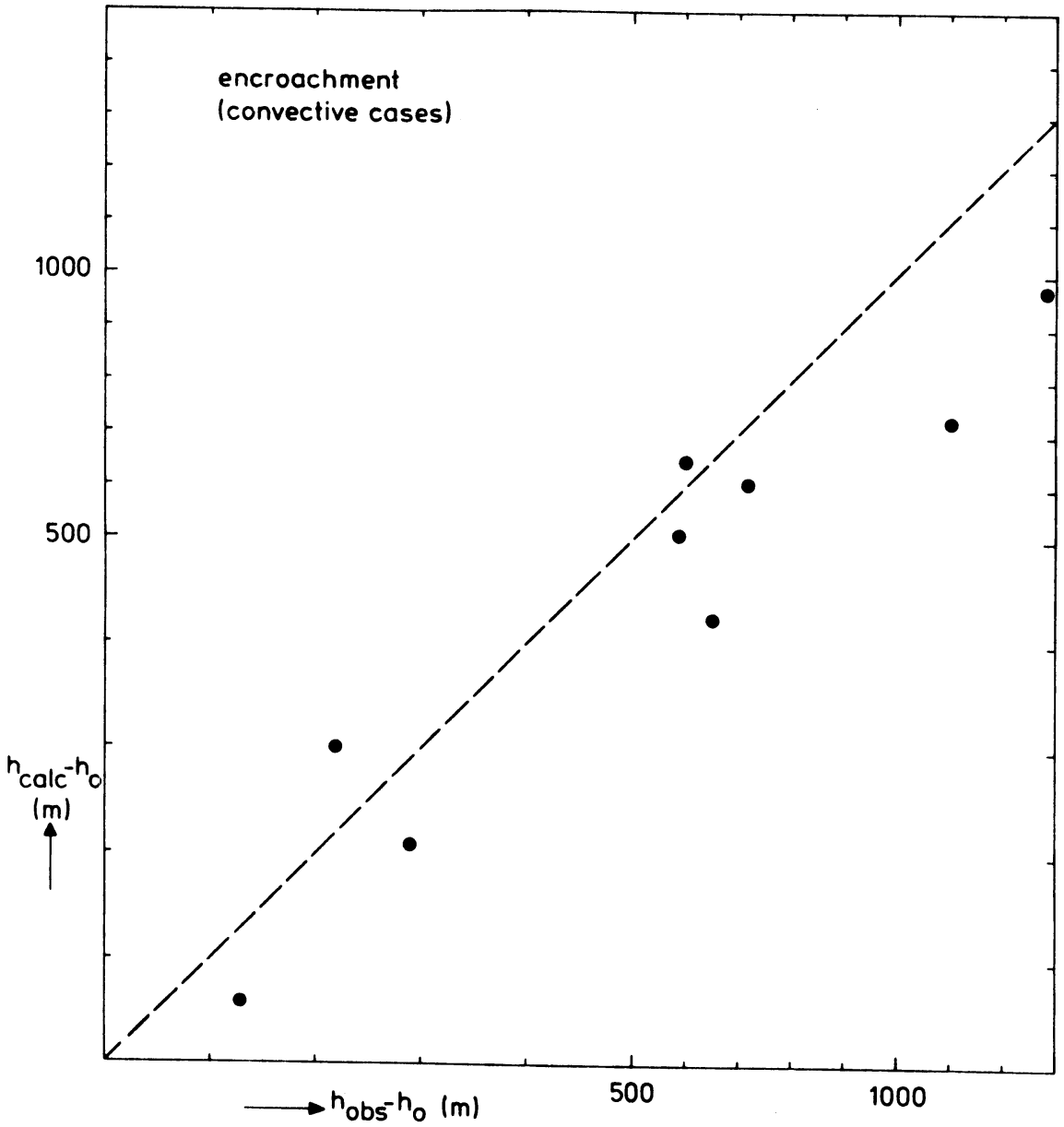

Figure 7.3. As Fig. 7.2 but now only for the cases which are dominated by convection.

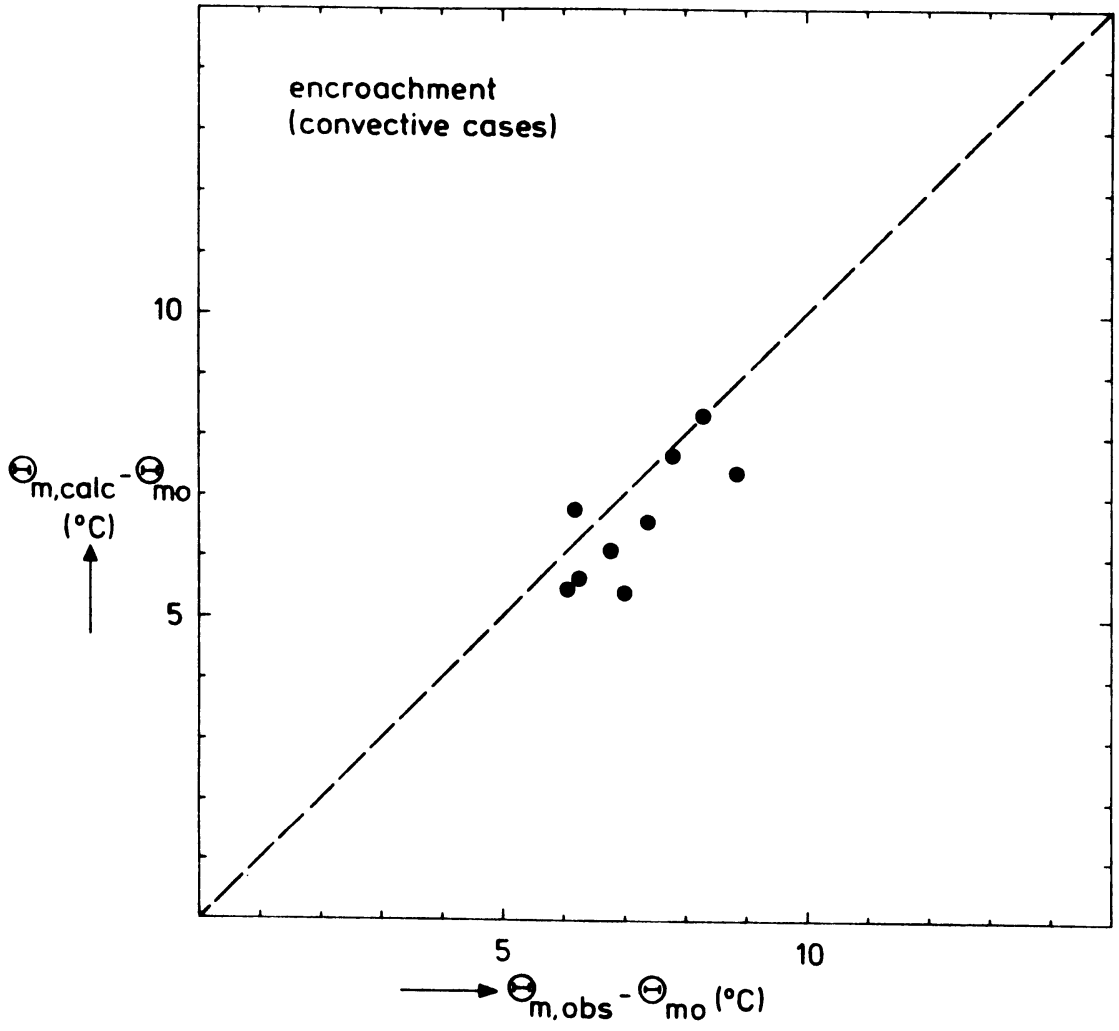

Figure 7.4. Increase in observed mixed-layer potential temperature compared with encroachment calculations for convective cases.

7.2. Tennekes' model.

As a first step in the incorporation of entrainment we use the model of Tennekes (1973), as described in section (3.6), (eqs. (3.43)-(3.51)), which we summarize here:

$$\frac{dh}{dt} = c_F \, \sigma_w^{\,3}/h\Delta b, \tag{7.3}$$

$$\sigma_w^{\,3} = w_*^{\,3} + (A/c_F)u_*^{\,3}. \tag{7.4}$$

For the moment we do not consider the effect of humidity on the buoyancy, so that $w_*^{\,3} = (g/T_o).\overline{\theta'w'}_o$. h, and $\Delta b = (g/T_o)\,\Delta\theta$.

This model involves two "constants" which are associated with two limiting cases of (7.4). When $u_* = 0$ the turbulence is of a purely convective nature and the entrainment is associated with the value of c_F. When $w_* = 0$ we have only mechanical turbulence and entrainment is governed by the value of A. In both limiting cases the solution of the mixed-layer model based on (7.3) and (7.4) will depend only on one constant: c_F or A. In the case of inversion rise on a clear day however the relative contribution of u_* and w_* in (7.4) will usually be a function of time: in the early morning w_* will be small, and later on the day w_* will be large compared to u_*. This means that the solution for h(t) will depend on the values of c_F and A in a way that depends on the time history of the ratio between $u_*^{\,3}$ and $w_*^{\,3}$. As long as this ratio is large (small heat flux) h(t) will be influenced most by the value of A. When this ratio is getting small, the influence of A decreases and that of c_F increases. This is an important point in the comparison of the solution of a mixed-layer model based on (7.3)-(7.4) with the observations: the solution for h(t) will depend on the constants c_F and A and on the whole time history of the forcing between t_o and t.

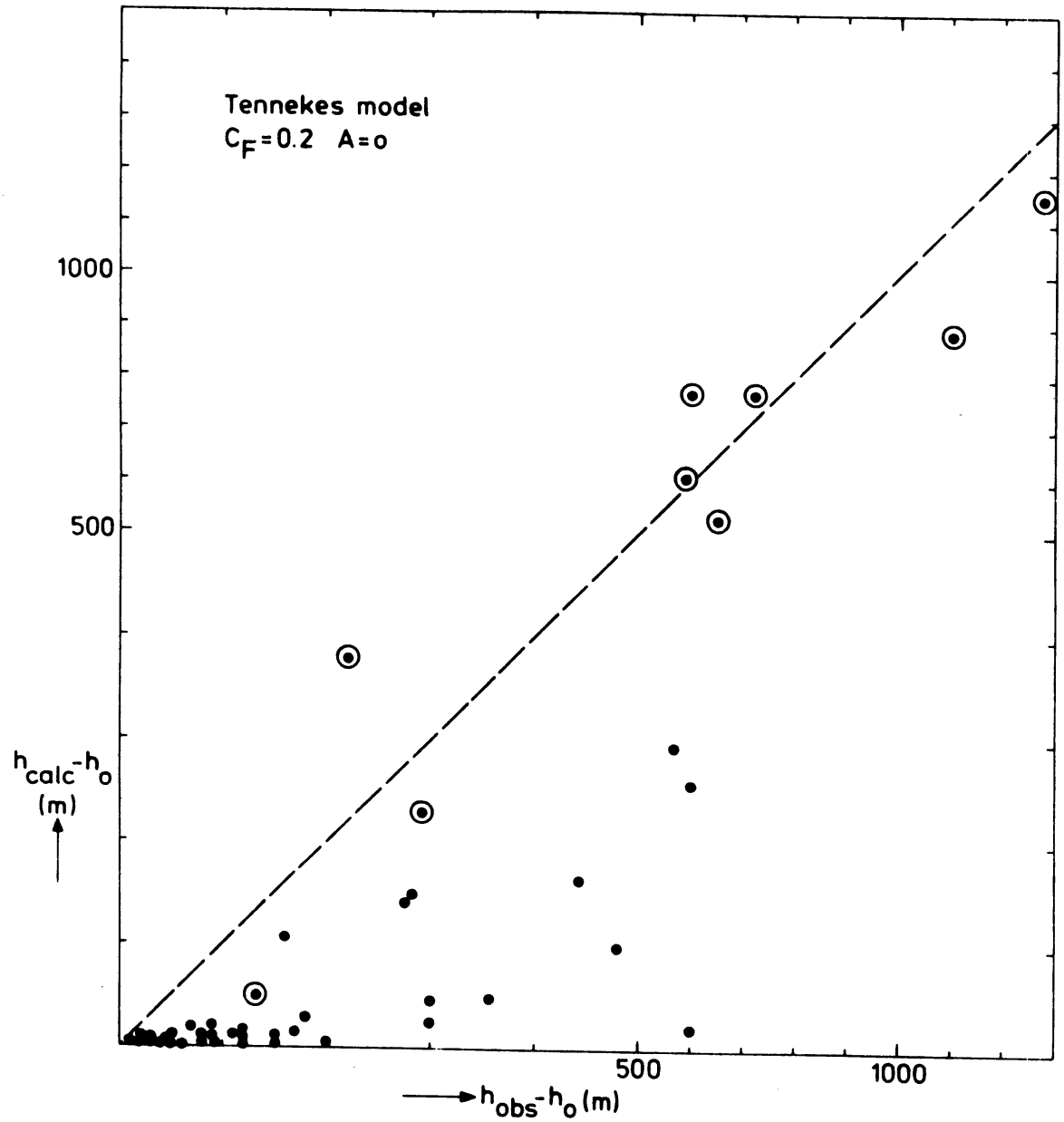

Figure 7.5. Results of Tennekes model. Only convective entrainment. All observations (●). Encircled are the cases in which u_*-term is unimportant.

In Fig. 7.5 we give the calculations for the case in which $c_F = 0.2$ and the mechanical term in (7.4) is neglected altogether. It is clear that this doesn't improve anything substantial compared to Fig. 7.2 (encroachment). This means that, for application on our measuring days, eq. (7.3) and (7.4) indeed are a two-parameter problem: both the value of c_F and A are important when we want to describe all our observations.

In section 6.2 we saw that for purely convective entrainment a change in c_F from 0 to 0.2 or from 0.2 to 0.5 affects the results for the calculated h(t) by about 20%. This makes clear that it is quite useless to puzzle too much about small variations in the value of c_F: observations of h at noon from radiosondes have a statistical error of ~100 m (section 5.2). What can we say about the effect of a variation in A on h(t)? To give an estimate for this we consider a situation with only mechanical entrainment ($w_* = 0$), with initial conditions $h_o = 0$, $\Delta\Theta_o = 0$ and stable temperature gradient γ (see Figure 7.6). At t_o we turn on a constant u_*.

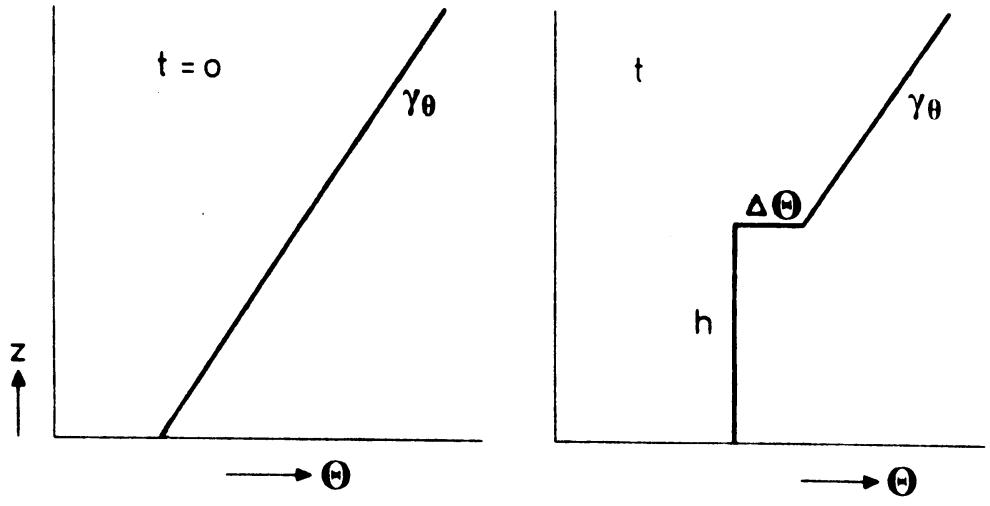

Figure 7.6. Mechanical entrainment in stratified fluid: $\Delta\Theta = \frac{1}{2}\gamma h$.

The temperature jump in this situation is governed by the diagnostic relation: $\Delta\theta = \frac{1}{2} \gamma h$. The solution of (7.3) is in this case:

$$\frac{1}{6} \gamma h^3 = A \cdot u_*^3 \frac{T_0}{g} t.$$

Thus a relative change in A of $\Delta A/A$ causes a change in h of $\Delta h/h = 1/3\ \Delta A/A$: for mechanical entrainment a change of A from 2.5 to 5 results in an increase in h of 30%. Besides, we see that a 10% error in u_* has the same effect on h as a 30% error in A, since A is associated with the cube of u_*. This makes it clear that for the value of A, as for c_F, it is quite useless to puzzle about small variations.

Convective situations: estimation of c_F.

For the description of all our cases convective entrainment alone is not enough (Fig. 7.5). However, we may choose a subset in which the influence of friction is small, and which is dominated by convection. For this purpose we selected the cases in which $u_* << w_*$ for a period of at least a few hours. These are the observations at noon on convective days because then w_* is large. When there was only little wind ($u_* \approx 0$) we selected all the observations on that particular day. To quantify this selection procedure we calculated the model of eqs. (7.3)-(7.4) for different combinations of c_F and A. As a convectively dominated subset of our observations we used the cases for which a change in c_F from 0.2 to 0.5 led to a change in the resulting mixed-layer height which was more than twice as large as when we changed A from 0 to 2.5. This means that in our subset indeed the influence of convection (associated with c_F) is much more important than friction (associated with A). These convectively dominated cases are encircled in Fig. 7.5 and separately plotted in Fig. 7.7 (page 109). The same data are tabulated in table 7.1.

Since it is not possible to determine c_F with great accuracy from atmospheric observations, we considered only three values: $c_F = 0$, representing encroachment (already investigated in section 7.1), $c_F = 0.2$ as suggested by Tennekes (1973) and given as a mean value of the experimental data collected by Stull (1976b), and $c_F = 0.5$ as the largest value reported from measurements (Carson, 1973; Tennekes and Van Ulden, 1974).

Table 7.1. Differences in observed and calculated mixed-layer height in convectively dominated cases for different values of c_F.

day number (see table 5.1)	time (GMT)	h_{obs} (m)	$h_{calc}-h_{obs}$ (m)		
			$c_F = 0$	$c_F = 0.2$	$c_F = 0.5$
77217	1230	900	-225	-100	+ 90
77257	1115	650	- 80	+ 20	+170
77262	912	340	- 80	- 50	+ 50
	1020	650	+ 50	+150	+330
	1130	1350	-330	-150	+ 80
78151	1230	1200	-360	-200	0
78152	946	300	+ 80	+140	+150
	1115	800	-110	+ 40	+310
78286	1200	230	- 70	- 40	+ 15
averages + standard dev.			-125±150	-20±125	+130±120

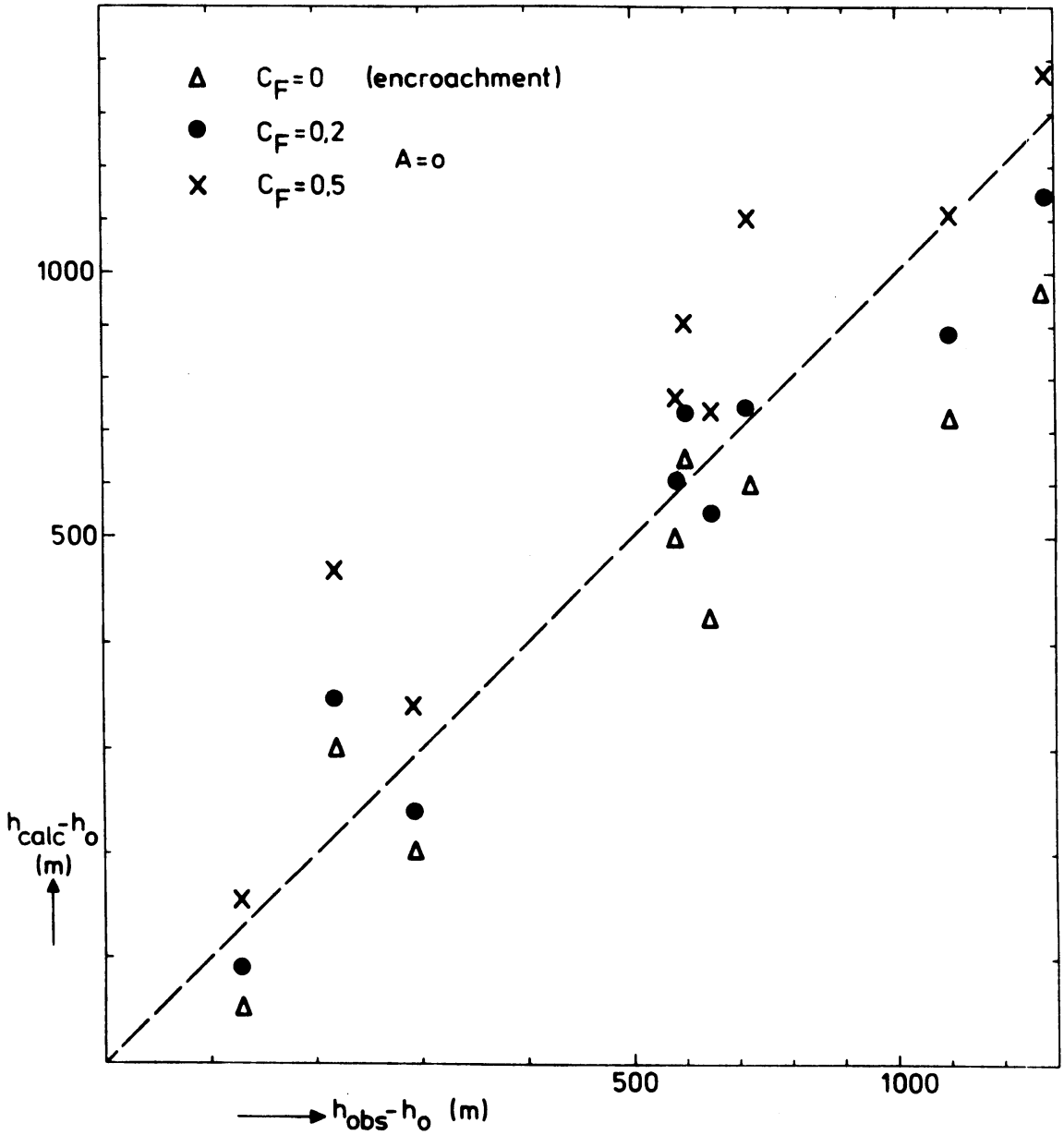

Figure 7.7. Convectively dominated mixed-layer heights, calculated with various values of the entrainment coefficient c_F *in eq. (7.3).*

From Fig. 7.7 and table 7.1 it may be concluded that the scatter in the results is about 125 m, which is also typically the statistical inaccuracy of the estimate of the ensemble-averaged value of h from one radiosonde. The differences between $c_F = 0$, $c_F = 0.2$ and $c_F = 0.5$ are on the average not very large but they are significant (smaller variations of c_F, e.g. $c_F = 0.2$ and $c_F = 0.3$ would lead to results which do not differ significantly). We must conclude that a value of $c_F = 0.2$ gives the best results for convective entrainment. A value of $c_F = 0.5$ predicts too large values of h.

Inclusion of mechanical entrainment: the value of A.

We will now investigate if inclusion of the mechanical entrainment in eq. (7.4) improves the calculations when we consider all our observations. This extra term may certainly play an important role in the early morning hours, when the heat flux is small. In various cases this term even contributes significantly throughout the whole day.

In the context of the entrainment model, that we use here, there is some controversy about the value of the coefficient A in (7.4) derived from laboratory experiments with shear-driven mixed layer. Kato and Phillips (1969) gave a value of $A = 2.5$ which was also used by Tennekes (1973). Later, however, Kantha et al. (1977) did analogue experiments and measured entrainment rates which were about twice as high, i.e. $A \approx 5$. Apart from this, their results also indicated that the simple modeling of the mechanical term in eq. (7.4) is not valid for all values of the Richardson number, $Ri_* = (g/T_o)h\,\Delta\theta/\sigma_w^2$, especially not for very low and very high Ri_*. In the atmosphere very high values of Ri_* (>100) hardly ever occur. The effect on the entrainment at very low Ri_* will be discussed in the next section. For the moment we may state that their results indicated $A \approx 5$ in eq. (7.4).

Since it doesn't make much sense to determine A with great accuracy from atmospheric observations, we compared the calculations for the two values of A cited above, i.e. A = 2.5 and A = 5, to see which one is best supported by our data. We thus integrated the model of eq. (7.3)-(7.4) together with eqs. (3.12)-(3.26) for these two values of A. The coefficient c_F was taken at $c_F = 0.2$.

The results are given in Figures 7.8 and 7.9 page 112-113, for all observations. Those cases that are dominated by the value of c_F rather than by A, are encircled.

A comparison of both Figures with Fig. 7.5, in which no mechanical entrainment was included, makes clear that the u_*-term gives a sizeable contribution to the mixed-layer growth in the early morning hours, when h is still low. The results for A = 5 are much better than for A = 2.5. A linear regression of $h_{calc} - h_o$ on $h_{obs} - h_o$ for those cases which are not encircled (not dominated by convection) gives: $h_{calc}-h_o = (0.6\pm0.2)\ (h_{obs}-h_o)$ for $c_F = 0.2$, A = 2.5, and $h_{calc}-h_o = (0.9\pm0.1)\ (h_{obs}-h_o)$ for $c_F = 0.2$, A = 5. In both cases the correlation coefficient is high (0.95).
When we also take into account the encircled points in Fig. 7.9, i.e. when we take $c_F = 0.2$, A = 5 for all cases, then the slope of the regression increases to 0.95. Thus the bias is quite small. Furthermore then the standard deviation of $h_{calc}-h_{obs}$ is $\approx$80 m (for all $h_{obs}-h_o > 100$ m), but only $\approx$40 m when we take $h_{obs}-h_o < 500$ m.

We conclude that mechanical entrainment in (7.4) improves the results significantly and that A = 5 leads to a good agreement between the calculated and observed mixed-layer heights.

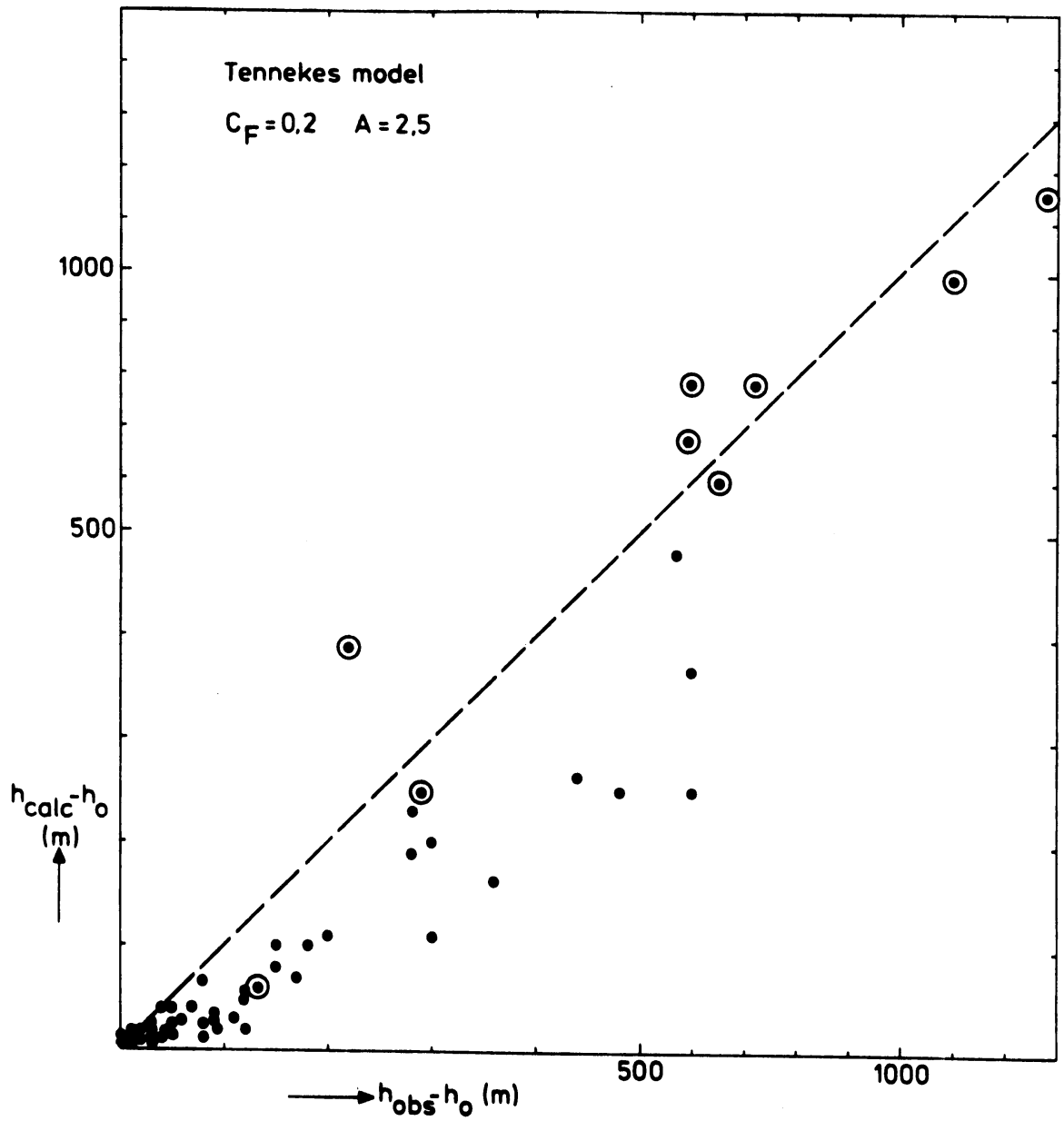

Figure 7.8. Tennekes model (eq. (7.3)-(7.4)). Mechanical entrainment included, with c_F=0.2 and A=2.5. Encircled are the convectively dominated cases.

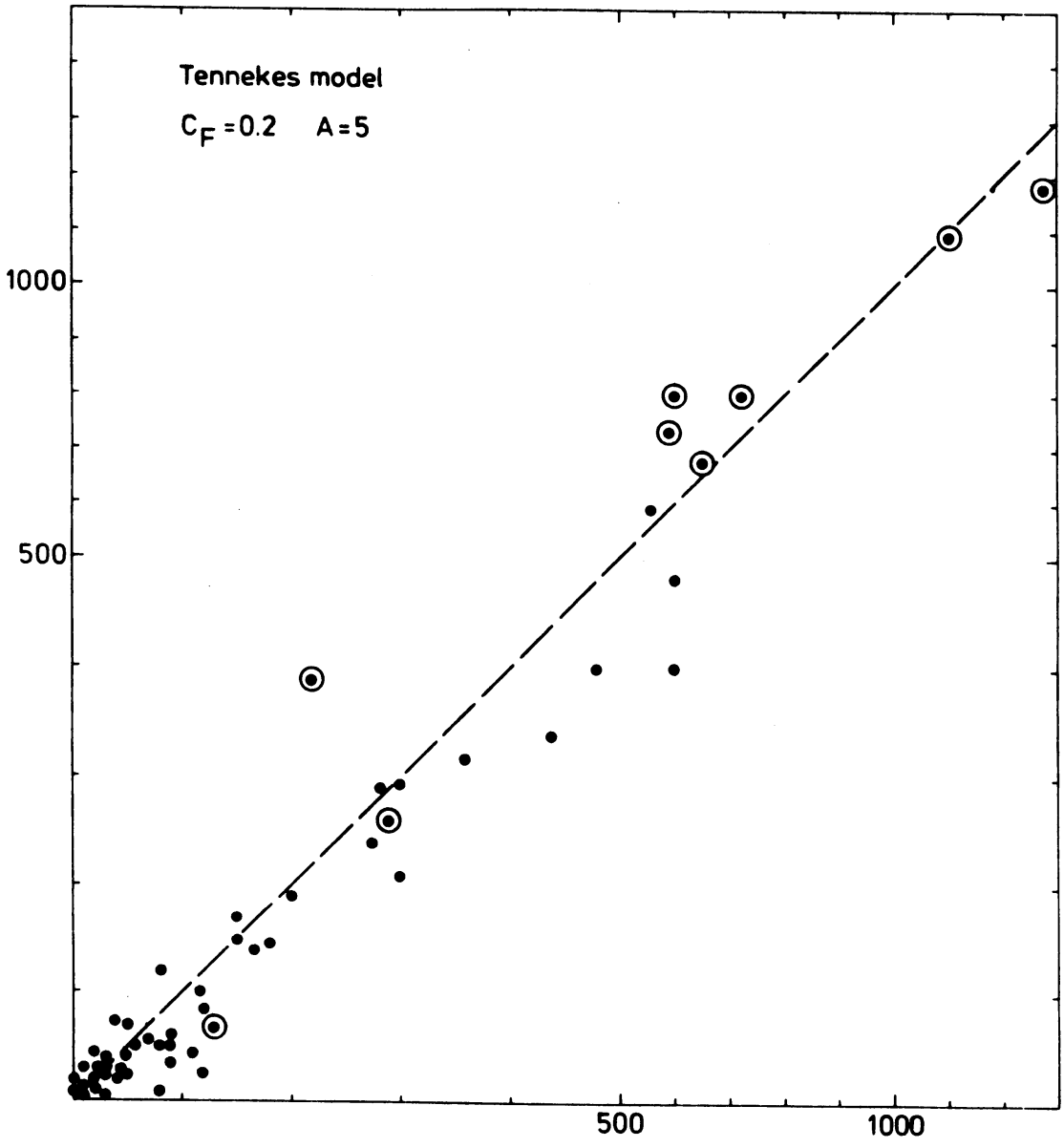

Figure 7.9. As Fig. 7.8 but now with c_F=0.2 and A=5.

We now come back to the issue of a variation of the convective entrainment coefficient c_F. We saw that $c_F = 0.2$ gave the best results in cases where mechanical entrainment is not important. We still have to look if the use of $c_F = 0.5$ can be discriminated from $c_F = 0.2$ if we consider all cases, thus including mechanical entrainment. We have to investigate if the cases that are not encircled in Fig. 7.8 and 7.9 do change significantly when we use $c_F = 0.5$ instead of $c_F = 0.2$. The results for $c_F = 0.5$ and A = 2.5 or A = 5 respectively are given in Figures 7.10 and 7.11 (page 116-117). The points in Fig. 7.10 indicate that there are two subsets in the calculations: those cases in which mechanical entrainment is not important (encircled) and for which h_{calc} is too high, and the other cases (not encircled) for which h_{calc} is too low. A change from A = 2.5 to A = 5 (Fig. 7.11) brings the latter subset in good agreement with the observations: $h_{calc}-h_o = 0.95\ (h_{obs}-h_o)$ for the not-encircled points. However, this differs only slightly from the results with $c_F = 0.2$, A = 5 (slope = 0.9, and about the same scatter). Thus we conclude that for this subset the value of c_F does not matter too much. In the subset of the convective cases, however, the calculated h with $c_F = 0.5$, A = 5 is significantly worse than with $c_F = 0.2$, A = 5. (Averaged over this subset $h_{calc}-h_{obs} = 220 \pm 130$m for $c_F = 0.5$, A = 5 in contrast to $h_{calc}-h_{obs} = 40 \pm 110$ m for $c_F = 0.2$, A = 5). We therefore conclude for all observations the model of eqs. (7.3)-(7.4) with $c_F = 0.2$, A = 5 is superior to the other combinations of c_F and A that we have considered.

In Fig. 12 (page 118-120) the time evolution of the mixed-layer height calculated with this model is shown in combination with our observations for each of the ten measuring days.

Conclusions.

The mixed-layer heights in convectively dominated situations, i.e. around noon on sunny days or even earlier when u_* is small, are quite well predicted by taking a value $c_F = 0.2$ and

neglecting mechanical entrainment in eq. (7.4): with this value the results have no bias and a standard deviation of ≈ 125 m.

In many cases the way in which the mixed-layer grows shortly after sunrise is strongly influenced by mechanical entrainment. The inclusion of this term in eq. (7.4) improves the model results significantly for these cases. Best results are obtained with a value of A = 5. This value is also suggested by the laboratory experiments of Kantha et al. (1977), and gives better results than the value A = 2.5, given by Kato and Phillips (1969).

When $c_F = 0.2$ and A = 5 are used in eqs. (7.3)-(7.4), and all cases are considered, then the mean deviation between calculations and observations is small (5%) and the overall standard deviation of $h_{calc}-h_{obs}$ is ≈ 80 m. When we confine ourselves to those cases for which $h_{obs}-h_o < 500$ m, then the standard deviation is only ≈ 40 m.

In the next few sections we are going to include more terms in the parameterization of the turbulent kinetic energy budget. However, since the model of this section already predicts the observed mixed-layer heights quite well, it is not very likely that more complicated models will lead to much better results.

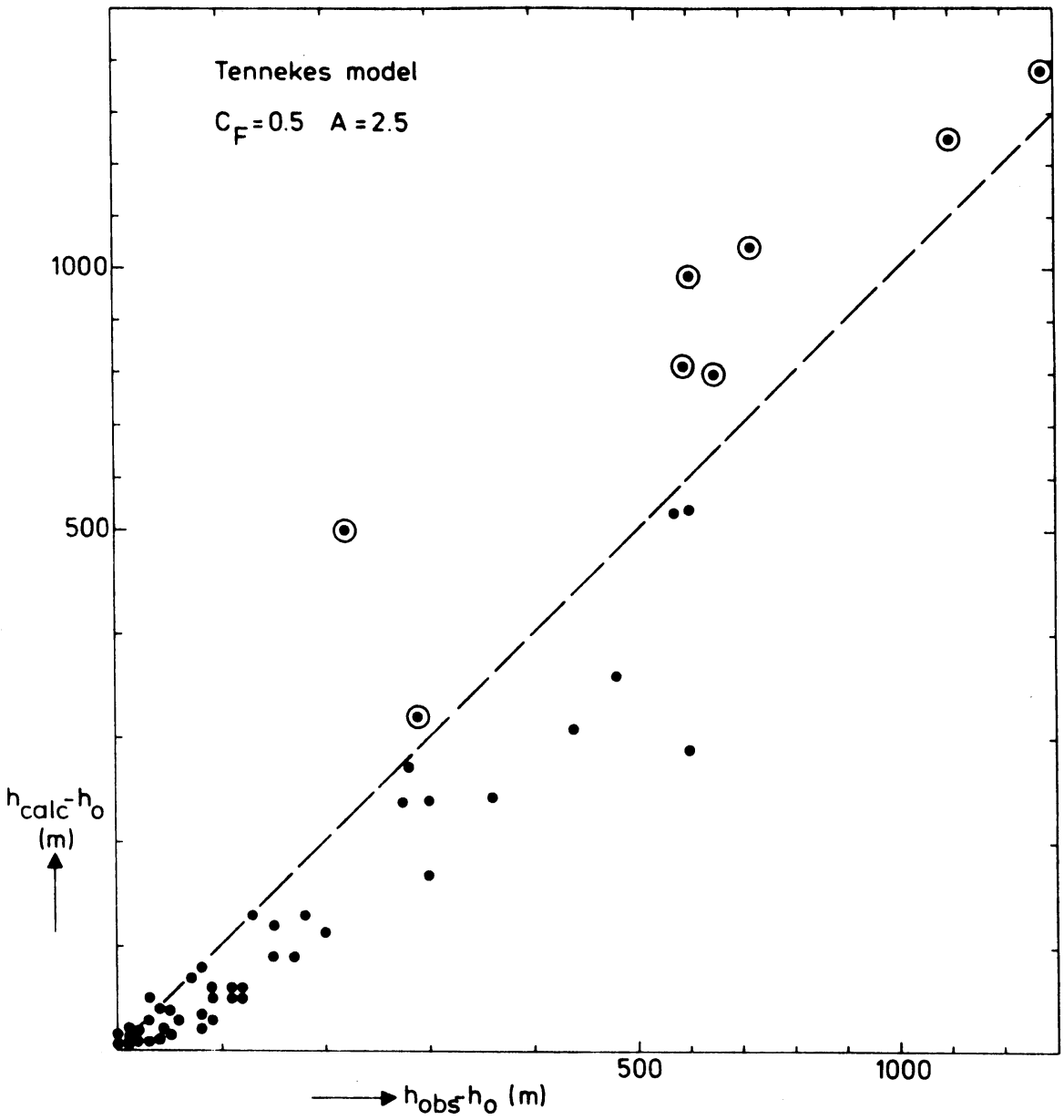

Figure 7.10. As Fig. 7.8 but now with c_F=0.5 and A=2.5.

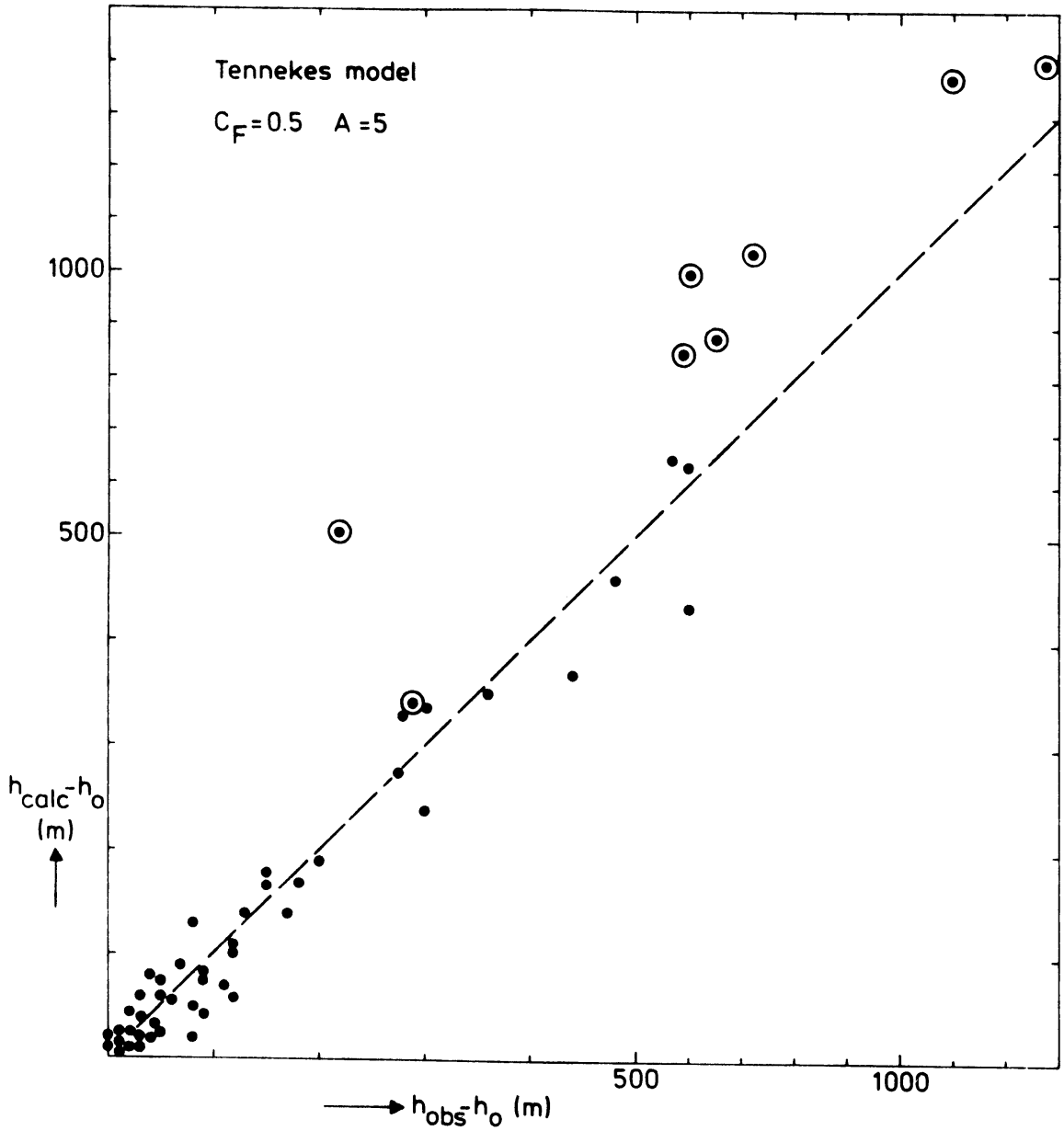

Figure 7.11. As Fig. 7.8 but now with c_F=0.5 and A=5.

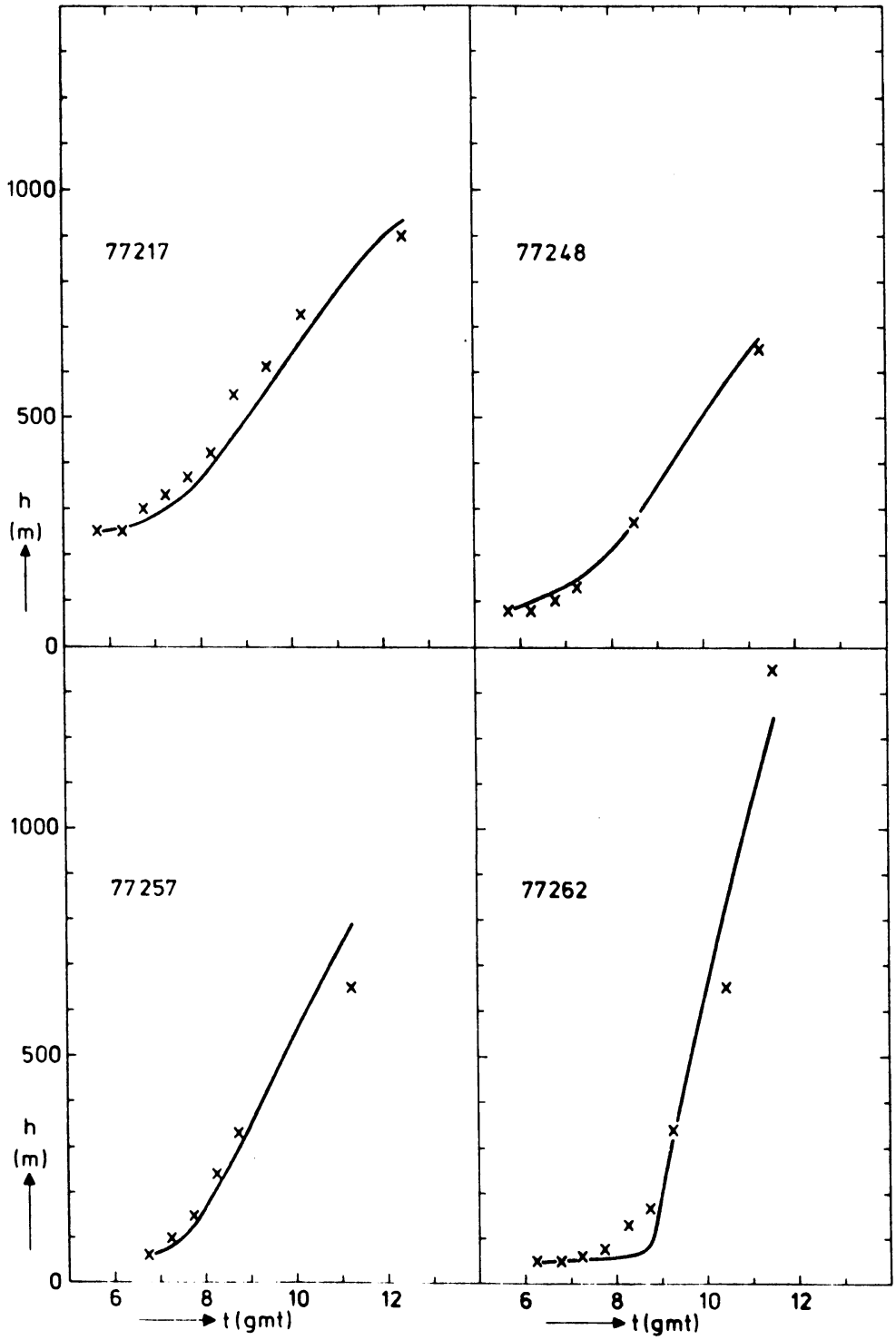

Figure 7.12. Comparison of the time evolution of the mixed-layer height as observed (✖) and calculated with Tennekes model (eq. (7.3) and (7.4)) with c_F=0.2 and A=5 (——), for each of the ten measuring days.

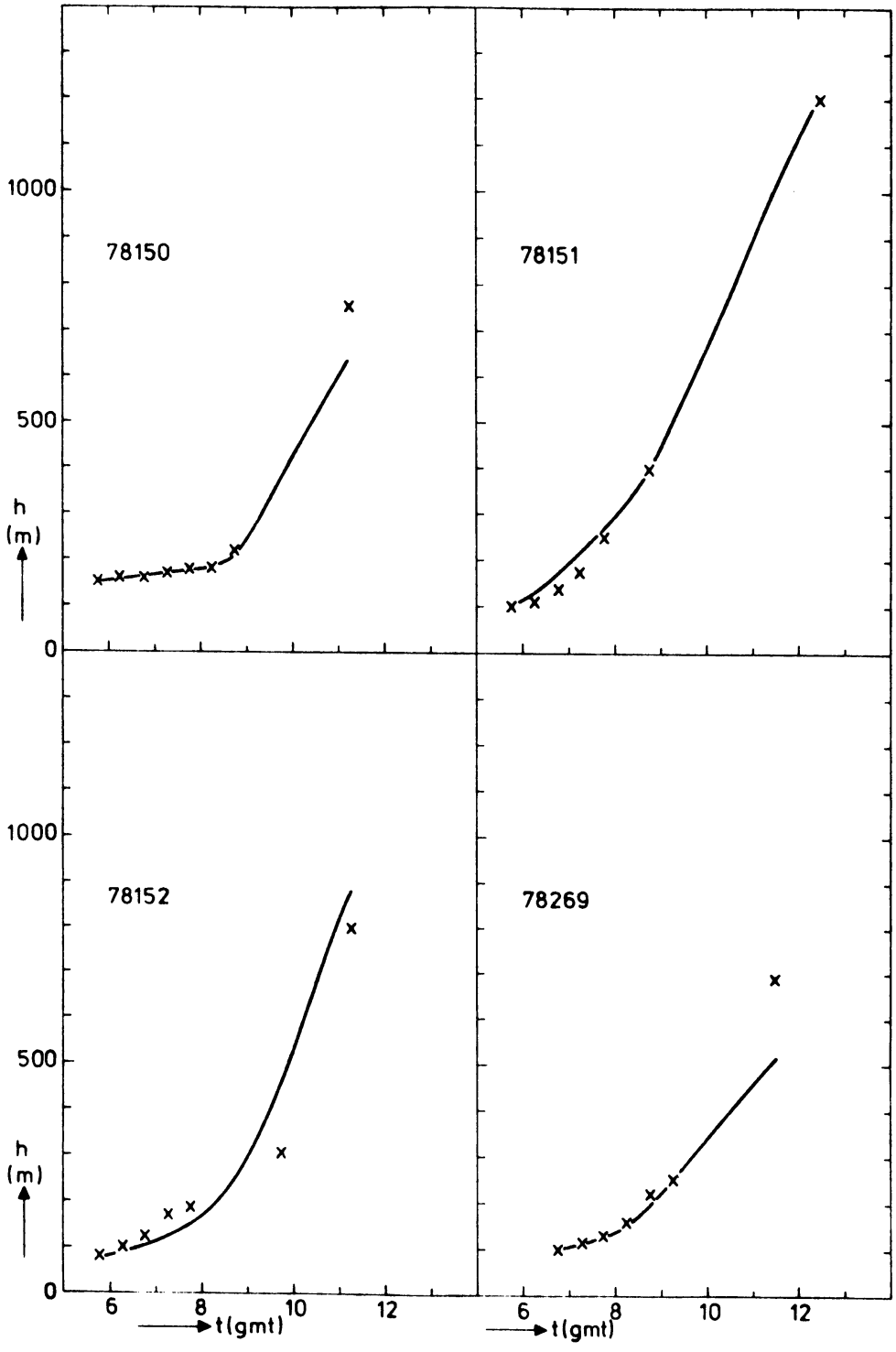

Figure 7.12 (continued).

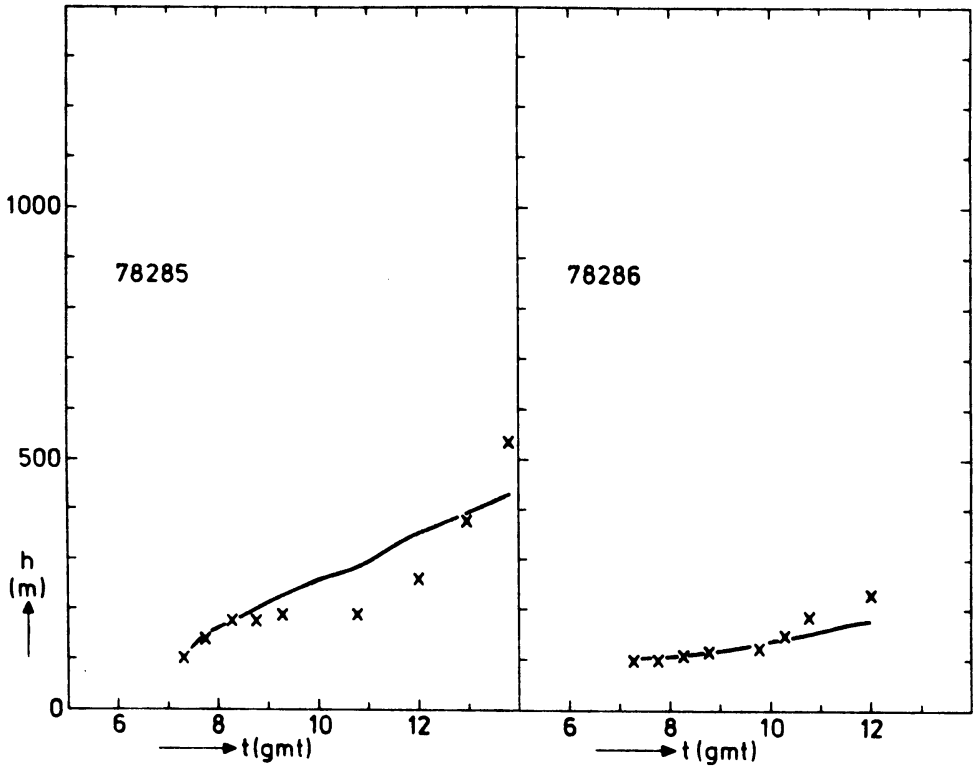

Figure 7.12 (continued).

7.3. The Zilitinkevich correction.

The model of section 7.2 cannot handle cases in which the Richardson number Ri_* gets very small (see section 3.6). In order to keep the entrainment rate finite an extra term has to be retained in the turbulent kinetic energy budget (Zilitinkevich, 1975). The combined Tennekes/Zilitinkevich model is given by eqs. (3.50) and (3.56), repeated here fore convenience:

$$\frac{dh}{dt} = \frac{c_F \sigma_w^3}{h\Delta b\ (1+c_T/Ri_*)}\ , \tag{7.5}$$

$$\sigma_w^3 = w_*^3 + (A/c_F)u_*^3, \tag{7.6}$$

where Ri_* is defined as $Ri_* = h\Delta b/\sigma_w^2$.

The value of c_T is not independent of c_F and A. We will continue to use $c_F = 0.2$ and $A = 5$. In section 3.6 we estimated in that context $c_T = 1.5$ from available laboratory experiments.

In comparison with the entrainment relation (7.3) of the foregoing section, eq. (7.5) differs by a factor of $1/(1+c_T/Ri_*)$. If we regard this effectively as a reduction factor of the entrainment coefficient c_F, we know from section 6.2 (eq. 6.14) that an appreciable effect on the solution for the mixed-layer height may be expected only for low values of Ri_* (of the same order as c_T).

The values of Ri_* in our observations were typically in the range 3-50, where the lower values occured later on the day. In order to see the effect of the Zilitinkevich term in (7.5), we selected for each day the observations for which $Ri_* < 10$ and compared the solutions for $c_T = 1.5$ and $c_T = 0$. The results are given in Fig. 7.13 (page 123). The values of h calculated with $c_T = 0$ are of course always higher than with c_T=1.5,

but the differences between the two are small, of the same order of magnitude as the measuring inaccuracy for h. Therefore we must state that in our measurements the effect of the Zilitinkevich term is negligibly small. It does not seem necessary to take it into account in atmospheric applications.

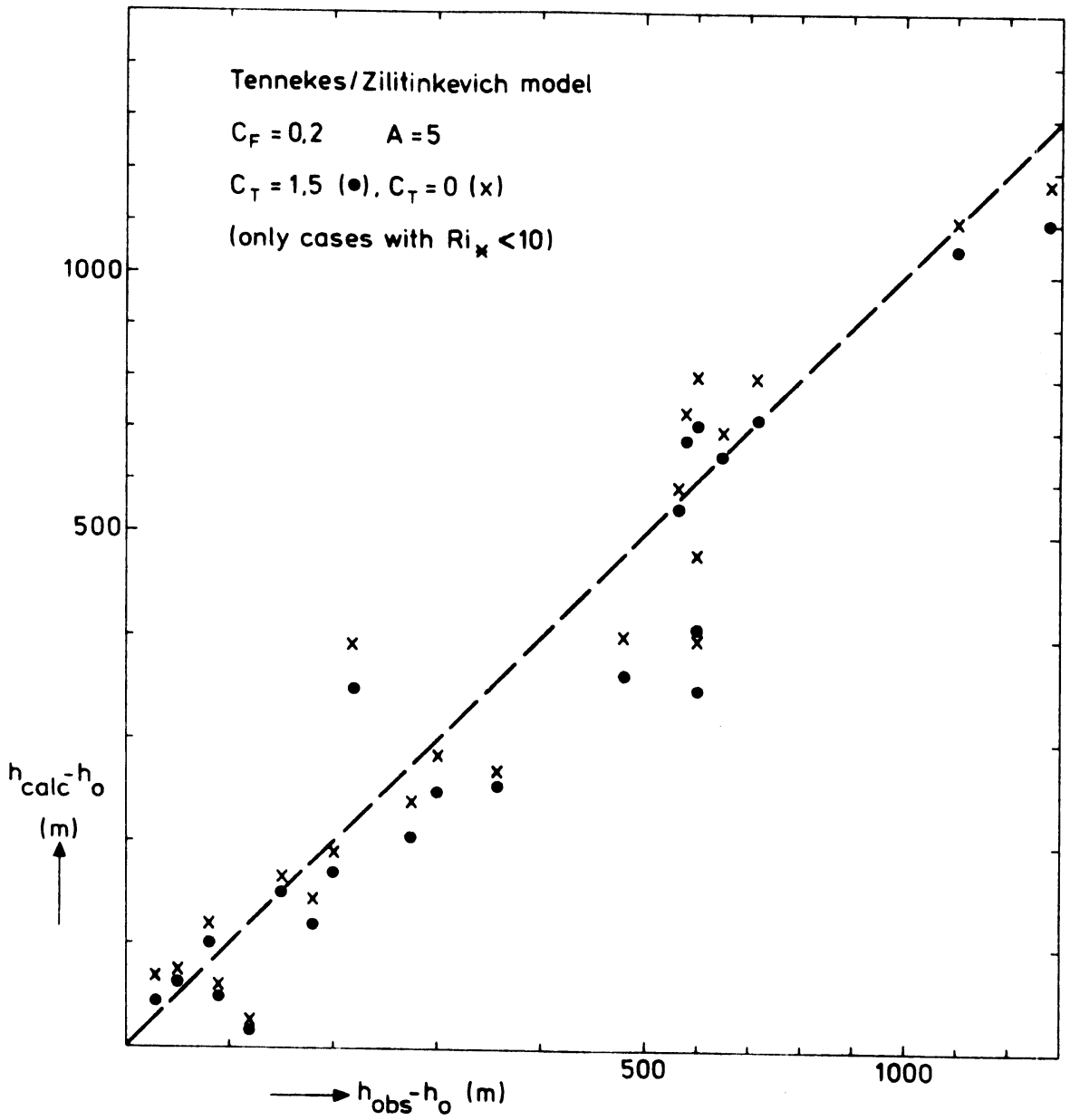

Figure 7.13. Results of the Tennekes/Zilintinkevich model (eq. (7.5)-(7.6)) with c_F=0.2 and A=5, for values c_T=0 (✖) and c_T=1.5 (●). Only cases with Ri_* < 10 are considered.

7.4. Zeman's model.

A further elaboration of the entrainment model was given by Zeman and Tennekes (1977). They tried to incorporate the limiting case of very large Richardson numbers. This model was discussed in section 3.6 and resulted in the following entrainment relations (see eqs. (3.60), (3.62), (3.65), (3.67):

$$\frac{dh}{dt} = \frac{c_F \sigma_w^3 - c_D \sigma_w^3 h/d}{h \Delta b (1+c_T/Ri_*)} , \tag{7.7}$$

$$\sigma_w^3 = w_*^3 + \eta^3 u_*^3, \tag{7.8}$$

where the dissipation length scale d is given by

$$d = \sigma_w/\omega_B . \tag{7.9}$$

The values of the coefficients were given in (3.68):

$$c_F=0.6 \quad c_D=0.03 \quad c_T=4.3 \quad \eta=2. \tag{7.10}$$

We do not yet include the effects of humidity so that $w_*^3 = (g/T_o)\overline{\theta'w'}_o\, h$ and $\Delta b = (g/T_o)\Delta\theta$.

Compared to the model of Tennekes (section 7.2) this model has various characteristic differences, partly compensating each other. The value of c_F is much large (0.6 versus 0.2), leading to higher entrainment rates. The second term in the nominator decreases the entrainment rate, and the same holds for the denominator.

Before we analyze these differences further, we first give in Fig. 7.14 (page 126) the results of h, calculated with (7.7)-(7.10). It is rather surprising that despite the considerably more

complicated model and different coefficients there is hardly any difference with Fig. 7.9, where we calculated h with Tennekes' model. How can we explain that?

We therefore repeat the entrainment rate of section 7.2 with its constants:

$$\left(\frac{dh}{dt}\right)_T = 0.2 \frac{(w_*^3 + 25\, u_*^3)}{h\, \Delta b} . \qquad (7.11)$$

After some algebra we can rewrite (7.7)-(7.10) in the form

$$\left(\frac{dh}{dt}\right)_Z = 0.6\, R \frac{(w_*^3 + 8\, u_*^3)}{h\, \Delta b} , \qquad (7.12)$$

where $R = (1 - 0.05\, h/d)/(1 + 4.3/Ri_*)$ can be regarded as a "reduction factor".
We monitored the value of R throughout our calculations. In cases where w_* was small compared to u_* (early morning hours) the value of R was about 1. Then the nominators of (7.11) and (7.12) have the same value ($5\, u_*^3$ and $4.8\, u_*^3$ respectively). When u_* was small compared to w_* (convective situations), the value of R was about 0.5. Then again the nominators of (7.11) and (7.12) are not significantly different ($0.2\, w_*^3$ and $0.3\, w_*^3$ respectively) in view of section 6.2.

We conclude that for practical applications in the atmosphere it is not necessary to use a complicated entrainment model. The simpler model of eqs. (7.3)-(7.4) with $c_F = 0.2$ and $A = 5$ gives the same results.

We also did calculations with another formulation for the dissipation length scale d, expressed in (3.61):

$$\tfrac{1}{2}\, \sigma_w^2 = \Delta b.d + \tfrac{1}{2}\, \omega_B^2 d^2. \qquad (7.13)$$

For small Δb, large ω_B this expression is equivalent to (7.9).

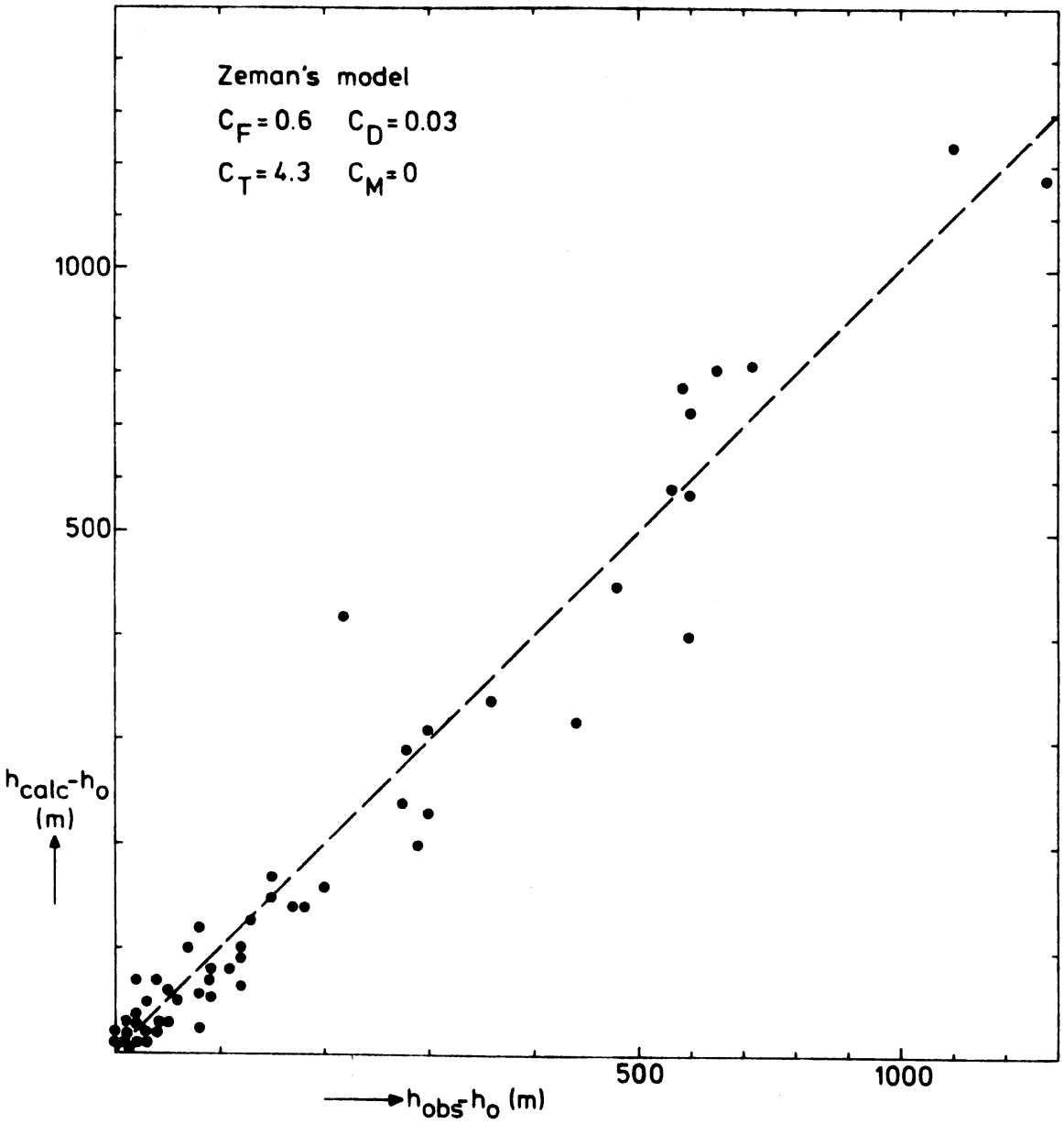

Figure 7.14. Results of Zeman's model (eq. (7.7)-(7.9)) with c_F=0.6, c_D=0.03, c_T=4.3 and n=2.

When Δb is large (not small compared to $\frac{1}{2}\ \omega^2_B d$), (7.13) results in a smaller value of d than (7.9). However, (7.7) leads only to realistic entrainment when $h/d < c_F/c_D = 20$, since we have to assure that $dh/dt > 0$. When we used (7.13) instead of (7.9) this constraint was frequently violated in the early morning hours, leading to unrealistic results. Therefore we must conclude that (7.13) should not be used in connection with (7.7).

7.5. Models based on the integrated budget for turbulent kinetic energy.

In the preceding sections we have considered entrainment models originating from the turbulent kinetic energy budget applied locally at the interface between turbulent and non-turbulent fluid, in conditions where there is no discontinuity in the wind at the top of the mixed layer, i.e. $\Delta\underset{\sim}{U} = 0$ (the influence of $\Delta\underset{\sim}{U}$ is discussed in section 7.7). Strictly speaking this local approach should also lead to the use of local length scales and velocity scales. This is not very attractive when separate equations for these local scales would be needed, because we would then lose the simple concept of the one-layer model. Therefore, in the parameterization of the local energy budget, local scales are avoided, and in most models instead velocity and length scales are used that are representative for the bulk of the mixed layer, i.e. σ_w or h.

The parameterization of the vertically integrated kinetic energy budget quite naturally leads to the use of these bulk scales. The result of this approach was formulated in eq. (3.71). When we consider cases for which $\Delta\underset{\sim}{U} = 0$, and for which we neglect the Zilitinkevich-correction, associated with B_4, then we may rewrite (3.71) as:

$$\frac{dh}{dt} = \frac{B_3 \, (w_*^3 + (B_1/B_3)u_*^3)}{h \, \Delta b} \, .$$

This has the same form as the model of Tennekes, formulated in (7.3) and (7.4):

$$\frac{dh}{dt} = \frac{c_F \, (w_*^3 + (A/c_F)u_*^3)}{h \, \Delta b} \, .$$

We thus see that the models which are based on the parameterization of the vertically integrated turbulent kinetic energy budget do not differ from the model that we already considered and which led to good agreement between calculations and observations.

7.6. The correction for humidity in buoyancy effects.

Thus far we have not considered the effects of humidity on buoyant accelerations. We have assumed that the air is dry, and therefore we wrote for the buoyancy $b = g\,\theta/T_o$.

We know however that humidity is not just a passive variable that only responds to the mixed-layer growth. Water vapor, like temperature, influences the density of air , and thus affects the buoyant accelerations.

Moist air is characterized by its potential temperature θ and its specific humidity q. The combined effects of θ and q on the density ρ may be represented by the virtual potential temperature $\theta_v = \theta\,(1+0.61\,q) + 0.61\,q\,T_o$ (see section 3.2). For the buoyancy $b = -g\rho/\rho_o$ we can write to first order in the deviations from a reference state:

$$b = g\,\frac{\theta_v}{T_o} = \frac{g}{T_o}\,(\theta + 0.61\,q\,T_o). \tag{7.14}$$

For the mixed-layer equations, the effects of humidity manifest themselves in the following way:

$$b_m = \frac{g}{T_o}\,(\theta_m + 0.61\,q_m\,T_o), \tag{7.15}$$

$$\Delta b = \frac{g}{T_o}\,(\Delta\theta + 0.61\,T_o\,\Delta q), \tag{7.16}$$

$$\overline{b'w'}_o = \frac{g}{T_o}\,(\overline{\theta'w'}_o + 0.61\,T_o\,\overline{q'w'}_o), \tag{7.17}$$

$$w_*^3 = h\,.\,\overline{b'w'}_o. \tag{7.18}$$

These equations contain some interesting features of the buoyancy flux $\overline{b'w'}_o$ and the buoyancy jump Δb.
Through the inclusion of humidity, $\overline{b'w'}_o$ increases by a factor of $(1 + 0.61\,T_o\,\overline{q'w'}_o/\overline{\theta'w'}_o)$ with respect to the

same without humidity. For c_p = 1000, L = 2.5 x 10^6, this is approximately equal to (1 + 0.07/B), where B is the Bowen ratio of the sensible and latent heat flux, B = H/LE = $c_p\overline{\theta'w'}_o/L\overline{q'w'}_o$. Thus for the surface buoyancy flux, the inclusion of humidity is equivalent to multiplying its dry value with a factor (1 + 0.07/B). For the days on which we took data the Bowen ratio was greater than 0.4 for most of the time, which makes this multiplication factor less than 20%. We have already seen in section 6.2 that such an increase in the surface heat input leads to changes in the mixed-layer height of the order of 10% (when the other variables remain unchanged).

Another effect of the inclusion of humidity is the decrease of Δb. This is due to the fact that $\Delta q < 0$ in almost all practical atmospheric conditions. Since moist air is lighter than dry air (with the same pressure and temperature), moisture effectively decreases the buoyancy jump by a factor of $(1 + 0.61\ T_o\ \Delta q/\Delta\theta)$. This reduction is usually small in the early stages of the inversion rise after a clear night, since $\Delta\theta$ is then quite large (if we take typical values $\Delta\theta$ = 4 °C, Δq = -2 gr/kg, T_o = 290 °K then the reduction of Δb due to humidity is less than 10%). Later on the day, however, $\Delta\theta$ usually gets small (especially when γ_θ is small) and the inclusion of humidity may drastically influence Δb. E.g. when $\Delta\theta$ = 0.5 °C, Δq = -2 gr/kg, T_o = 290 °K then Δb is reduced to $\approx$30% of its original value. Since dh/dt is proportional to the inverse of Δb, we may expect that under certain conditions dh/dt is largely influenced by the effect of Δq on Δb. This is quite embarassing from the point of view of measurements: humidity is less accurately determined with radiosondes than temperature while it might have a considerable impact.

We calculated the effects of humidity with the model of Tennekes (section 7.2) with c_F = 0.2 and A = 5. We first simulated the effect of humidity on the surface buoyancy flux, i.e. we used (7.17) but did not consider the effect of Δq on Δb in (7.16). For this purpose we increased the surface heat input in the dry version of the model with 20%. Next we integrated the

model, fully accounting for the humidity effects through (7.16) and (7.17). The results are given in table 7.2. Since humidity has small effects in the initial stage of mixed layer growth, we selected only those observations for which $h > 2\ h_o$. This table shows that the mixed-layer heights for the model which includes humidity in the buoyancy are always larger than the results for the dry model. In most cases the differences are smaller than 10%. However, some results which are underlined show differences that are larger than 20%, sometimes even much larger. These large differences occur on days with a small stable temperature gradient γ_θ, and thus small values of $\Delta\theta$. Then the humidity correction in Δb is relatively important, which makes the results sensitive to humidity measuring errors.

Table 7.2. Effect of humidity on h. Entrainment model: $dh/dt = 0.2\ \sigma_w^3/h\Delta b$, $\sigma_w^3 = w_*^3 + 25\ u_*^3$.
h_1: no humidity included (dry model).
h_2: dry model with surface heat flux increased by 20%.
h_3: humidity included.

day	time (gmt)	h_{obs} (m)	h_1 (m)	h_2 (m)	h_3 (m)
77217	849	550	460	465	485
	922	610	520	540	585
	1005	730	650	655	680
	1230	900	935	1040	1040
77248	829	280	270	270	300
	1115	650	670	690	720
77257	815	240	205	220	225
	845	335	300	320	320
	1115	650	790	860	830
77262	845	170	75	90	100
	912	340	310	460	485
	1020	650	850	980	1015
	1130	1350	1230	1375	1410
78150	845	220	205	215	220
	1115	750	630	810	955
78151	750	250	265	270	280
	850	400	385	410	430
	1230	1200	1260	1440	1590
78152	945	300	470	590	630
	1115	800	880	1150	1450
78269	915	250	255	260	265
	1130	700	500	520	560
78285	1257	380	390	410	410
	1353	540	430	450	455
78286	1200	230	170	200	200

7.7. The effect of wind shear at the inversion base.

Thus far we were only concerned with entrainment caused by turbulence produced in the bulk of the mixed layer or generated at the lower surface. Another mechanism, associated with turbulence produced by local wind shear at the top of the mixed layer, might be important too. In the turbulent kinetic energy budget the net contribution of this mechanism to the buoyancy flux at the interface, $\overline{b'w'}_h$, was parameterized as (see section 3.7):
$B_2\left(|\Delta \underset{\sim}{U}|^2/h \right) dh/dt$, where B_2 is a constant.

There are severe problems with this term when we apply it to the atmosphere.

The momentum jump $\Delta \underset{\sim}{U}$, just like the other jumps, is calculated by means of a rate equation. We recapitulate these rate equations for ΔU and ΔV (eq. (3.17), (3.18), where for the moment we assume that $(dU/dz)_+ = (dV/dz)_+ = 0$ and where we neglect the last (small) terms in these equations. We also use (3.22) and (3.23). There results:

$$\frac{d}{dt}(h\,\Delta U) = -\overline{u'w'}_o + f\,h\,\Delta V, \tag{7.19}$$

$$\frac{d}{dt}(h\,\Delta V) = -\overline{v'w'}_o - f\,h\,\Delta U. \tag{7.20}$$

These equations permit a solution in the form of an inertial oscillation. If we write $\Delta W = \Delta U + i\,\Delta V$, then the solution is (for constant surface fluxes):

$$h\,\Delta W = C_o\, e^{-ift} + (-\overline{u'w'}_o - i\,\overline{v'w'}_o)/if\ . \tag{7.21}$$

The equations for ΔU, ΔV thus allow an inertial oscillation with an amplitude C_o that is completely determined by the initial conditions!
However, as we have shown in chapter 5, the initial conditions

for ΔU, ΔV could only be determined very roughly. This makes the calculated ΔU, ΔV suspicious during the whole day and makes the use of terms in the entrainment model that are based on them of doubtful value.

Our calculations with an entrainment model including this inversion-based wind shear were indeed of poor value. We used the model of eq. (3.71) but abandoned the last term (the Zilitinkevich-correction). Using (3.26), we can re-arrange this equation to

$$(\Delta b - B_2 \, |\Delta \underset{\sim}{U}|^2/h) \, \frac{dh}{dt} = B_1 u_*^3 + B_3 w_*^3.$$

The right hand side is always positive. In order to assure that $dh/dt > 0$ (otherwise the model is not valid) we must have

$$\Delta b > B_2 \, |\Delta \underset{\sim}{U}|^2/h.$$

In our calculations this constraint was frequently violated, leading to unrealistic results.

In section 8.3 we will give detailed results for the wind regime in the mixed layer. They also show poor agreement with the observations, indicating that the mixed-layer equations do not behave well for momentum.

7.8. Conclusions about the mixed-layer height.

We have calculated the mixed-layer height with the equations (3.12)-(3.26), supplemented by an entrainment model of increasing complexity.

On convective days, encroachment explains about 80% of the observed increase in h at noon. The rest has to be explained by entrainment. The model of Tennekes (1973), including only convective entrainment with an entrainment coefficient of $c_F = 0.2$, predicts the mixed-layer height in convectively dominated cases without bias and with a standard deviation of ≈ 125 m, which is comparable to the error in h determined from a radiosonde profile at noon.

A model which includes only convective entrainment does not predict the observed mixed-layer height well when w_* is small compared to u_*. This is usually the case in the first few hours after sunrise. The predicted h then is much too low.

When mechanical entrainment is included in Tennekes' model with an entrainment coefficient A = 5, the predicted h corresponds to the observations with a bias of only -5%. The remaining variance of $h_{calc}-h_{obs}$ is ≈ 80 m when we consider all cases, and only ≈ 40 m when $h_{obs}-h_o < 500$ m. The value A = 5 is supported by the laboratory experiments of Kantha et al. (1977).

The incorporation of the Zilitinkevich correction term, which accounts for a finite entrainment velocity at very low Richardson numbers, only weakly affects our results. For atmospheric applications it is apparently small.

The model of Zeman (Zeman and Tennekes, 1977) leads to results which are not significantly different from Tennekes' model in all cases. Its complexity is not justified by the results of our observations.

Models based on the integrated turbulent kinetic energy budget are not different from Tennekes' model and lead to the same results.

Incorporation of humidity in the buoyancy affects the mixed-layer equations in two ways. The surface buoyancy flux increases with respect to the dry case with a factor which depends on the surface Bowen ratio. In our observations this increase was at most 15-20%. The second effect is that the buoyancy jump at the interface decreases with respect to the dry case with a factor $1 + 0.61\ T_o\ \Delta q/\Delta\theta$, since $\Delta q < 0$. This effect of humidity may occasionally lead to a sharp increase in h_{calc} in situations with small $\Delta\theta$, small γ_θ. However, measurements of the humidity profiles are not very accurate.

The effect of wind shear at the inversion base was also considered. The results were quite disappointing. This is partly due to the difficulty in defining the correct initial conditions from observed profiles, partly due to the existence of spurious oscillations in the model.

We conclude that our observations on the height of the mixed layer agree with the model of Tennekes (section 7.2) if $c_F = 0.2$ and $A = 5$ are used.

8. OBSERVATIONS AND CALCULATIONS OF OTHER VARIABLES.

Apart from the height, mixed-layer models also predict the behavior of the mean mixed-layer temperature, humidity, and momentum. We will now compare our observations of these quantities with the calculations from the entrainment model of section 7.2.

8.1. Mixed-layer potential temperature.

In section 6.2 we have seen that the mixed-layer temperature in convectively dominated cases is not very sensitive to the entrainment model: a change in the entrainment coefficient c_F from 0.2 to 0.5 changes Θ_m at noon less than 0.1 ^{o}C. The temperature is more sensitive to changes in the integral heat input and in the stable gradient γ_θ.

In cases where mechanical entrainment is also important, the calculated mixed-layer temperature does of course depend on the entrainment model: the negative heat flux at the inversion base may be larger than the surface heat flux.

The calculated and observed increase in Θ_m are compared in Fig. 8.1. The agreement is generally good. The standard deviation is $\pm$ 0.5 ^{o}C, and the maximum differences are less than 1 ^{o}C except for a few points, which come from days 78150, 78285 and 78286. On these days the observed temperature at noon is up to 2 ^{o}C larger than the calculated one. On days 78285 and 78286 the mixed layer is capped by a layer with a large stable gradient ($\gamma_\theta \approx$10-20 K/km). Therefore the increase in h over the day is only small (h $\sim$300 m at noon). In those cases the temperature increase is much more sensitive than h to a small change in γ_θ or in the integral heat input. When we varied γ_θ with 1 K/km and the heat flux with 10%, then the calculated temperature at noon varied as much as 1 ^{o}C, while h hardly changed. This indicates that in such situations the mixed-layer temperature calculations are not very accurate. On day 78150 the differences could not be attributed to the model characteristics, but was caused by advective temperature changes.

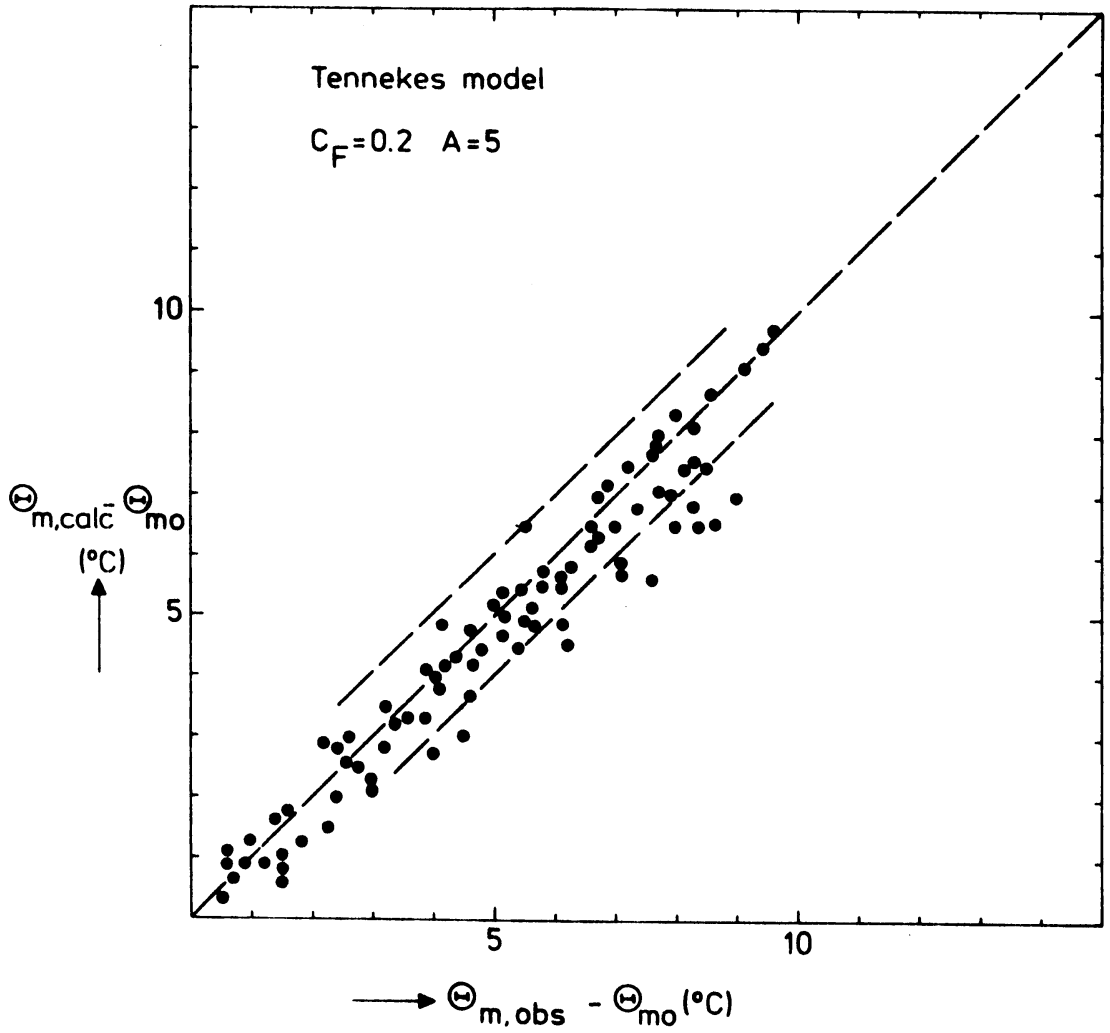

Figure 8.1. Calculated and observed increase in mixed-layer potential temperature.

8.2. Mixed-layer humidity.

We discussed the effects of humidity on the buoyancy in section 7.6. These effects are twofold: the surface buoyancy flux increases and the buoyancy jump decreases. We concluded that the resulting effect on the mixed-layer height may be large in cases where the lapse rate γ_θ is small. Then the buoyancy jump may be appreciably affected by Δq. However, in those cases the calculated h was much larger than the observed value. We attributed this to inaccurate measurements of the humidity profile by radiosondes and excluded the humidity from the buoyancy for best predictions of h.

The mean humidity in the mixed layer, q_m, may be calculated by eqs. (3.15), (3.20) and (3.25), provided that γ_q and $\overline{q'w'}_o$ are given.

For those days on which humidity measurements were available, the calculated and observed values of q_m are given in Fig. 8.2. For the calculations we used the model of section 7.2 with $c_F = 0.2$ and $A = 5$. The results are reasonably good, except on a few days (77248, 78151, 78286). Especially on day 77248 the different behavior of observations and calculations in striking.

For an analysis of the mechanisms that influence q_m we refer to eq. (3.15) and (3.25) which we repeat here in combined form:

$$\frac{dq_m}{dt} = \overline{q'w'}_o + \Delta q \frac{dh}{dt}. \qquad (8.1)$$

The first term on the right hand side, the surface moisture flux $\overline{q'w'}_o$, is positive in daytime, tending to increase q_m, just like the surface heat input tends to increase the mixed-layer temperature. The second term represents the change in q_m due to entrainment. Since $\Delta q < 0$ and $dh/dt > 0$, this term represents a loss for q_m. This is in contrast with the cor-

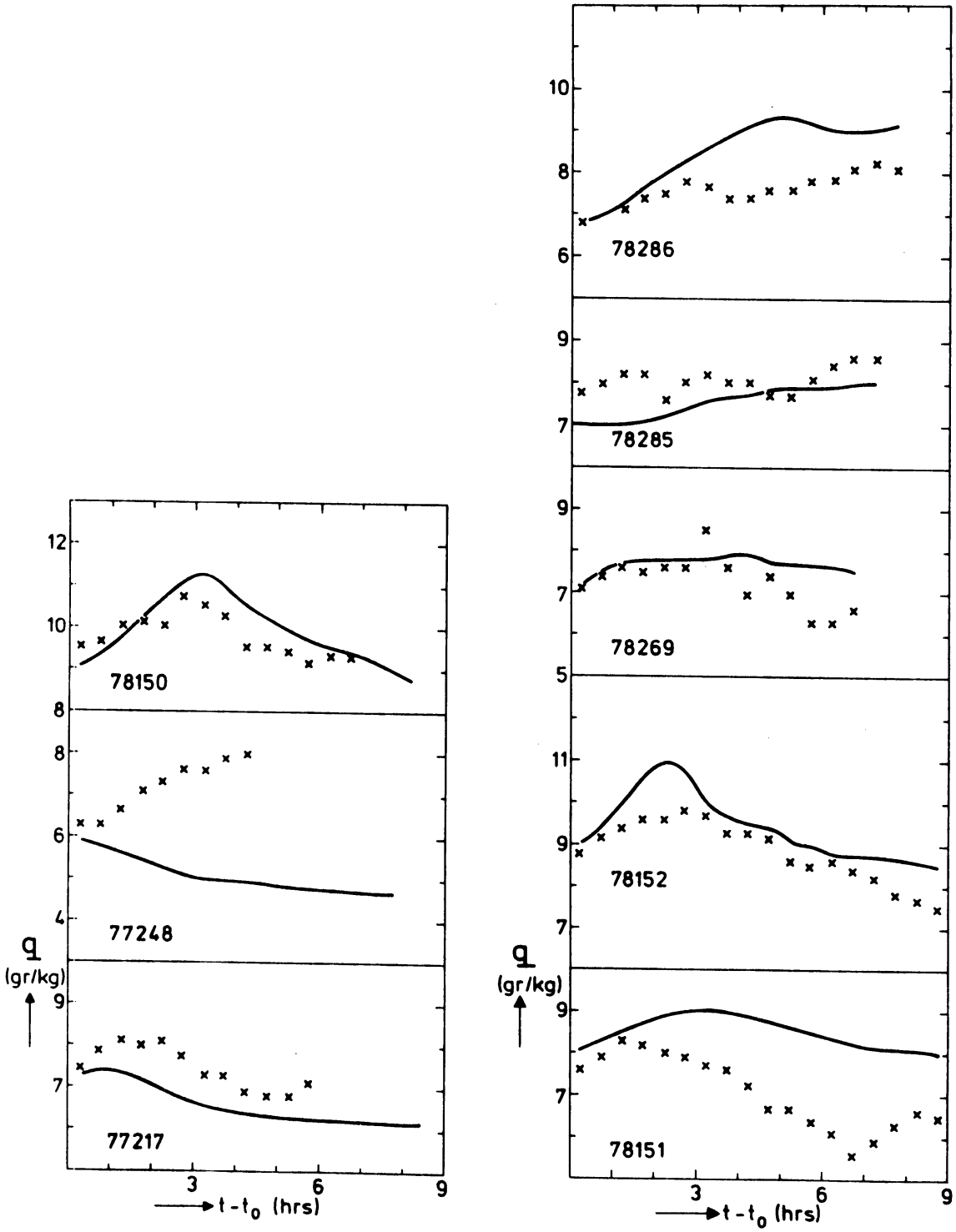

Figure 8.2. Calculated (——) and observed (×) mixed-layer specific humidity.

responding equation for Θ_m, where entrainment always gives a positive contribution to $d\Theta_m/dt$, since $\Delta\Theta > 0$. Even when $\overline{q'w'}_o > 0$ these different signs in (8.1) may thus lead to a decrease in q_m due to the combined effect of Δq and dh/dt (and γ_q). Accurate measurements of Δq and γ_q are thus required for the prediction of q_m.

8.3. Mixed-layer momentum.

We will now look more closely into the equations governing the mixed-layer momentum and the velocity jumps. We repeat them here for convenience:

$$\frac{dU_m}{dt} = f\,(V_m - V_{gm}) + (\overline{u'w'}_o + \Delta U\,\frac{dh}{dt})/h, \tag{8.2}$$

$$\frac{dV_m}{dt} = -f\,(U_m - U_{gm}) + (\overline{v'w'}_o + \Delta V\,\frac{dh}{dt})/h, \tag{8.3}$$

$$\frac{d\Delta U}{dt} = \gamma_u\,\frac{dh}{dt} - (\overline{u'w'}_o + \Delta U\,\frac{dh}{dt})/h + f\,\Delta V, \tag{8.4}$$

$$\frac{d\Delta V}{dt} = \gamma_v\,\frac{dh}{dt} - (\overline{v'w'}_o + \Delta V\,\frac{dh}{dt})/h - f\,\Delta U. \tag{8.5}$$

In (8.2)-(8.5) we have combined eqs. (3.12), (3.13), (3.17), (3.18), (3.22) and (3.23) and we have written $\gamma_u = (\partial U/\partial z)_+$, $\gamma_v = (\partial V/\partial z)_+$. Furthermore we have put $\overline{w}_h = 0$ and neglected the last term in eqs. (3.17) and (3.18).

The characteristics of eqs. (8.2)-(8.5) differ essentially from their counterparts, e.g. for temperature, in the action of the Coriolis force and the pressure gradient, through which both components of the wind interact.

We will now look first at the behavior of the wind above the mixed layer, in particular at the behavior of γ_u and γ_v. In contrast to e.g. temperature, these stable gradients are not steady. Above the mixed layer the turbulent momentum flux is zero and it is easy to show that γ_u, γ_v are governed by:

$$\frac{\partial}{\partial t}\,\gamma_u = f(\gamma_v - \gamma_{vg}), \tag{8.6}$$

$$\frac{\partial}{\partial t}\gamma_v = -f(\gamma_u - \gamma_{ug}), \tag{8.7}$$

where $\gamma_{ug} = (\partial U_g/\partial z)_+$, $\gamma_{vg} = (\partial V_g/\partial z)_+$. The solution of (8.6)-(8.7) is quite simple when the geostrophic wind is stationary. If we write $W = U + i\,V$ and $W_g = U_g + i\,V_g$, then the solution is:

$$\gamma_W = \gamma_{Wo}\, e^{-ift} + \gamma_{Wg}, \tag{8.8}$$

where γ_{Wo} is determined by the initial conditions. We thus see that the gradients in the wind above the boundary layer are in general a function of time, even when γ_{Wg} is not.

We now assume that the geostrophic wind is stationary and independent of height, i.e. $\gamma_{Wg} = 0$. If then at $t = t_o$ the actual wind is also independent of height (not necessarily equal to the geostrophic wind), it follows from (8.8) that $\gamma_W = 0$ for all times. However, even in this case the actual wind above the mixed layer may still depend on time. Integration of (8.8) gives:

$$W = W_g + (W_o - W_g)\, e^{-ift}, \tag{8.9}$$

which represents an inertial oscillation.
Furhtermore we have seen in section 7.7 that, with $\gamma_W = 0$ and with a constant friction, eqs. (8.4)-(8.5) also have a solution in the form of an inertial oscillation for the velocity jump:

$$h\,\Delta W = C_o\, e^{-ift} - i\,u_*^2/f, \tag{8.10}$$

where we have taken the x-axis along the constant friction. C_o is determined by the initial conditions:
$C_o = h_o\,\Delta W_o + i\,u_*^2/f$. With the relation $W_m = W - \Delta W$, we can now write the solution for the mixed-layer momentum in this case:

$$W_m = (W_g + i\,\frac{u_*^2}{fh}) + (W_o - W_g - \frac{C_o}{h})\,e^{-ift} \quad . \tag{8.11}$$

This solution represents an inertial oscillation of W_m around $W_g + i\,u_*^2/fh$, with period $T = 2\pi/f$ and amplitude $|W_o - W_g - \frac{C_o}{h}|$. At $t = t_o$ this amplitude is $|W_{mo} - W_g - i\,u_*^2/fh_o|$.

When we further simplify the situation by taking $W = W_g$, i.e. the wind above the mixed layer is always geostrophic, then (8.11) reduces to:

$$W_m = (W_g + i\,\frac{u_*^2}{fh}) + (-\Delta W_o\,\frac{h_o}{h} - i\,\frac{u_*^2}{fh})\,e^{-ift}. \tag{8.12}$$

Again an inertial oscillation. The amplitude decreases with h_o/h which is not very fast. Further the center point shifts with respect to W_g with $i\,u_*^2/fh$. This is not a small shift in the early morning hours: e.g. for $u_* \approx 0.3$ m/s, $f = 10^{-4}$ s^{-1}, $h = 200$ m, u_*^2/fh amounts to 5 m/s.

It is quite intriguing that despite all the simplifications the behavior of the mixed-layer momentum remains quite complicated. Inertial oscillations make the solutions dependent on the initial conditions.

We will now compare the model solutions with our observations. Since we measured the wind profile above the mixed layer with radiosondes, we have an estimate of γ_u and γ_v. From surface pressure observations we determined the geostrophic wind at the surface. We now follow two procedures. First we suppose that the geostrophic wind has no vertical gradient, i.e. we use everywhere the surface geostrophic wind. Second we take the geostrophic wind above the mixed layer equal to the wind as measured by the radiosondes.

We first used eqs. (8.2)-(8.5) in the form as they are given. We determined γ_u, γ_v from the radiosondes, U_g and V_g were taken independent of height, $\overline{u'w'}_o$ and $\overline{v'w'}_o$ are measured and prescribed as a function of time. For the entrainment we used the model of section 7.2 with $c_F = 0.2$ and $A = 5$. The comparison of these calculations with the observations is given in Figure 8.3. These results are quite remarkable: in most cases the calculated mixed-layer wind starts an inertial oscillation after $t = t_o$ and deviates largely from the observed wind in which such an oscillation is hardly seen.

The second procedure that we considered was to take the geostrophic wind above the mixed layer equal to the measured wind. As a consequence, eqs. (8.4)-(8.5) for ΔU, ΔV, change into:

$$\frac{d\Delta U}{dt} = \gamma_u \frac{dh}{dt} - \frac{dU_m}{dt} , \tag{8.13}$$

$$\frac{d\Delta V}{dt} = \gamma_v \frac{dh}{dt} - \frac{dV_m}{dt} . \tag{8.14}$$

We solved eqs. (8.2), (8.3) in combination with (8.13), (8.14) instead of (8.4), (8.5). The results are shown in Figure 8.4. The changes with respect to Figure 8.3a-c are only small compared to the differences between the calculations and observations.

Apparently the mixed-layer momentum equations do not behave well when we prescribe all forcing terms. They allow for large amplitude inertial oscillations which depend on the geostrophic wind, the initial conditions, the friction, and the mixed layer height. Inaccurate determination of one of these will lead to large deviations from the actual mixed layer wind, because the inertial oscillations are only weakly damped.

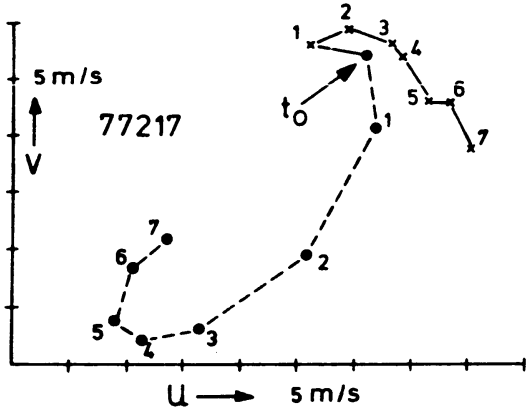

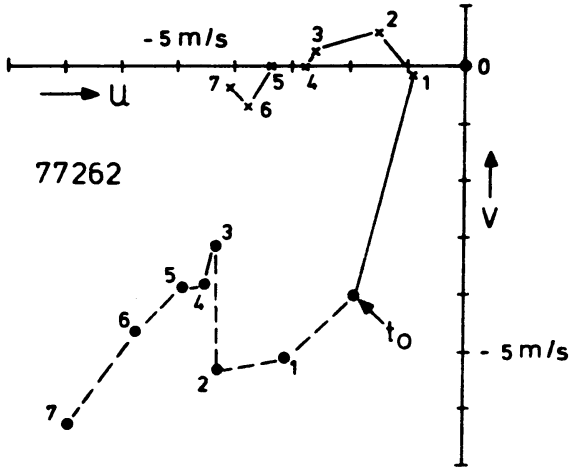

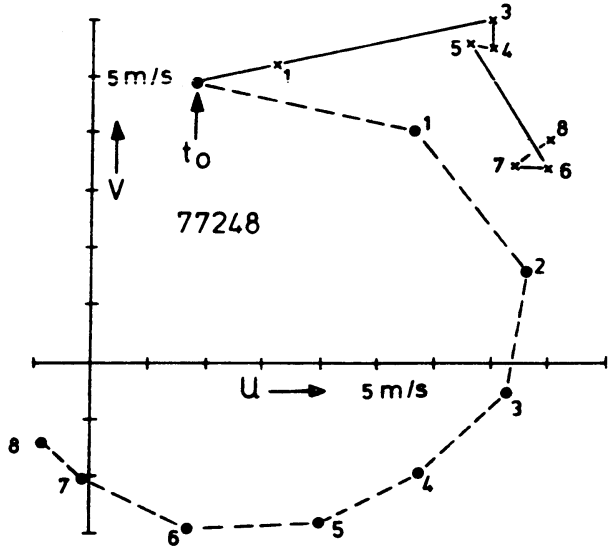

Figure 8.3. Calculated (•——•) and observed (✖——✖) mixed- layer wind. Geostrophic wind taken to be constant with height. Values of γ_u, γ_v from radiosondes.

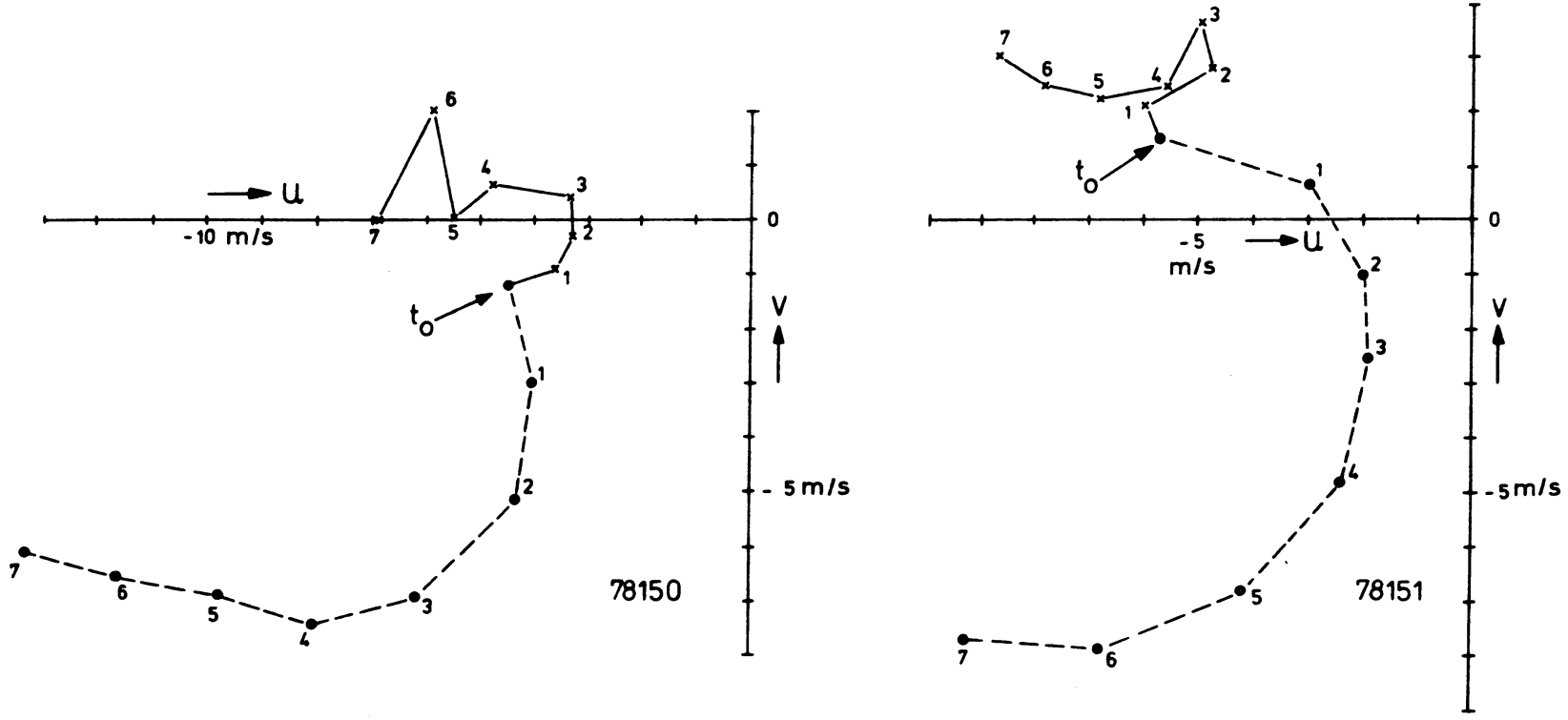

Figure 8.3 (continued)

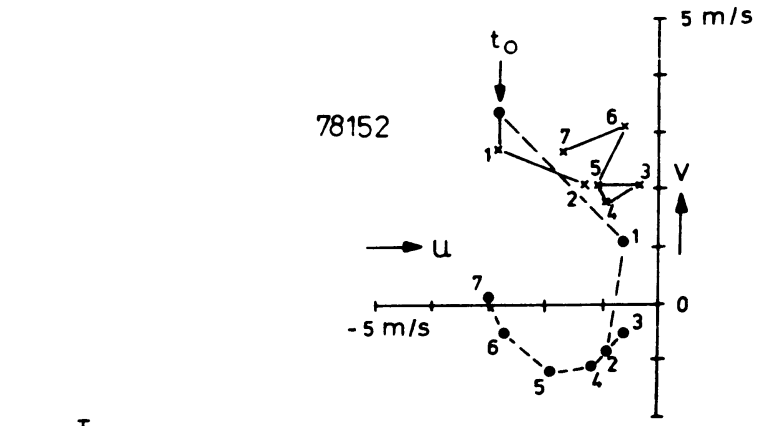

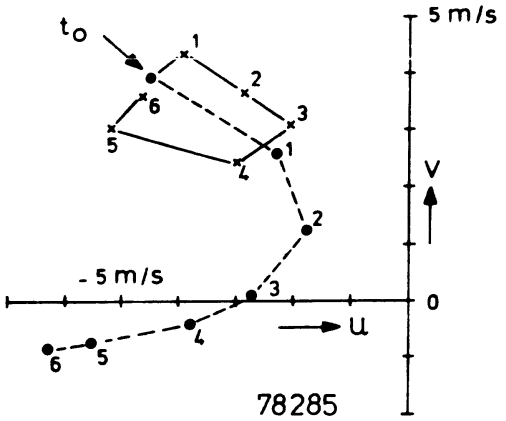

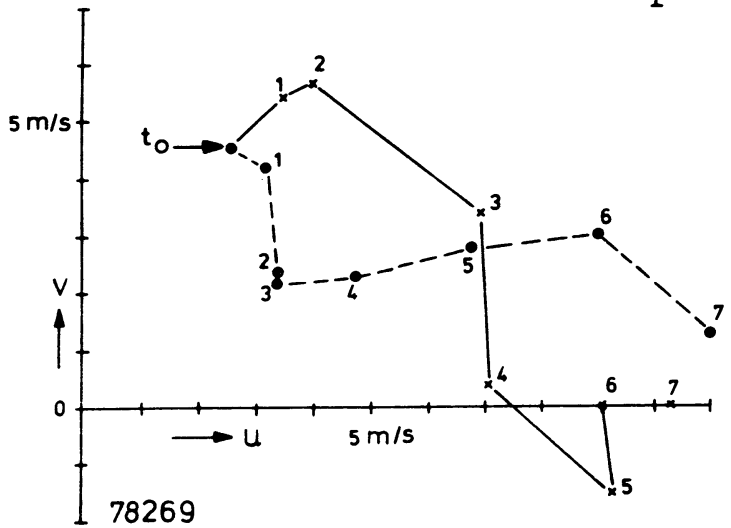

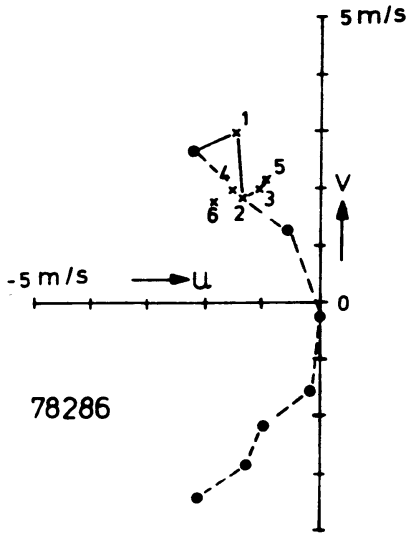

Figure 8.3 (continued)

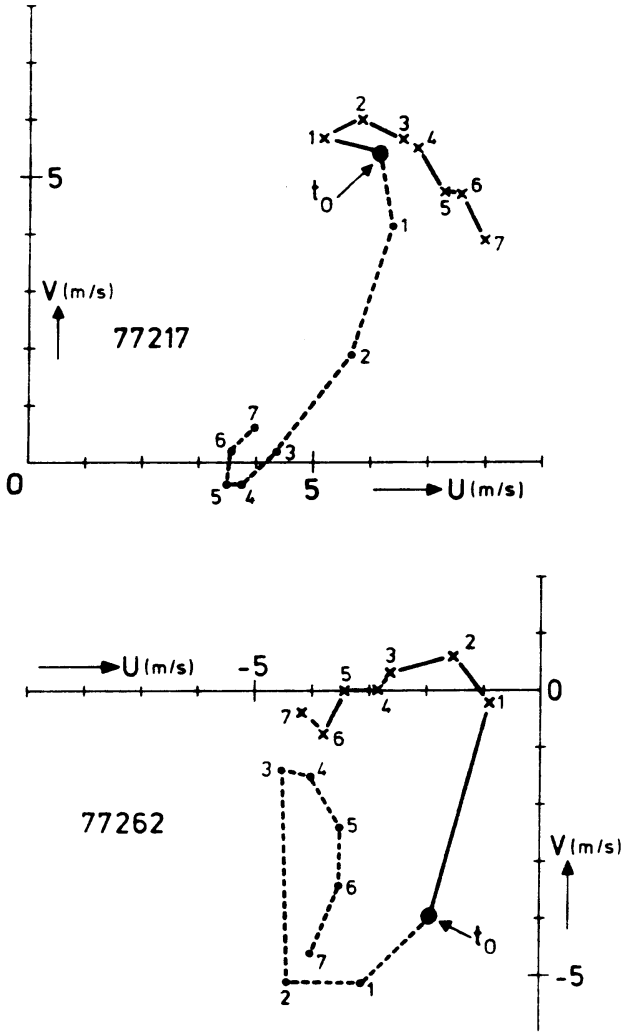

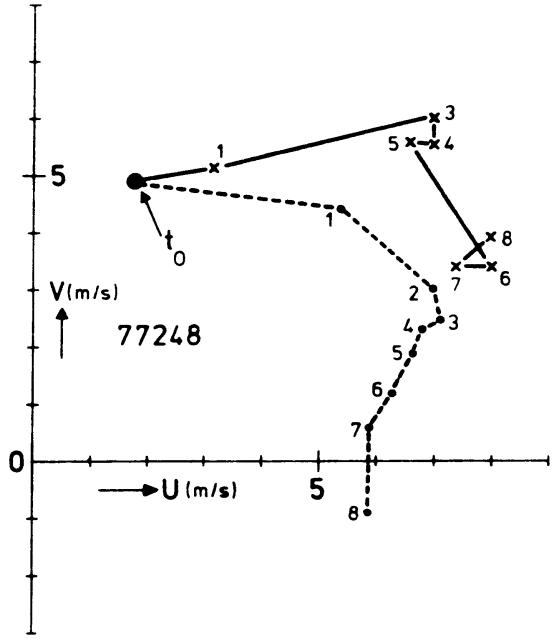

Figure 8.4. As Fig. 8.3, but now with the geostrophic wind above the mixed layer taken to be equal to the wind observed by the radiosondes.

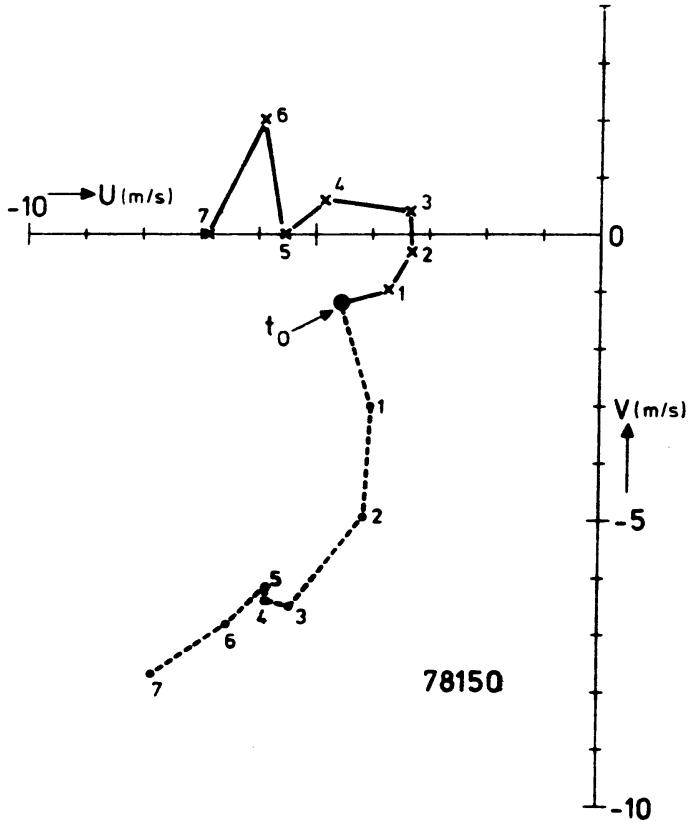

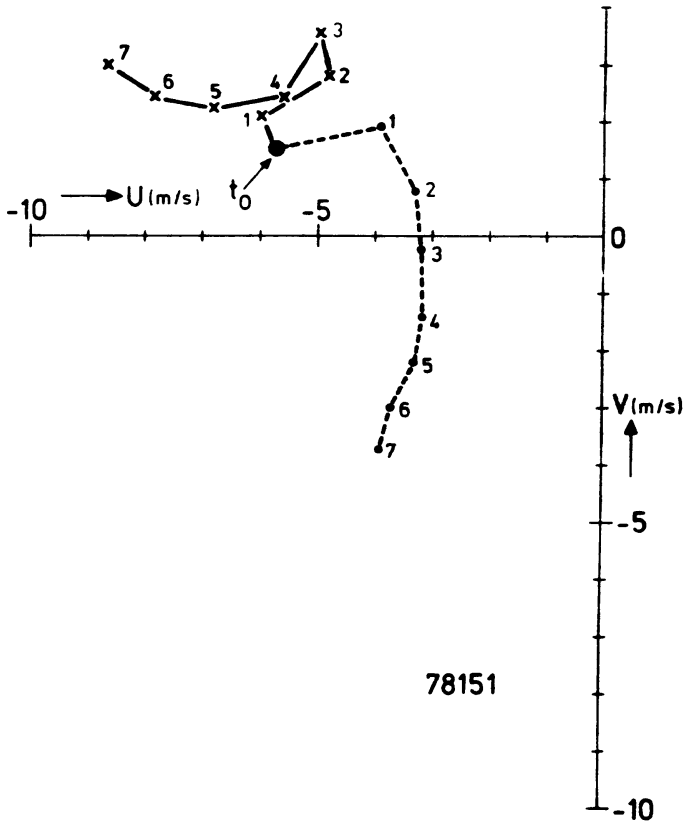

Figure 8.4 (continued)

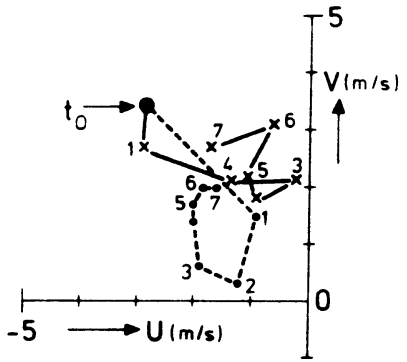

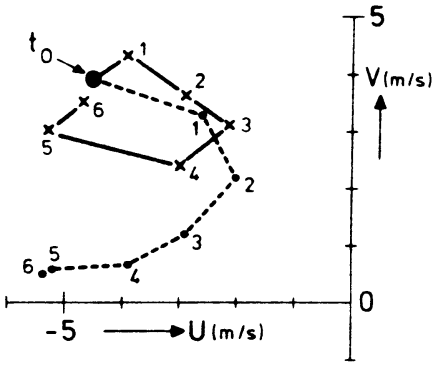

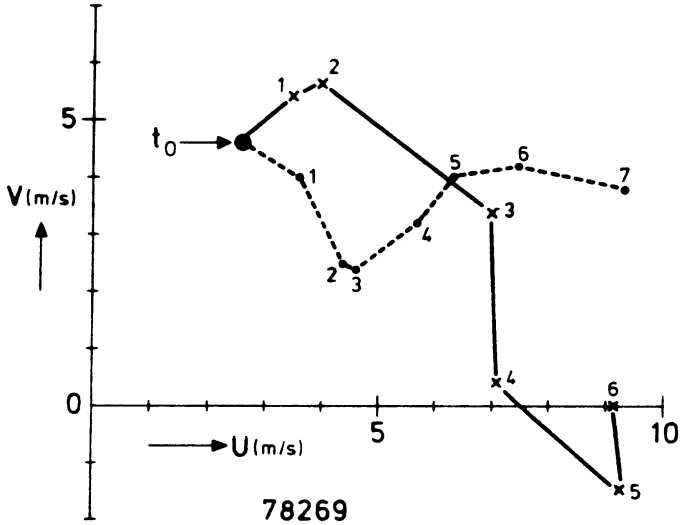

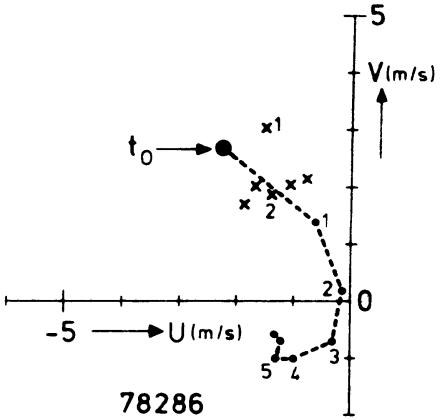

Figure 8.4 (continued)

8. CONCLUSIONS

Due to the heat input from the surface, the state of the atmospheric boundary layer continuously changes during the course of a clear day. Its height, temperature, humidity, and momentum are a function of time. In this study we have compared the results of various models for this time-dependent behavior with a set of field experiments.

Observations of the vertical profile of potential temperature in the boundary layer in case of vigorous turbulent mixing by convection reveal a typical structure. In a thin layer close to the heated ground the vertical gradient of potential temperature is large, in the bulk of the boundary layer this gradient is nearly zero, and in a thin layer at the interface between the turbulent mixed layer and the quiet, stably stratified air aloft the gradient of potential temperature is large again.

For the calculation of the evolution of the boundary layer we used so-called slab models or jump models which are based on a schematization of this observed structure. These models are characterized by a vertically uniform distribution of potential temperature, specific humidity and momentum within the boundary layer (mixed layer). At the top a jump in these variables represents the transition to the stable air above. The thickness of the surface layer, where also large gradients occur, is neglected in comparison with the mixed-layer height.

Starting from the general conservation equations, these model assumptions are used to derive simplified budgets for heat, momentum and moisture.
The bookkeeping with these quantities is straightforward, but the resulting set of equations still suffers from the usual closure problem.

One of the jump conditions at the top of the mixed layer indicates that entrainment of warmer air from the stable environment aloft into the cooler boundary layer requires a downward heat flux at the inversion base. Since warmer air prefers to rise, this downward heat flux must be associated with an expenditure of energy, presumably made available by the turbulence that maintains the downward heat flux.

This line of reasoning forces one to turn to the budget for turbulent kinetic energy. Here all entrainment modeling problems originate. Turbulence has a habit of dissipating almost all of the energy supplied to it. Only a few percent of the gross energy consumption of the boundary layer is available for entrainment. Parameterization of the energy budget requires estimates for small differences between large quantities and this is not a situation in which it is easy to decide which particular parameterization is best.

In geophysical flows three production mechanisms leading to entrainment in the mixed layer can be distinguished: convective turbulence produced from the heated surface, mechanical turbulence produced by surface friction and mechanical turbulence produced by local wind shear at the top of the mixed layer. In chapter 3 we received the parameterizations of the turbulent kinetic energy budget that account for these production mechanisms. It cannot be expected that the scaling of the various terms in the energy budget can deal with the interaction between these mechanisms. They are considered independently and simple interpolation formulae are used when more than one is present simultaneously.

Some parameterizations originate from a vertically integrated (bulk) energy budget, others from a local energy budget applied at the inversion base. We have shown that the differences in these approaches are minimal, since in both cases the same velocity and length scales have to be chosen for the most important terms in the energy budget. The application of a local length scale for the shear production at the inversion base is neither attractive nor justified.

Care has to be exercised with the parameterization of the energy budget in cases with very low or very high Richardson numbers. At very low values one has to account for the fact that the entrainment rate must remain finite. The energy consumed by the entrained air when becoming turbulent then has to be taken into account. At very high Richardson numbers the situation is quite complicated and no satisfactory solution has been found yet. Several proposals have been made. One of them is the inclusion of a dissipation term at the inversion base which can also account for a loss of energy due to internal waves. Another way is to make all the coefficients dependent on the Richardson number. Neither of these is fully satisfactory. Field experiments are not accurate enough to provide an answer to these questions.

It was over purpose to determine the practical applicability of these models to the evolution of the atmospheric boundary layer on a clear day. Measuring compaigns were carried out on ten days in 1977 and 1978.

Our observations included measurements of the vertical profiles of potential temperature, humidity, and momentum. These profiles were obtained along the 200 m mast, and with radiosondes. In the early morning hours the boundary-layer height was determined with an acoustic echo sounder (Sodar). The forcing functions (surface heat flux, friction velocity) were also measured.

Mixed-layer models are based on an idealized form of the structure of the vertical profiles. In reality deviations from this schematic picture are possible and we had to define an objective procedure to transform a measured profile in such a way that the model variables could be extracted. This transformation was carried out with the constraint that the total heat content of the boundary layer remained unchanged.

We were especially concerned with the determination of the height of the mixed layer (h). In the early morning hours it is not possible to do this from the temperature profile alone. Then the data from the sodar were of great value since the top of its echo corresponds with the height of the turbulent layer. The accuracy of the sodar data on h is estimated to be $\pm$ 20 m.
Later in the day we had to use temperature-profiles, obtained with radiosondes, for the determination of h. Since convective plumes and billows distort the local interface between turbulent and non-turbulent air considerably, an instantaneous value of h from a radiosonde profile has a statistical sampling error. We estimated this error to be $\pm$ 100 m in our conditions. In the atmosphere this type of error is inevitable and differences between model results which are smaller must be regarded as insignificant.

For a comparison with the observations we integrated the model equations in time. We compared the solutions for the dependent variables rather than the differential equations themselves, because derivatives cannot be determined from atmospheric observations with reasonable accuracy. A sensitivity analysis of the exact solution of a simple entrainment model showed that the dependent variables are not very sensitive to variations in the model constants. In view of this and of the accuracy of our observations we conclude that only relatively large variations between the models can be assessed in the atmosphere.

For a further evaluation of the predicted mixed-layer height h we separated our observations in two groups according to the dominant entrainment mechanisms. One group consisted of the convectively dominated cases in which the heat flux is large, and another group contained the cases in which mechanical entrainment is important (small heat flux).

For convectively dominated cases, an encroachment model (no fluxes at all at the top of the mixed layer) explained about 80% of the observed increase in h. An entrainment model in which the negative heat flux at the top is proportional to the surface heat flux predicted the observed mixed-layer height in these cases without bias and with a standard deviation of $\pm$ 125 m, when we took a proportionality factor $c_F = 0.2$. This standard deviation is about the same as the estimated error in the observations.

A model which only takes into account the entrainment caused by convective turbulence does not predict the observed mixed-layer height correctly when the surface heat flux is small. In these cases mechanical entrainment is also important. This is usually the case in the first few hours after sunrise.

When we included mechanical entrainment in the model of Tennekes (1973), all observations of h were quite well predicted with $c_F = 0.2$ and $A = 5$. The predicted h then had a bias of only -5%. The remaining scatter was $\pm$ 80 m when we considered all cases, and $\pm$ 40 m as long as $h_{obs} - h_o < 500$ m. The choice $A = 5$ is supported by the laboratory experiments of Kantha et al. (1977).

Further complications of the entrainment model did not improve the results significantly. The Zilitinkevich correction term, accounting for a finite entrainment velocity at low Richardson numbers, only weakly affected the mixed-layer height in atmospheric applications. The corrections were smaller than the scatter in the data. The model of Zeman did not lead to results that were significantly different from Tennekes' model. The average difference was smaller than 5%.

Inclusion of humidity in the buoyancy affects the mixed-layer growth in two ways. The surface buoyancy flux increases with respect to the dry case with a factor that depends on the Bowen ratio. In our observations this increase was at most 15-20%. The second effect is

the decrease of the buoyancy jump at the interface with a factor $1 + 0.61\ T_o\ \Delta q/\Delta\theta$. Since usually $\Delta q < 0$, this reduces the buoyancy jump. These two humidity effects on the buoyancy may occasionally lead to large increases of h with respect to the dry case. This is especially so when $\Delta\theta$ and γ_θ are small. However, the measurements of humidity were not very accurate and we cannot conclude from our observations that the inclusion of humidity effects in the buoyancy leads to better predictions. Further study on this matter seems necessary, especially because it is associated with the prediction of the formation of clouds at the top of the mixed layer.

We also compared predictions and observations of the other variables in the mixed layer: potential temperature, humidity, and momentum.

The calculated mixed-layer potential temperature does not depend very much on the entrainment model that is used. It is more sensitive to the external forcing functions (surface heat input, stable gradient). The observed temperature increase during the day was predicted with a standard deviation of $\pm$ 0.5 ^{o}C. On convective days the temperature at noon was also well described by considering encroachment alone.

Mixed-layer humidity was reasonably well predicted except in a few cases. It was clear that the results depend more on the quality of the humidity measurements than on the entrainment model. Accurate humidity measurements are required for the application of these models to the prediction of clouds at the top of the mixed layer. Further study in this direction would be interesting.

The wind in the mixed layer was poorly predicted by the mixed-layer models. This is more a consequence of the typical character of the mixed-layer equations for momentum than of the formulation of the entrainment. The equations may exhibit large-amplitude inertial oscillations, which depend on the geostrophic wind, initial conditions, friction, and the mixed-layer height. These

oscillations are only weakly damped, and inaccuracies will lead to large deviations from the actually observed wind.

What is the picture that emerges at the end of this study? Observations in the atmosphere inevitably show large scatter. This is not due to errors made in the design of experiments, but is caused by the natural variability of atmospheric phenomena. Models predict the behavior of averaged variables, but the data often refere to local, instantaneous values. The verification of models with the aid of field observations thus can be successful only when the physical processes involved are sufficiently pronounced. Subtle changes or small differences cannot be discovered in this way; fortunately, they often are of little practical value.

REFERENCES

André, J.C., de Moor, G., Lacarrère, P., Therry, G., and R. du Vachat, 1978: Modeling the 24-hour evolution of the mean and turbulent structure of the planetary boundary layer. J. Atmos. Sci., 35, 1861-1883.

Arnold, A., and J.R. Rowland, 1976: Fine-scale observations of free convection in the atmosphere. Third Symp. on Atmos. Turbulence, Diffusion and Air Quality, Rayleigh. Amer. Meteor. Soc., Boston, pp. 1-8.

Artaz, M.A., and J.C. André, 1980: Similarity studies of entrainment in convective mixed layers. Boundary-Layer Meteor., 19, 51-66.

Ball, F.K., 1960: Control of inversion height by surface heating. Quart. J. Roy. Meteor. Soc., 86, 483-494.

Benkley, C.W., and L.L. Schulman, 1979: Estimating hourly mixing depths from historical meteorological data. J. Appl. Meteor., 18, 772-780.

Betts, A.K., 1973: Non-precipitating cumulus convection and its parameterization. Quart. J. Roy. Meteor. Soc., 99, 178-196.

Busch, N.E., 1973: On the mechanics of turbulence. In: Workshop on micrometeorology, Ed. D.A. Haugen. Amer. Meteor. Soc., Boston, pp. 1-65.

Carson, D.J., 1973: The development of a dry, inversion-capped, convectively unstable boundary layer. Quart. J. Roy. Meteor. Soc., 99, 450-467.

Cats, G.J., 1977: The calculation of the geostrophic wind. KNMI Scientific Report 77-2.

Cattle, H., and K.J. Weston, 1975: Budget studies of the heat flux profiles in the convective boundary layer over land. Quart. J. Roy. Meteor. Soc., 101, 353-363.

Caughey, S.J., 1979: Some aspects of turbulent structure through the depth of the convective boundary layer. Quart. J. Roy. Meteor. Soc., 105, 811-827.

Clarke, R.H., Dyer, A.J., Brook, R.R., Reid, D.G., and A.J. Tromp, 1971: The Wangara experiment: Boundary-Layer data. Division of Meteorological Physics, Technical Paper No. 19, CSIRO, Melbourne, Australia, 350 pp.

Crapper, P.F., and P.F. Linden, 1974: The structure of turbulent density interfaces. J. Fluid Mech., 65, 45-63.

Coulman, C.E., 1978a: Boundary-Layer evolution and nocturnal inversion dispersal. Part I. Boundary-Layer Meteor., 14, 471-491.

Coulman, C.E., 1978b: Boundary-Layer evolution and nocturnal inversion dispersal. Part II. Boundary-Layer Meteor., 14, 493-513.

Coulter, R., 1979: A comparison of three methods for measuring mixing-layer height. J. Appl. Meteor., 18, 1495-1499.

Deardorff, J.W., 1973: An explanation of anomalously large Reynolds stresses within the convective planetary boundary layer. J. Atmos. Sci., 30, 1070-1076.

Deardorff, J.W., 1974a: Three-dimensional numerical study of the height and mean structure of a heated planetary boundary layer. Boundary-Layer Meteor., 7, 81-106.

Deardorff, J.W., 1974b: Three-dimensional numerical study of turbulence in an entraining mixed layer. Boundary-Layer Meteor., 7, 199-226.

Deardorff, J.W., 1979: Prediction of convective mixed-layer entrainment for realistic capping inversion structure. J. Atmos. Sci., 36, 424-436.

Deardorff, J.W., Willis, G.E., and D.K. Lilly, 1969: Laboratory investigation of non-steady penetrative convection. J. Fluid Mech., 35, 7-31.

Denman, K.L., 1973: A time-dependent model of the upper ocean. J. Phys. Oceanogr., 3, 173-184.

Denman, K.L., and M. Miyake, 1973: Upper layer modification of ocean station "Papa": observations and simulation. J. Phys. Oceanogr., 3, 185-196.

de Szoeke, R.A., and P.B. Rhinés, 1976: Asymptotic regimes in mixed-layer deepening. J. Marine Res., 34, 111-116.

Dop, H. van, Steenkist, R., Altena, D., and R. Scholten, 1978: The use of acoustic methods for boundary layer studies near the coast of the Netherlands. Proc. 4th Symp. on Meteor. Observ. and Instr., Denver. Amer. Meteor. Soc., Boston, pp. 326-329.

Driedonks, A.G.M., van Dop, H., and W. Kohsiek, 1978: Meteorological observations on the 213 m mast at Cabauw in the Netherlands. Proc. 4th Symp. on Meteor. Observ. and Instr., Denver. Amer. Meteor. Soc., Boston, pp. 41-46.

Driedonks, A.G.M., Nieuwendijk, P.A.T., and C.J. Goes, 1980: A set of computer programs to process turbulence data measured at the 200 m mast at Cabauw. KNMI Scientific Report 80-3.

Farmer, D.M., 1975: Penetrative convection in the absence of mean shear. Quart. J. Roy. Meteor. Soc., 101, 869-891.

Garnich, N.G., and S.A. Kitaygorodskii, 1977: On the rate of deepening of the oceanic mixed layer. Izv. Akad. Nauk. USSR, Atmos. and Ocean. Phys., 13, 1287-1296.

Garnich, N.C., and S.A. Kitaygorodskii, 1978: On the theory of the upper quasi-homogeneous ocean layer owing to the processes of purely wind-induced mixing. Izv. Akad. Nauk. USSR, Ocean. and Atmos. Phys., 14, 748-755.

Garwood, R.W., 1977: An oceanic mixed-layer model capable of simulating cyclic states. J. Phys. Oceanogr., 7, 456-468.

Gill, G.C., Olson, L.E., Sela, J., and M. Suda, 1967: Accuracy of wind measurements on towers and stacks. Bull. Amer. Meteor. Soc., 48, 665-674.

Heidt, F.D., 1977: The growth of the mixed layer in a stratified fluid due to penetrative convection. Boundary-Layer Meteor., 12, 439-461.

Holton, J.R., 1973: An introduction to dynamic meteorology. Academic Press, New York. 319 pp.

Jensen, N.O., and D.H. Lenschow, 1978: An observational study of penetrative convection. J. Atmos. Sci., 35, 1924-1933.

Kaimal, J.C., 1972: Spectral characteristics of surface layer turbulence. Quart. J. Roy. Meteor. Soc., 98, 563-589.

Kantha, L.H., 1975: Turbulent entrainment at the density interface of a two-layer stably stratified fluid system. Ph. D. Dissertation, The John Hopkins Univ.

Kantha, L.H., Phillips, O.M., and R.S. Azad, 1977: On turbulent entrainment at a stable density interface. J. Fluid Mech., 79, 753-768.

Kato, H., and O.M. Phillips, 1969: On the penetration of a turbulent layer into stratified fluid. J. Fluid Mech., 37, 643-655.

Kim, J.W., 1976: A generalized bulk model of the oceanic mixed layer. J. Phys. Oceanogr., 6, 686-695.

Kitaygorodskii, S.A., and N.G. Kozhelupova, 1978: Entrainment rate in the penetrative convection regime in unsteady-state boundary layers of the atmosphere and the ocean. Izv. Akad. Nauk. USSR, Atmos. and Ocean. Phys., 14, 453-458.

Klöppel, M., and G. Stilke, 1978: Untersuchungen der Vorgänge beim Auf- und Abbau von Bodeninversionen. Hamburger Geophys. Einzelschriften, Reihe A, Heft 38.

Kraus, E.B., 1972: Atmosphere-ocean interaction. Clarendon Press, Oxford.

Kraus, E.B., 1977 (ed.): Modelling and prediction of the upper layers of the ocean. Pergamon Press, Oxford

Kraus, E.B., and J.S. Turner, 1967: A one-dimensional model of the seasonal thermocline. Part 2: The general theory and its consequences. Tellus, 19, 98-106.

Lenschow, D.H., and P.L. Stephens, 1978: Airborne measurements of the structure of thermals. Aero-Revue, 12, 780-784.

Lilly, D.K., 1968: Models of cloud-topped mixed layers under a strong inversion. Quart. J. Roy. Meteor. Soc., 94, 292-309.

Linden, P.F., 1975: The deepening of a mixed layer in a stratified fluid. J. Fluid Mech., 71, 385-405.

Lofquist, K., 1960: Flow and stress near an interface between stratified liquids. Phys. of Fluids, 3, 158-175.

Long, R.R., 1975: The influence of shear on mixing across density interfaces. J. Fluid Mech., 70, 305-320.

Mahrt, L., 1979: Penetrative convection at the top of a growing boundary layer. Quart. J. Roy. Meteor. Soc., 105, 469-485.

Mahrt, L., and D.H. Lenschow, 1976: Growth dynamics of the convectively mixed layer. J. Atmos. Sci., 33, 41-51.

Mahrt, L., Heald, R.C., Lenschow, D.H., and B.B. Stankov, 1979: An observational study of the structure of the nocturnal boundary layer. Boundary-Layer Meteor., 17, 247-264.

Manton, M.J., 1977: On the structure of convection. Boundary-Layer Meteor., 12, 491-504.

Manton, M.J., 1978: On dry penetrative convection. Boundary-Layer Meteor., 14, 301-322.

Melgarejo, J.W., and J.W. Deardorff, 1974: Stability functions for the boundary-layer resistance laws based upon observed boundary-layer heights. J. Atmos. Sci., 31, 1324-1333.

Mellor, G.L., and T. Yamada, 1974: A hiercharchy of turbulent closure models for planetary boundary layer models. J. Atmos. Sci., 31, 1791-1806.

Mellor, G.L., and P.A. Durbin, 1975: The structure and dynamics of the ocean surface. J. Phys. Oceanogr., 5, 718-728.

Monin, A.S., and A.M. Yaglom, 1971: Statistical Fluid Mechanics: Mechanics of turbulence. Volume 1. The MIT Press, Cambridge, Mass. 769 pp.

Monna, W.A.A., and A.G.M. Driedonks, 1979: Experimental data on the dynamic properties of several propeller vanes. J. Appl. Meteor., 18, 699-702.

Moore, M.J. and R.R. Long, 1971: An experimental investigation of turbulent stratified shearing flow. J. Fluid Mech., 49, 635-655.

Munk, W.H., and E.R. Anderson, 1948: Notes on a theory of the thermocline. J. Marine Res., 7, 276-295.

Nieuwstadt, F.T.M., 1978: The computation of the friction velocity u_* and temperature scale T_* from temperature and velocity profiles by least-square methods. Boundary-Layer Meteor., 14, 235-246.

Nieuwstadt, F.T.M., 1980a: The steady-state height and resistance laws of the nocturnal boundary layer: theory compared with Cabauw observations. To appear in Boundary-Layer Meteor.

Nieuwstadt, F.T.M., 1980b: A rate equation for the nocturnal boundary-layer height. Submitted to J. Atmos. Sci.

Nieuwstadt, F.T.M., and A.G.M. Driedonks, 1979: The nocturnal boundary layer: a case study compared with model calculations. J. Appl. Meteor., 18, 1397-1404.

Niiler, P.P., 1975: Deepening of the wind-mixed layer. J. Marine Res., 33, 405-422.

Niiler, P.P., 1977: One-dimensional models of the seasonal thermocline. In: The Sea, volume 6, Wiley, New York, pp. 97-115.

Niiler, P.P., and E.B. Kraus, 1977: One-dimensional models of the upper ocean. In: Modelling and Prediction of the upper layers of the ocean. Pergamon Press, Oxford, pp. 143-172.

Palmer, S.G., and S.J. Caughey, 1979: An observational study of entraining convection using balloon-borne turbulence probes and high-power doppler radar. Boundary-Layer Meteor., 16, 261-278.

Pandolfo, J.P., and C.A. Jacobs, 1972: Numerical simulation of the tropical air-sea planetary boundary layer. Boundary-Layer Meteor., 3, 15-46.

Phillips, O.M., 1972: The entrainment interface. J. Fluid Mech., 51, 97-118.

Phillips, O.M., 1977: Entrainment. In: Modelling and Prediction of the upper layers of the ocean. Pergamon Press, Oxford, pp. 92-101.

Pollard, R.T., Rhines, P.B., and R.O.R.Y. Thompson, 1973: The deepening of the wind-mixed layer. Geophys. Fluid Dyn., 3, 381-404.

Price, J.F., 1979: On the scaling of stress-driven entrainment experiment. J. Fluid Mech., 90, 509-529.

Price, J.F., Mooers, C.N.K., and J.C. van Leer, 1978: Observation and simulation of storm-driven mixed-layer deepening. J. Phys. Oceanogr., 8, 582-599.

Rayment, R.M., and C.J. Readings, 1974: A case study of the structure and energetics of an inversion. Quart. J. Roy. Meteor. Soc., 100, 221-233.

Resnyanski, Yu.D., 1975: On the parameterization of the bulk dissipation of turbulent energy in the upper quasi-homogeneous layer of the ocean. Izv. Akad. Nauk. USSR, Atmos. and Ocean. Phys., 11, 726-733.

Richards, J.M., 1961: Experiments on the penetration of an interface by buoyant thermals. J. Fluid Mech., 11, 369-384.

Sherman, F.S., Imberger, J., and G.M. Corcos, 1978: Turbulence and mixing in stably stratified waters. Ann. Rev. Fluid Mech., 10, 267-288.

Slob, W., 1978: The accuracy of aspiration thermometers. KNMI Scientific Report 78-1.

Stilke, G., Wamser, C., and G. Peters, 1976: Untersuchungen über den Abbau einer Bodeninversion mit direkten und indirekten Messverfahren. Meteor. Rundschau, 29, 1-11.

Stull, R.B., 1973: Inversion-rise model based on penetrative convection. J. Atmos. Sci., 30, 1092-1099.

Stull, R.B., 1975: Temperature inversions capping atmospheric boundary layers. Ph. D. Dissertation, the University of Washinton.

Stull, R.B., 1976a: The energetics of entrainment across a density interface. J. Atmos. Sci., 33, 1260-1267.

Stull, R.B., 1976b: Mixed-layer depth model based on turbulent energetics. J. Atmos. Sci., 33, 1268-1278.

Stull, R.B., 1976c: Inertial gravity waves generated by penetrative convection. J. Atmos. Sci., 33, 1279-1286.

Tennekes, H., 1973: A model for the dynamics of the inversion above a convective boundary layer. J. Atmos. Sci., 30, 558-567.

Tennekes, H., 1975: Reply to Zilitinkevich. J. Atmos. Sci., 32, 992-995.

Tennekes, H., and J.L. Lumley, 1972: A first course in turbulence. MIT Press, Cambridge, Mass., 300 pp.

Tennekes, H., and A.P. van Ulden, 1974: Short term forecasts of temperature and mixing height on sunny days. Preprints 2nd Symposium on Atmos. Turbulence, Diffusion, and Air Quality, Santa Barbara, Amer. Meteor. Soc., Boston, pp. 35-40.

Tennekes, H., and A.G.M. Driedonks, 1981: Basic entrainment equations for the atmospheric boundary layer. To appear in Boundary-Layer Meteorology.

Thompson, R.O.R.Y., 1979: A re-interpretation of the entrainment process in some laboratory experiments. Dyn. of Atmos. and Oceans, 4, 45-55.

Thompson, S.M., and J.S. Turner, 1975: Mixing across an interface due to turbulence generated by an oscillating grid. J. Fluid Mech., 67, 349-368.

Thorpe, S.A., 1973: Turbulence in stratified fluids: a review of laboratory experiments. Boundary-Layer Meteor., 5, 95-119.

Turner, J.S., 1968: The influence of molecular diffusivity on turbulent entrainment across a density interface. J. Fluid Mech., 33, 639-656.

Turner, J.S., 1973: Buoyancy effects in fluids. Cambridge University Press.

Turner, J.S., and E.B. Kraus, 1967: A one-dimensional model of the seasonal thermocline. Part 1: a laboratory experiment and its interpretation. Tellus, 19, 88-97.

Ulden, A.P. van, van der Vliet, J.G., and J. Wieringa, 1976: Temperature and wind observations at heights from 2 m to 200 m at Cabauw in 1973. KNMI Sci. Rep. 76-7.

Wieringa, J., 1967: Evaluation and design of wind vanes. J. Appl. Meteor., 6, 1114-1122.

Wieringa, J., 1972: Tilt errors and precipitation effects in trivane measurements of turbulent fluxes over water. Boundary-Layer Meteor., 2, 406-426.

Wieringa, J., 1973: Gust factors over open water and built-up country. Boundary-Layer Meteor., 3, 424-441.

Wieringa, J., and F.X.C.M. van Lindert, 1971: Application limits of double fin and coupled wind vanes. J. Appl. Meteor., 10, 137-145.

Willis, G.E., and J.W. Deardorff, 1974: A laboratory model of the unstable planetary boundary layer. J. Atmos. Sci., 31, 1297-1307.

Wolanski, E.J., and L.M. Brush, 1975: Turbulent entrainment across stable density step structures. Tellus, 27, 259-268.

Wu, J., 1973: Wind-induced turbulent entrainment across a stable density interface. J. Fluid Mech., 61, 275-287.

Wyngaard, J.C., 1973: On surface layer turbulence. In: Workshop on micrometeorology, ed. D.A. Haugen. Amer. Meteor. Soc., Boston, pp. 101-150.

Wyngaard, J.C., and O.R. Coté, 1974: The evolution of a convective planetary boundary layer - a higher-order - closure model study. Boundary-Layer Meteor., 7, 289-308.

Yamada, T., and S. Berman, 1979: A critical evaluation of a simple mixed-layer model with penetrative convection. J. Appl. Meteor., 18, 781-786.

Yamamoto, S., Gamo, M., and O. Yokoyama, 1977: Airborne measurements of turbulent heat flux. J. Meteor. Soc. Japan, 55, 533-545.

Zeman, O., 1975: The dynamics of entrainment in the planetary boundary layer: a study in turbulence modeling and parameterization. Ph. D. Dissertation, the Pennsylvania State Univ.

Zeman, O., and J.L. Lumley, 1976: Modeling buoyancy driven mixed layers. J. Atmos. Sci., 33, 1974-1988.

Zeman, O., and H. Tennekes, 1977: Parameterization of the turbulent kinetic energy budget at the top of the daytime boundary layer. J. Atmos. Sci., 34, 111-123.

Zilitinkevich, S.S., 1975: Comments on a paper by H. Tennekes. J. Atmos. Sci., 32, 991-992.

Zilitinkevich, S.S., Chalikov, D.V., and Yu.D. Resnyansky, 1979: Modeling the oceanic upper layer. Oceanologica Acta, 2, 219-240.

Appendix A. Frequency response functions of the turbulence instrumentation.

The turbulence measuring system consists of first order systems (propeller, thermocouple array) and second order systems (vane).

a. First order systems

The governing equation for the output X(t) of a first order system with time constant 1/K in response to a forcing F(t) reads:

$$\frac{dX}{dt} + K\,X = K\,F(t). \qquad (A.1)$$

When F(t) is a periodic forcing: $F(t) = F_o + \alpha \sin \gamma t$, then the solution of (A.1) is:

$$X(t) = A \sin(\gamma t + \delta) + F_o\ , \qquad (A.2)$$

where $A = \alpha\,(1 + \gamma^2/K^2)^{-\frac{1}{2}}$ and $\operatorname{tg} \delta = -\gamma/K$ $(-\pi/2 \leqslant \delta \leqslant 0)$.

The amplification factor (gain) of the system is $b = A/\alpha$ and the phase shift is δ.

In terms of the response length $D = F_o/K$ of the system and the wave length $\lambda = 2\pi F_o/\gamma$ of the forcing, we get:

$$b = (1 + 4\,\pi^2 D^2/\lambda^2)^{-\frac{1}{2}}$$

$$\operatorname{tg} \delta = -\,2\pi D/\lambda\ .\quad (-\pi/2 \leqslant \delta \leqslant 0).$$

These functions are depicted in Fig. A.1a.

b. Second order system

The equation of motion for a wind vane with damping ratio h and undamped oscillation frequency ω_o reads (Mitsuta, 1966):

$$\frac{d^2\beta}{dt^2} + 2\,h\,\omega_o \frac{d\beta}{dt} + \omega_o^{\,2}\,\beta = \omega_o^{\,2}\,\alpha(t), \qquad (A.3)$$

where β is the angle of the vane with respect to the mean

wind direction and $\alpha(t)$ is the angle of the forcing wind with respect to its mean direction. This equation is approximately valid for $\alpha, \beta < 15^{o}$.
When the forcing is periodic $\alpha(t) = \alpha_o \sin \gamma t$, then the solution of (A.3) is:

$$\beta(t) = A \sin (\gamma t + \varepsilon), \qquad (A.4)$$

where $A = \alpha_o \left((1 - \gamma^2/\omega_o^2)^2 + 4h^2\gamma^2/\omega_o^2 \right)^{-\frac{1}{2}}$ and

$$\operatorname{tg} \varepsilon = 2h\omega_o\gamma/(\gamma^2 - \omega_o^2), \quad (-\pi \leqslant \varepsilon \leqslant 0).$$

In terms of the undamped wave length of the instrument: $Ut_o = 2\pi U/\omega_o$ and the wave length $\lambda = 2\pi U/\gamma$ of the forcing, the gain $b = A/\alpha_o$ and phase shift ε are given by

$$b = \left((1 - (Ut_o/\lambda)^2)^2 + 4h^2 (Ut_o/\lambda)^2 \right)^{-\frac{1}{2}},$$

$$\operatorname{tg} \varepsilon = 2h(Ut_o/\lambda) \Big/ \left((Ut_o/\lambda)^2 - 1 \right), \quad (-\pi \leqslant \varepsilon \leqslant 0).$$

These functions are depicted in Fig. A.1b.

c. The correlation of a first and second order variable, e.g. temperature and elevation, will also be modified by the response characteristics. In case that the forcings of these variables are both periodic with the same period γ, the ratio of this modified correlation to the original one can be calculated from (A.2) and (A.4). After some algebra there results:

$$\frac{cor'}{cor} = \left(1 + 4\pi^2(D/\lambda)^2 \right)^{-1} \cdot \left((1 - (Ut_o/\lambda)^2)^2 + 4h^2(Ut_o/\lambda)^2 \right)^{-1} \cdot$$

$$\left(1 - (Ut_o/\lambda)^2 + 4\pi h (D/\lambda)(Ut_o/\lambda) \right). \qquad (A.5)$$

This ratio is depicted in Fig. A.1c, for D=0.5 m, Ut_o=3.3 m, h=0.56.

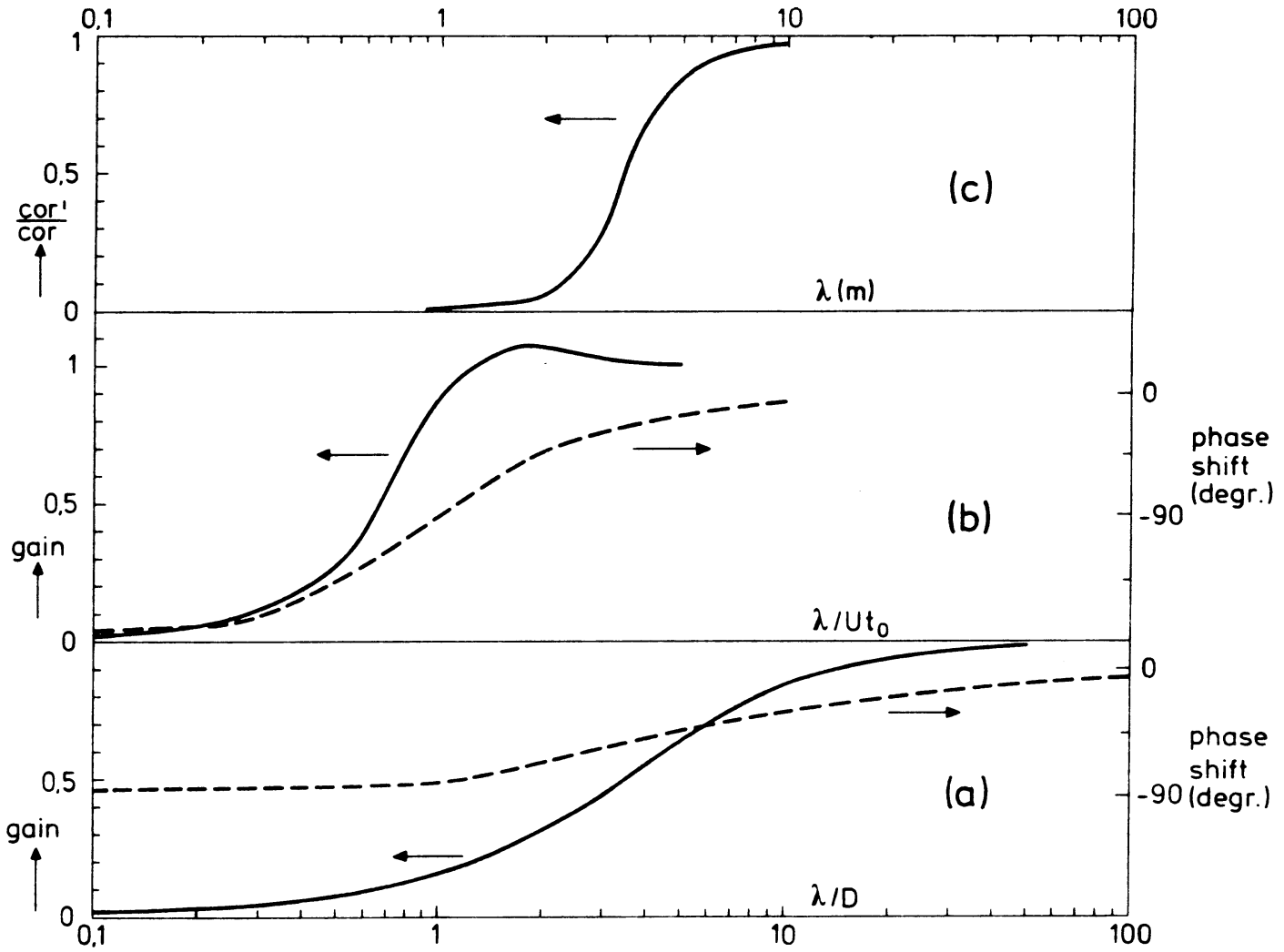

Figure A.1. *(a). Gain and phase shift for a first-order system as a function of the non-dimensional wavelength.*

(b). Same as (a), but for a second-order system.

(c). Modification of the correlation between a first-order and second-order system due to instrument lag, applied to the turbulence instrumentation.

Appendix B. Correction of temperature profiles from radiosondes for instrument lag.

The temperature sensor of the radiosonde is a first order system and thus governed by eq. (A.1). After transformation to the vertical coordinate $z = w_u.t$, where w_u is the updraft speed of the sonde, we get:

$$dX/dz + K\,X = K\,F(z) \qquad (B.1)$$

where K is now equal to $1/(w_u.T)$, with T the lag time of the sensor. Since w_u was kept at about 4 m/s, and $T \approx 5$ s, K has a value of about 1/20.
The original temperature profile F(z) can be retrieved from the measured one, X(z), by using (B.1). This will be an inaccurate procedure due to the large variability of dX/dz in a real signal from the sonde. We are not interested in all the small ripples in a radiosonde profile and therefore chose the following pragmatic method to correct the measured inversion height and thickness.
We supposed the true temperature profile to consist of a composition of linear fractions (see Fig. B.1). The transformation of this profile can easily be calculated with (B.1).

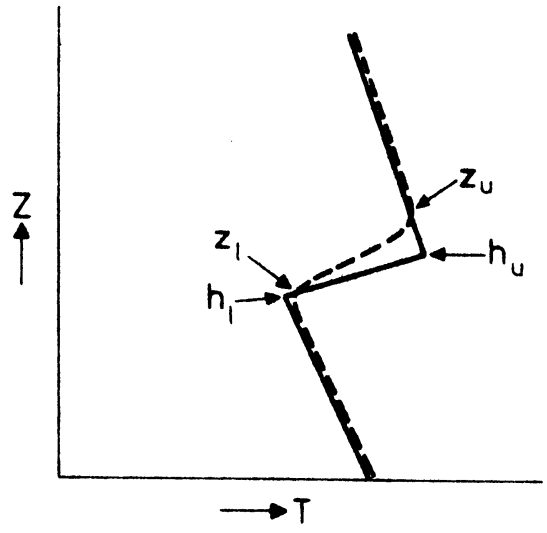

B.1. Original temperature profile (——) and transformation due to instrument lag of a radiosonde (----).

We are mainly interested in the differences between h_u, h_l and z_u, z_l where the latter are the points where the measured temperature gradient is zero (the lower and upper bound of the inversion). The difference between z_l and h_l is very small when the temperature gradient β within the inversion is positive, the difference between z_u and h_u however may be rather large. In good approximation the real inversion thickness $\Delta h = h_u - h_l$ is related to the observed inversion thickness $\Delta h_{obs} = z_u - z_l \approx z_u - h_l$ by

$$e^{K\Delta h} = \frac{\gamma}{\gamma-\beta} \; e^{K\Delta h_{obs}} - \frac{\beta-\alpha}{\gamma-\beta}$$

where γ is the lapse rate above the inversion (usually $\gamma < 0$, $\beta < 0$), and α the lapse rate below the inversion (≈ -0.01). E.g. for $\alpha = -0.01$, $\gamma \doteq -0.01$, $\beta = +0.05$, $K = 1/20$, $\Delta h_{obs} = 100$ m, then $\Delta h \approx 65$ m, which is a significant reduction. When in the same case $\beta = +0.01$, then $\Delta h \approx 90$ m. Only for strong, sharp inversions the reduction due to the correction for the lag-time of the sonde is necessary.

Appendix C. Tabulated data set for mixed-layer models for ten measuring days.

For each day the initial conditions, the forcing functions, and the observed values of the mixed-layer variables are given. Standard averaging time is 30 min.

Symbols and units.

t (GMT)	:	all times are in GMT,
h (m)	:	mixed-layer height,
θ_m (^oC)	:	potential temperature,
q_m (gr/kg)	:	specific humidity,
U_m (m/s)	:	wind (East-component),
V_m (m/s)	:	wind (North-component),
$\Delta\theta_o$ (^oC)	:	initial values of jumps of the mixed-layer variables at z=h ,
Δq_o (gr/kg)	:	
ΔU_o (m/s)	:	
ΔV_o (m/s)	:	
γ_θ (K/m)	:	gradient of pot. temp. for different height intervals in the stable air,
γ_q ((gr/kg)/m)	:	the same for specific humidity,
γ_u (s^{-1})	:	for the East-component of the wind,
γ_v (s^{-1})	:	for the North-component of the wind,
H_s (W/m^2)	:	surface sensible heat flux ($= \rho c_p \overline{\theta'w'}_o$),
LE_s (W/m^2)	:	surface latent heat flux ($= \rho L \overline{q'w'}_o$),
Q^* (W/m^2)	:	surface net radiation,
u_* (m/s)	:	surface friction velocity,
U_g (m/s)	:	geostrophic wind (East),
V_g (m/s)	:	geostrophic wind (North),

YEAR : 1977 DAY : 77217 (5 Aug)

Initial conditions

t_o : 0530-0600

h_o : 250

θ_{mo} = 13.2 $\Delta\theta_o$ = 6.1

q_{mo} = 7.4 Δq_o = -4.2

U_{mo} = 6.2 ΔU_o = 4.3

V_{mo} = 5.4 ΔV_o = -5.4

γ_θ = 5.6 $*10^{-3}$ z < 1200 m

1.6 $*10^{-3}$ 1200-2000 m

γ_q = 4.7 $*10^{-4}$ z < 2000 m

γ_u = 1.8 $*10^{-3}$ z < 1000 m

-4.8 $*10^{-3}$ 1000-1500 m

1.0 $*10^{-3}$ 1500-2000 m

γ_v = 2.8 $*10^{-3}$ z < 1000 m

1.8 $*10^{-3}$ 1000-1500 m

1.2 $*10^{-3}$ 1500-2000 m

sunrise : 0408

Forcing functions

	time	H_s	LE_s	Q^*	u_*	U_g	V_g
	0400-0430	-21	1	-20			
	0430-0500	-20	7	-12		8.9	3.4
	0500-0530	-18	35	17			
t_o	0530-0600	+3	56	58	.35	8.9	3.4
	0600-0630	22	83	105	.38		
	0630-0700	45	108	153	.46	9.2	3.1
	0700-0730	54	122	176	.52		
	0730-0800	93	163	256	.59	8.7	3.3
	0800-0830	115	189	303	.62		
	0830-0900	138	218	355	.58	6.6	1.9
	0900-0930	165	241	406	.57		
	0930-1000	182	250	432	.56	5.5	0.9
	1000-1030	190	259	449	.62		
	1030-1100	142	230	372	.51	5.7	0.5
	1100-1130	180	266	446	.40		
	1130-1200	199	269	469	.52		
	1200-1230	194	267	461			
	1230-1300	188	262	450			
	1300-1330	174	256	430			
	1330-1400	158	238	397			
	1400-1430	116	206	322			

Mixed-layer data

time	h	θ_m	q_m	U_m	V_m
0530-0600	250	13.2	7.4	6.2	5.4
0600-0630	250	13.7	7.4	5.7	5.4
0630-0700	300	14.7	7.8	5.2	5.5
0700-0730	330	15.5	8.0	5.0	5.3
0730-0800	370	16.2	8.0	5.9	5.9
0800-0830		17.1	8.1	6.1	5.4
0805	420				
0830-0900		17.9	7.8	6.6	5.6
0849	550				
0900-0930		18.4	7.3	7.4	5.2
0922	610				
0930-1000		19.0	7.3	6.8	5.5
1000-1030		19.8	6.9	7.2	4.2
1005	730				
1030-1100		19.8	6.8	7.3	4.6
1100-1130		20.4	6.8	7.4	4.3
1130-1200		20.9	7.2	7.7	4.6
1200-1230		21.2		6.8	4.0
1230	900	21.5			
1230-1300		21.8		8.1	3.8
1300-1330		22.4			
1330-1400		22.6			
1400-1430		22.8			

YEAR : 1977 DAY : 77248 (5 Sept)

Initial conditions

t_o : 0530-6

h_o : 80

θ_{mo} = 12.2 $\Delta\theta_o$ = 3.0

q_{mo} = 6.5 Δq_o = -3.0

U_{mo} = 1.8 ΔU_o = 9.2

V_{mo} = 4.9 ΔV_o = 1.4

$\gamma_\theta = 6.6 * 10^{-3}$ z < 2000 m

$\gamma_q = -5.0 * 10^{-4}$ z < 2000 m

$\gamma_u = 0$ z < 2000 m

$\gamma_v = -2.6 * 10^{-3}$ z < 1500 m

= 0 1500 - 2000 m

sunrise : 0458

Forcing functions

	time	H_s	LE_s	Q^*	u_*	U_g	V_g
	0430-0500	-17	- 1	-18	.23	7.4	3.5
	0500-0530	- 6	2	- 3	.24		
t_o	0530-0600	+20	-15	6	.26	7.9	2.4
	0600-0630	-25	43	18	.28		
	0630-0700	-14	55	41	.30	6.3	1.3
	0700-0730	+12	87	99	.34		
	0730-0800	4	70	74	.40	7.7	2.4
	0800-0830	8	80	87	.44		
	0830-0900	29	111	139	.46	7.7	2.5
	0900-0930	58	148	206	.48		
	0930-1000	82	163	246	.50	7.5	2.1
	1000-1030	92	166	257	.52		
	1030-1100	69	136	204	.72	6.5	1.1
	1100-1130	77	109	185	.57		
	1130-1200	10	65	75	.58	5.7	0.2
	1200-1230	77	126	203	.58		
	1230-1300	52	93	146	.60	3.1	-2.6
	1300-1330	23	57	80	.59		
	1330-1400	9	45	55	.54	3.9	-0.7

Mixed-layer data

time	h	θ_m	q_m	U_m	V_m
0530-0600	80	12.2	6.5	1.8	4.9
0600-0630	80	12.2	6.4	2.2	5.1
0630-0700	100	12.8	6.4	3.2	5.3
0700-0730	130	13.2	6.7	3.6	5.6
0730-0800			7.1		
0800-0830			7.3	7.1	4.8
0829	280	15.0			
0830-0900		15.4	7.6	6.6	6.0
0900-0930		15.9	7.6	7.6	6.1
0930-1000		16.3	7.9	7.0	5.5
1000-1030		16.6	8.0	6.9	5.0
1030-1100		16.8		6.5	5.6
1100-1130		17.2		6.5	4.9
1115	650				
1130-1200		17.3		8.0	3.4
1200-1230		16.9		7.7	3.0
1230-1300		16.9		7.4	3.5
1300-1330		16.5		7.7	3.8
1330-1400		16.5		8.0	3.9

YEAR : 1977 DAY : 77257 (14 Sept)

Initial conditions

t_o : 0630-7

h_o : 60

θ_{mo} = 9.8 $\Delta\theta_o$ = 2.3

q_{mo} = 6.5 Δq_o =

U_{mo} = ΔU_o =

V_{mo} = ΔV_o =

γ_θ = 6.5 * 10^{-3} z < 620 m

5.2 * 10^{-3} 620 < z < 1390

27.5 * 10^{-3} 1390 < z < 1550

14.7 * 10^{-3} 1550 < z < 1850

2.7 * 10^{-3} 1850 < z < 2000

γ_q

γ_u not determined (no radio soundings at Cabauw)

γ_v

sunrise : 0513

Forcing functions

time	H_s	LE_s	Q^*	u_*	U_g	V_g	
0500-0530			-8	.03			
0530-0600			1	.02	2.5	-3.9	
0600-0630			24	.03			
0630-0700	2	68	57	.17	5.4	-2.3	t_o
0700-0730	22	89	108	.23			
0730-0800	48	103	158	.26	5.7	-2.3	
0800-0830	34	93	137	.35			
0830-0900	92	129	236	.34	7.2	-2.6	
0900-0930	115	128	265	.47			
0930-1000	127	138	289	.46	6.9	-4.6	
1000-1030	165	151	342	.50			
1030-1100	145	120	296	.45	6.3	-5.4	
1100-1130	138	114	283	.55			
1130-1200	165	127	326	.61	7.2	-5.8	
1200-1230	138	114	284	.59			
1230-1300	86	92	202	.61	6.9	-5.8	
1300-1330	132	117	274	.62			
1330-1400	79	84	188	.64	5.8	-6.9	
1400-1430	70	79	169	.65			
1430-1500	62	73	153	.63	5.8	-6.9	
1500-1530	46	66	131	.62			
1530-1600	2	38	49	.55	4.0	-6.9	

Mixed-layer data

time	h	θ_m	q_m	U_m	V_m
0630-0700	60	9.8	6.5		
0700-0730	100	10.5	6.8		
0730-0800	150	11.4	7.1		
0800-0830	240	12.5	7.3		
0830-0900	335	13.2	7.7		
0900-0930		14.0	8.2		
0930-1000		14.6	8.3		
1000-1030		15.3	8.6		
1030-1100		15.9	8.7		
1100-1130		16.1	8.8		
1115	650	16.0			
1130-1200		16.4			
1200-1230					
1230-1300					
1300-1330					
1330-1400					
1400-1430					
1430-1500					
1500-1530		17.4			
1530-1600		17.2			

YEAR : 1977 DAY : 77262 (19 Sept)

Initial conditions

t_o : 0600-0630

h_o : 50

θ_{mo} = 6.0 $\Delta\theta_o$ = 5.3

q_{mo} = 4.8 Δq_o = -0.8

U_{mo} = -1.9 ΔU_o = -2.6

V_{mo} = -4.0 ΔV_o = +4.0

γ_θ = $1.5 * 10^{-3}$ z < 1500 m

$3.4 * 10^{-3}$ 1500 < z < 2000 m

γ_q = $-1.0 * 10^{-3}$ z < 2000 m

γ_u = 0 z < 1000 m

$-3.8 * 10^{-3}$ 1000 < z < 1500 m

0 1500 < z < 2000 m

γ = 0 z < 2000 m

sunrise : 0521

Forcing functions

time	H_s	LE_s	Q^*	u_*	U_g	V_g	
0500-0530	-10			.03			
0530-0600	- 3		0	.01	-5.7	-1.1	
0600-0630	- 5	19	24	.03			t_o
0630-0700	+10	49	59	.04	-5.3	-1.7	
0700-0730	20	80	100	.05			
0730-0800	37	75	121	.10	-5.6	-0.7	
0800-0830	44	100	160	.11			
0830-0900	61	122	206	.16	-6.9	-0.8	
0900-0930	86	135	250	.25			
0930-1000	103	146	281	.21	-7.8	-2.5	
1000-1030	118	159	306	.31			
1030-1100	110	155	300	.28	-7.5	-2.9	
1100-1130	127	152	318	.31			
1130-1200	101	135	270	.35	-7.5	-3.1	
1200-1230	133	158	323	.34			
1230-1300	137	149	322	.39	-8.5	-3.1	
1300-1330	109	144	287	.36			
1330-1400	66	109	190	.41	-10.4	-3.8	
1400-1430	61	100	179	.35			
1430-1500	39	88	140	.32	-9.4	-3.4	
1500-1530	1	34	30	.29			
1530-1600	- 1	28	28	.18	-9.4	-3.4	
1600-1630	0	33	27	.14			
1630-1700	3	-5	-15	.23	-8.5	-3.1	

Mixed-layer data

time	h	θ_m	q_m	U_m	V_m
0600-0630	50	6.0	4.8	-1.9	-4.0
0630-0700	50	6.0			
0700-0730	60	7.5		-0.9	0
0730-0800	80	9.4		-1.2	3.4
0800-0830	130	10.6		-1.5	0.6
0830-0900	170	11.4		-1.8	0.2
0900-0930		12.1		-2.6	-0.3
0912	340		4.5		
0930-1000		12.4		-2.7	-0.3
1000-1030		12.8		-2.8	0
1020	650		3.5		
1030-1100		13.1		-3.4	0
1100-1130		13.4		-3.4	0
1130	1350	13.4			
1130-1200		13.6		-3.8	-0.7
1200-1230		13.8		-3.8	-0.7
1230-1300		14.0		-4.1	-1.3
1300-1330		14.2		-4.1	0.4
1330-1400		14.1		-4.3	-1.8
1400-1430		14.3		-3.2	-2.4
1430-1500		14.4		-3.0	-2.3
1500-1530		14.2			
1530-1600		14.0			
1600-1630		14.2			
1630-1700		13.8			

YEAR : 1978 DAY : 78150 (30 May)

Initial conditions

t_o : 0530-0600

h_o : 150

θ_{mo} = 15.7 $\Delta\theta_o$ = 5.6

q_{mo} = 8.9 Δq_o = -0.9

U_{mo} = -4.5 ΔU_o = -1.9

V_{mo} = -1.2 ΔV_o = -0.7

$\gamma_\theta = 3.3 * 10^{-3}$ $z < 500$ m

$1.2 * 10^{-3}$ $500 < z < 1000$ m

$0.5 * 10^{-3}$ $1000 < z < 2000$ m

$\gamma_q = -1.4 * 10^{-3}$ $z < 2000$ m

$\gamma_u = 2.8 * 10^{-3}$ $z < 1000$ m

$2.0 * 10^{-3}$ $1000 < z < 1500$ m

0 $z < 1500$ m

$\gamma_v = 0$

sunrise : 0327

Forcing functions

time	H_s	LE_s	Q^*	u_*	U_g	V_g
0330-0400	-14	-14	-42	.08	-10.3	-1.3
0400-0430	-10	- 7	-26	.12		
0430-0500	- 9	22	9	.11	- 9.9	-1.4
0500-0530	- 4	30	36	.15		
t_o 0530-0600	0	30	33	.18	-10.1	-1.1
0600-0630	23	83	117	.24		
0630-0700	17	83	114	.27	-10.7	-1.2
0700-0730	51	147	218	.27		
0730-0800	58	174	260	.21	-10.1	-0.5
0800-0830	76	214	326	.21		
0830-0900	89	247	376	.29	-10.5	-1.6
0900-0930	99	274	410	.34		
0930-1000	57	178	287	.44	-10.6	-1.7
1000-1030	54	179	291	.50		
1030-1100	101	346	510	.43	-10.3	-1.5
1100-1130	93	298	458	.43		
1130-1200	66	215	349	.50	-11.7	-1.1
1200-1230	41	246	338	.33		
1230-1300	38	268	348	.50	-12.0	-0.8
1300-1330	96	337	491	.56		
1330-1400	87	310	453	.42	-13.4	-1.2
1400-1430	74	302	426	.50		
1430-1500	52	272	372	.30	-11.8	-1.4
1500-1530	17	213	273	.30		
1530-1600	0	224	246	.34	-10.9	-2.2
1600-1630	- 4	216	234	.41		
1630-1700	-42	96	61	.31	-11.6	-1.7
1700-1730	-34	74	43	.28		
1730-1800	-30	61	32	.32	-11.4	-0.9
1800-1830	-18	27	8	.24		
1830-1900			-26	.20	-11.4	0

Mixed-layer data

time	h	θ_m	q_m	U_m	V_m
0530-0600	150	15.7	8.9	-4.5	-1.2
0600-0630	160	15.9	9.5	-4.0	-0.7
0630-0700	160	16.5	9.6	-3.7	-0.9
0700-0730	170	17.6	10	-3.2	-0.6
0730-0800	180	18.9	10.1	-3.3	-0.3
0800-0830	180	19.7	10	-3.2	0
0830-0900	220	21.0	10.8	-3.3	+0.4
0900-0930		21.9	10.5	-4.2	0.4
0930-1000		22.8	10.3	-4.8	0.6
1000-1030		23.5	9.5	-5.7	0
1030-1100		24	9.5	-5.5	0
1100-1130		24.4	9.4	-5.3	1.5
1115	750				
1130-1200		24.7	9.1	-5.9	2.0
1200-1230		24.6	9.3	-5.7	0
1230-1300		24.6	9.3	-6.9	0
1300-1330		24.9		-6.9	2.1
1330-1400		25.1		-5.5	1.0
1400-1430		25.2		-5.8	0
1430-1500		25.4		-5.1	0
1500-1530		25.5		-5.7	1.5
1530-1600		25.6		-5.7	0
1600-1630		25.7		-5.9	0
1630-1700		25.4		-7.6	0

YEAR : 1978 DAY : 78151 (31 May)

Initial conditions

t_o : 0530-0600

h_o = 100

θ_{mo} = 16.3 $\Delta\theta_o$ = 4.3

q_{mo} = 7.7 Δq_o = -0.3

U_{mo} = -5.7 ΔU_o = -2.8

V_{mo} = 1.5 ΔV_o = 6.2

γ_θ = $7.6 * 10^{-3}$ z < 350 m

$4.6 * 10^{-3}$ 350 < z < 500 m

$1.7 * 10^{-3}$ 500 < z < 2000 m

γ_q = $-1.5 * 10^{-3}$ z < 2000 m

γ_u = $10 * 10^{-3}$ z < 500 m

0 500 < z < 1000 m

$-3 * 10^{-3}$ 1000 < z < 2000 m

γ_v = $-11.7 * 10^{-3}$ z < 500 m

$-1 * 10^{-3}$ 500 < z < 1000 m

$+3 * 10^{-3}$ 1000 < z < 2000 m

sunrise : 0327

Forcing functions

	time	H_s	LE_s	Q^*	u_*	U_g	V_g
	0330-0400	-39	-2	-54	-	-10.5	2.1
	0400-0430	-33	4	-39	.10		
	0430-0500	- 3	2	- 8	.19	-10.2	1.9
	0500-0530	-18	54	+32	.32		
t_o	0530-0600	- 3	80	77	.35	-9.7	3.0
	0600-0630	18	104	127	.38		
	0630-0700	31	137	178	.44	-8.8	2.2
	0700-0730	47	165	227	.37		
	0730-0800	58	189	271	.37	-8.2	2.1
	0800-0830	66	231	323	.44		
	0830-0900	81	256	369	.47	-8.4	1.9
	0900-0930	92	286	410	.48		
	0930-1000	94	292	433	.51	-8.1	1.6
	1000-1030	98	310	460	.57		
	1030-1100	102	322	477	.55	-8.5	0.4
	1100-1130	107	325	491	.48		
	1130-1200	110	328	499	.57	-8.5	-0.7
	1200-1230	110	324	496	.64		
	1230-1300	116	303	477	.59	-9.0	-0.8
	1300-1330	100	291	446	.50		
	1330-1400	101	262	414	.51	-8.4	-0.9
	1400-1430	75	225	342	.41		
	1430-1500	81	226	348	.39	-9.3	-1.1
	1500-1530	57	196	289	.34		
	1530-1600	31	176	235	.20	-9.1	-1.4
	1600-1630	-16	99	97	.18		
	1630-1700	-17	35	24	.17	-9.5	-1.6
	1700-1730	-17	42	30	.16		
	1730-1800	-14	27	18	.14	-8.3	-0.1
	1800-1830	-15	30	18	.16		
	1830-1900			-10	.19	-7.6	1.7

Mixed-layer data

time	h	θ_m	q_m	U_m	V_m
0530-0600	100	16.3	7.7	-5.7	1.5
0600-0630	110	16.9	7.7	-5.1	1.4
0630-0700	140	18	7.9	-6	2.1
0700-0730	180	18.5	8.3	-5.6	2.5
0730-0800		19.6	8.2	-4.8	2.8
750	250				
0800-0830		20.6	8.0	-4.7	3.8
0830-0900		21.1	7.9	-5.0	3.6
850	400				
0900-0930		21.7	7.7	-5.4	3.2
0930-1000		22.5	7.6	-5.6	2.4
1000-1030		23.3	7.2	-6.1	2.2
1030-1100		23.9	6.7	-6.8	2.2
1100-1130		24.2	6.7	-6.8	2.2
1130-1200		24.6	6.4	-7.8	2.4
1200-1230		24.9	6.1	-8.6	3.0
1230-1300		25.2	5.6	-8.7	3.0
1230	1200	25.2			
1300-1330		25.4	5.9	-6.7	2.3
1330-1400		25.6	6.3	-5.9	2.1
1400-1430		25.8	6.6	-5.9	1.4
1430-1500		26.0	6.5	-5.9	1.4
1500-1530		26.1	6.5	-6.3	1.2
1530-1600		26.2	6.5	-6.0	1.6
1600-1630		26.9		-7.8	1.4

YEAR : 1978 DAY : 78152 (1 June)

Initial conditions

t_o : 0530-0600

h_o = 80

θ_{mo} = 17.6 $\Delta\theta_o$ = 5.7

q_{mo} = 8.5 Δq_o = -0.4

U_{mo} = -2.8 ΔU_o = -0.9

V_{mo} = 3.4 ΔV_o = 2.3

γ_θ = $3.8 * 10^{-3}$ z < 500 m

$2.5 * 10^{-3}$ 500 < z < 700 m

$1.3 * 10^{-3}$ 700 < z < 1000 m

$0.6 * 10^{-3}$ 1000 < z < 2000 m

γ_q = $-1.5 * 10^{-3}$ z < 2000 m

γ_u = $14 * 10^{-3}$ z < 200 m

$-1.4 * 10^{-3}$ 200 < z < 2000 m

γ_v = $-25 * 10^{-3}$ z < 200 m

$2.2 * 10^{-3}$ 200 < z < 2000 m

sunrise : 0327

Forcing functions

time	H_s	LE_s	Q^*	u_*	U_g	V_g
0330-0400	-20	-3	-34		-4.1	2.8
0400-0430	-29	12	-25			
0430-0500	-24	32	3	.29	-4.5	2.8
0500-0530	-10	49	36	.25		
0530-0600	7	67	77	.26	-4.8	1.5
0600-0630	25	88	122	.24		
0630-0700	40	111	168	.27	-3.6	2.0
0700-0730	51	144	220	.14		
0730-0800	66	170	269	.16	-3.2	1.9
0800-0830	75	197	314	.18		
0830-0900	87	220	354	.24	-3.0	1.4
0900-0930	96	246	386	.18		
0930-1000	92	241	395	.11	-3.0	1.3
1000-1030	104	272	443	.19		
1030-1100	114	289	470	.05	-3.1	0.8
1100-1130	112	301	485	.13		
1130-1200	74	251	386	.31	-2.6	0.3
1200-1230	48	214	315	.18		
1230-1300	17	179	231	.12	-2.0	0.7
1300-1330	38	230	310	.19		
1330-1400	56	266	374	.17	-2.4	-0.2
1400-1430	62	262	378	.10		
1430-1500	57	246	352	.22	-2.1	-1.5
1500-1530	-20	75	76	.12		
1530-1600	-13	36	27	.11	-1.5	-2.2

Mixed-layer data

time	h	θ_m	q_m	U_m	V_m
0530-0600	80	17.6	8.5	-2.8	3.4
0600-0630	100	18.5	8.8	-3.0	3.2
0630-0700	125	19.2	9.2	-2.4	2.7
0700-0730	170	20.2	9.4	-1.1	2.9
0730-0800	190	20.9	9.6	-1.3	2.1
0800-0830		21.7	9.6	-0.2	2.6
0830-0900		22.3	9.8	-0.3	2.1
0900-0930		23	9.7	0	2.4
0930-1000		23.8	9.3	-0.9	1.8
946	300				
1000-1030		24.5	9.3	-1.0	1.9
1030-11		25	9.2	-1.1	2.1
1100-1130		25.4	8.6	-1	2.8
1115	800				
1130-1200		25.7	8.5	-0.6	3.2
1200-1230		25.9	8.6	-1.3	2.3
1230-1300		26.1	8.4	0	2.5
1300-1330		26.2	8.2	-1.6	2.7
1330-1400		26.6	7.8	0	2.7
1400-1430		26.9	7.2	+0.6	2.7
1430-1500		27	7.0	1.8	3.0
1500-1530		27.2		0	2.3
1530-1600		26.9		2.8	2.8
1600-1630		26.6		5.3	1.0
1630-1700		26.1		4.0	0

YEAR : 1978 DAY : 78269 (26 Sept)

Initial conditions

t_o : 0630-0700

h_o = 100

θ_{mo} = 9.5 $\Delta\theta_o$ = 4.8

q_{mo} = 6.9 Δq_o = 0.3

U_{mo} = 2.6 ΔU_o = 5.5

V_{mo} = 4.6 ΔV_o = -1.9

γ_θ = 2.9	$* 10^{-3}$	z < 500 m
1.2	$* 10^{-3}$	500 < z < 1800 m
30	$* 10^{-3}$	1800 < z < 2000 m
γ_q = -2.6	$* 10^{-3}$	z < 1000 m
-0.8	$* 10^{-3}$	1000 < z < 1500 m
-4	$* 10^{-3}$	1500 < z < 2000 m
γ_u = -2.7	$* 10^{-3}$	z < 500 m
+2.3	$* 10^{-3}$	500 < z < 2000 m
γ_v = 2	$* 10^{-3}$	z < 500 m
-2.6	$* 10^{-3}$	500 < z < 1000 m
0.9	$* 10^{-3}$	1000 < z < 2000 m

sunrise : 0532

Forcing functions

	time	H_s	LE_s	Q^*	u_*	U_g	V_g
	0530-0600 } no data						
	0600-0630 }						
t_o	0630-0700	-2	28	21	.28	8.3	3.1
	0700-0730	4	60	64	.24		
	0730-0800	10	76	89	.34	8.5	2.5
	0800-0830	25	77	108	.39		
	0830-0900	31	90	130	.45	9.2	1.9
	0900-0930	18	59	84	.44		
	0930-1000	23	74	105	.36	8.2	-0.7
	1000-1030	41	91	145	.28		
	1030-1100	20	81	115	.29	8.2	-2.1
	1100-1130	18	145	170	.59		
	1130-1200	18	163	190	.49	8.3	-2.2
	1200-1230	35	167	215	.51		
	1230-1300	51	194	257	.53	7.8	-3.7
	1300-1330	6	120	134	.50		
	1330-1400	- 4	97	97	.46	9.6	-3.1
	1400-1430	-11	63	54	.41		
	1430-1500	- 4	98	96	.48	10.3	-2.2
	1500-1530	-14	46	31	.46		
	1530-1600	-13	31	15		12.0	-1.2
	1600-1630	-12	23	9			
	1630-1700			-6		11.9	-1.4

Mixed layer data

time	h	θ_m	q_m	U_m	V_m
0630-0700	100	9.5	6.9	2.6	4.6
0700-0730	110	10.0	7.1	2.2	5.5
0730-0800	130	11.0	7.4	3.5	5.4
0800-0830	160	11.9	7.6	2.9	5.7
0830-0900	220	12.5	7.5	4.0	5.7
0900-0930	250	12.7	7.6	5.9	4.9
0930-1000		12.9	7.6	7.0	3.4
1000-1030		13.4	8.5	6.8	1.4
1030-1100		14.3	7.6	7.1	0.4
1100-1130		14.8	6.0	10.2	-2.0
1130-1200		15	6.4	9.3	-1.5
1145	700	15			
1200-1230		15.2	6.0	8.7	-0.9
1230-1300		15.4	5.3	9.1	0
1300-1330		15.3	5.3	9.2	0
1330-1400		15.3	5.6	10.3	0

YEAR : 1978 DAY : 78285 (12 Oct)

Initial conditions

t_o : 0700-0730

h_o = 100

θ_{mo} = 10.5 $\Delta\theta_o$ = 3.0

q_{mo} = 7.6 Δq_o = -1.6

U_{mo} = -4.5 ΔU_o = -2.1

V_{mo} = 3.9 ΔV_o = 4.0

γ_θ = 22 $*$ 10^{-3} z < 500 m

15.5 $*$ 10^{-3} 500 < z < 770 m

γ_q = -0.8 $*$ 10^{-3} z < 1000 m

γ_u = 46 $*$ 10^{-3} z < 200 m

-5 $*$ 10^{-3} 200 < z < 500 m

-1.2 $*$ 10^{-3} 500 < z < 1000 m

γ_v = -12 $*$ 10^{-3} z < 200 m

-9 $*$ 10^{-3} 200 < z < 500 m

8.2 $*$ 10^{-3} 500 < z < 1000 m

sunrise : 0559

Forcing functions

	time	H_s	LE_s	Q^*	u_*	U_g	V_g
	0600-0630	-24	-14	-58	.28		
	0630-0700	-21	- 3	-40	.33	-4.5	5.0
t_o	0700-0730	-13	21	- 2	.41		
	0730-0800	4	38	40	.41	-4.5	5.6
	0800-0830	14	52	71	.35		
	0830-0900	29	81	119	.39	-3.1	6.5
	0900-0930	39	100	155	.41		
	0930-1000	48	118	184	.31	-3.8	6.5
	1000-1030	53	114	192	.30		
	1030-1100	58	130	214	.29	-4.6	6.5
	1100-1130	59	131	216	.45		
	1130-1200	58	130	215	.38	-4.2	8.2
	1200-1230	54	131	208	.35		
	1230-1300	47	126	192	.47	-6.1	5.4
	1300-1330	35	114	165	.50		
	1330-1400	19	91	126	.46	-6.0	4.6
	1400-1430	2	63	77	.37		
	1430-1500	- 5	36	41	.29	-7.0	3.4
	1500-1530	- 4	9	9	.15		
	1530-1600	-57	43	-13	.14	-6.3	3.9
	1600-1630	-27	- 3	-36	.11		
	1630-1700	-24	- 9	-48	.16	-5.6	4.9

Mixed-layer data

time	h	θ_m	q_m	U_m	V_m
0700-0730	100	10.5	7.6	-4.5	3.9
0730-0800	140	11.3	7.8	-4.2	4.5
0800-0830	180	11.8	8.0	-3.9	4.3
0830-0900	180	12.4	8.2	-3.6	3.5
0900-0930	190	12.9	8.2	-2.9	3.6
0930-1000	170	13.5	7.6	-1.7	3.6
1000-1030	170	14.5	8.0	-2.1	3.1
1030-1100	190	15.3	8.2	-2.5	2.9
1100-1130		16.1	8.0		
1130-1200		16.8	8.0	-3.0	2.4
1200	260	17.0			
1200-1230		17.7	7.7		
1230-1300		18.2	7.7	-5.2	3.0
1257	380	18.3			
1300-1330		18.9	8.1		
1330-1400		19.5	8.4	-5.6	3.9
1353	540	19.5			
1400-1430		19.9	8.6		
1430-1500		20.0	8.6	-4.6	4.6
1500-1530		20.1	8.5		
1530-1600		20.2	8.4	-4.8	5.0

YEAR : 1978 DAY : 78286 (13 Oct)

Initial conditions

t_o : 0700-0730

h_o = 100

θ_{mo} = 10.2 $\Delta\theta_o$ = 5.9

q_{mo} = 6.7 Δq_o = -0.2

U_{mo} = -2.2 ΔU_o = 1.2

V_{mo} = +2.7 ΔV_o = 2.2

γ_θ = $8.2 * 10^{-3}$ z < 600 m

γ_q = $-1.2 * 10^{-3}$ z < 1000 m

γ_u = $10 * 10^{-3}$ z < 200 m

$-7.5 * 10^{-3}$ 200 < z < 1000 m

γ_v = $-14 * 10^{-3}$ z < 200 m

$5 * 10^{-3}$ 200 < z < 800 m

$-3.5 * 10^{-3}$ 800 < z < 1000 m

sunrise : 0601

Forcing functions

	time	H_s	LE_s	Q^*	u_*	U_g	V_g
	0600-0630	-3	-1	-33	.12		
	0630-0700	1	1	-19	.12	-3.4	1.4
t_o	0700-0730	12	5	7	.19		
	0730-0800	8	35	48	.23	-2.4	1.4
	0800-0830	22	55	92	.21		
	0830-0900	34	74	131	.19	-1.9	1.5
	0900-0930	42	91	161	.19		
	0930-1000	46	98	174	.21	-2.1	1.5
	1000-1030	45	87	166	.14		
	1030-1100	52	101	191	.06	-2.3	0.9
	1100-1130	48	111	196	.09		
	1130-1200	47	106	189	.10	-2.9	0.1
	1200-1230	39	106	178	.14		
	1230-1300	38	100	167	.14	-2.2	0.5
	1300-1330	30	88	142	.21		
	1330-1400	20	72	112	.18	-2.1	0.7
	1400-1430	10	52	78	.13		
	1430-1500	1	28	41	.12	-1.5	1.0
	1500-1530	- 1	3	9	.10		
	1530-1600	-41	23	-18	.08	-1 8	0.4
	1600-1630	-27	3	-32	.01		
	1630-1700	-14	-7	-38	.04	-1.6	0.4

Mixed layer data

time	h	θ_m	q_m	U_m	V_m
0700-0730	100	10.2	6.7	-2.2	2.7
0730-0800	100	10.7	6.8	-2.0	3.0
0800-0830	110	11.5	-	-1.5	3.0
0830-0900	115	12.2	7.1	-1.4	2.3
0900-0930	110	13.2	7.4	-1.4	1.8
0930-1000	125	14.2	7.5	-1.0	2.2
1000-1030	150	14.9	7.8	-1.1	2.0
1030-1100	190	15.9	7.7	-1.1	1.5
1100-1130		16.4	7.4	-1.5	2.0
1130-1200		17.0	7.4	-1.4	1.6
1200	230	17.2			
1200-1230		17.4	7.6	-1.0	2.0
1230-1300		17.9	7.6	-1.6	1.6
1300-1330		18.2	7.8	-1.9	1.9
1330-1400		18.5	7.8	-1.5	2.0
1400-1430		18.6	8.1	-1.0	2.1
1430-1500		18.7	8.2	-1.0	2.8
1500-1530		18.8	8.1		
1530-1600		18.9	8.1	-1.2	3.3
1600-1630		18.9	8.1		
1630-1700		19	7.8	-0.4	3.5

LIST OF TABLES

LIST OF FIGURES

LIST OF SYMBOLS

A	constant in entrainment model.
B_1, B_2, B_3, B_4	constants in entrainment model.
b	buoyancy, $b = -g\rho/\rho_o$.
b_m	value of b in the mixed layer.
b_{mo}	initial value of b_m.
Δb	jump in buoyancy at top of mixed layer.
Δb_o	initial value of Δb.
$\overline{b'w'}$	vertical turbulent buoyancy flux.
$\overline{b'w'}_o$	value of $\overline{b'w'}$ at the surface.
$\overline{b'w'}_h$	value of $\overline{b'w'}$ at z=h.
C	any quantity, conserved under adiabatic vertical mixing.
c_p	specific heat at constant pressure.
c_v	specific heat at constant volume.
c_F, c_T, c_D, c_M	constants in entrainment model.
d	thickness of interfacial layer between turbulent and non-turbulent fluid, penetration depth of turbulent eddies into non-turbulent fluid.
e	turbulent kinetic energy ($= \frac{1}{2}(\overline{u'^2} + \overline{v'^2} + \overline{w'^2})$).
$\overline{ew'}$	vertical transport of TKE.
f	Coriolis parameter.
G	heat flux into the soil.
g	gravity acceleration.
H	vertical flux of sensible heat, ($\rho_o c_p \overline{\theta'w'}$).
H_s	surface flux of sensible heat, ($\rho_o c_p \overline{\theta'w'}_o$).
h	mixed layer height.
h_o	initial value of h.
K	eddy diffusivity.
L	latent heat of vaporization ($L \approx 2.5\ 10^6$ J/kg).
LE	vertical flux of latent heat, ($\rho_o L \overline{q'w'}$).
LE_s	surface flux of latent heat, ($\rho_o L \overline{q'w'}_o$).
p_o	reference pressure.
p	deviation from reference pressure.
Q_T	diabatic heating term.
Q^*	net radiation at the surface.

LIST OF SYMBOLS (continued)

q	specific humidity.
q_m	mixed-layer humidity.
q_{mo}	initial value.
Δq	jump in humidity at z=h.
Δq_o	initial value.
$\overline{q'w'}$	moisture flux.
$\overline{q'w'}_o$	surface moisture flux.
$\overline{q'w'}_h$	moisture flux at z=h.
Ri	gradient Richardson number, $Ri = (\partial b/\partial z)/(\lvert \partial \underset{\sim}{U}_H/\partial z \rvert)^2$.
Ri_*	bulk Richardson number for the mixed layer, $Ri_* = h\Delta b/\sigma_w^2$.
Ri_b	bulk Richardson number for the mixed layer, based on $\Delta\underset{\sim}{U}$; $Ri_b = h\Delta b/\lvert\Delta\underset{\sim}{U}\rvert^2$.
S	salinity.
T_o	reference temperature for an adiabatic atmosphere.
T_v	virtual temperature.
t	time.
$\underset{\sim}{U}_H$	horizontal wind vector.
U, V	horizontal wind components (East, North).
U_m, V_m	wind in the mixed layer.
U_{mo}, V_{mo}	initial values.
ΔU, ΔV	jumps in wind components at z=h.
ΔU_o, ΔV_o	initial values.
$\overline{u'w'}$, $\overline{v'w'}$	turbulent momentum transports.
$\overline{u'w'}_o$, $\overline{v'w'}_o$	values at the surface.
$\overline{u'w'}_h$, $\overline{v'w'}_h$	values at z=h.
u_*	surface friction velocity, $u_* = (\overline{u'w'}_o^{\,2} + \overline{v'w'}_o^{\,2})^{1/4}$.
U_g, V_g	components of the geostrophic wind.
w	vertical wind component.
$\overline{w}_h$	mean vertical wind at z=h.
w_*	convective velocity scale, $w_*^3 = \overline{b'w'}_o\, h$.
z	vertical coordinate (positive upward).

LIST OF SYMBOLS (continued)

Greek symbols

α	thermal expansion coefficient for water.
β	salinity expansion coefficient for water.
$\gamma_b = (\partial b/\partial z)_+$	stable gradient of buoyancy outside the mixed layer.
$\gamma_q = (\partial q/\partial z)_+$	gradient of specific humidity outside the mixed layer.
$\gamma_\theta = (\partial \Theta/\partial z)_+$	gradient of potential temperature outside the mixed layer.
$\gamma_u = (\partial u/\partial z)_+$ $\gamma_v = (\partial v/\partial z)_+$	gradients of wind outside the mixed layer.
$\gamma_\rho = (\partial \rho/\partial z)_+$	gradient of potential density outside the mixed layer.
ε	dissipation rate of turbulent kinetic energy.
$\underset{\sim}{\eta}$	unit vector in vertical direction.
η	constant in entrainment model.
Θ	potential temperature.
Θ_v	virtual potential temperature.
θ'	fluctuating component of $\Theta = \overline{\Theta} + \theta'$.
Θ_m	mixed-layer potential temperature.
Θ_{mo}	initial value of Θ_m.
$\Delta\Theta$	jump in potential temperature at z=h.
$\Delta\Theta_o$	initial value.
$\overline{\theta'w'}$	vertical kinematic heat flux.
$\overline{\theta'w'}_o$	surface kinematic heat flux.
$\overline{\theta'w'}_h$	kinematic heat flux at inversion base z=h.
ρ_o	reference density for an adiabatic atmosphere.
$\tilde{\rho}$	actual density.
ρ	potential density, deviation from reference density.
ρ'	fluctuating component of $\rho = \overline{\rho} + \rho'$.
ρ_m	mean value of density in the mixed layer.
$\Delta\rho$	jump in density at z=h.
σ_w	turbulent velocity scale in the mixed layer.
$\underset{\sim}{\tau}_H$	horizontal components of the Reynolds stress, $\underset{\sim}{\tau}_H = -\rho_o\,(\overline{u'w'}, \overline{v'w'})$.
ω_b	Brunt-Vaisala frequency, $\omega_B = \gamma_b^{\frac{1}{2}}$.